CHARACTERIZING HUMAN VISUAL CORTEX DEVELOPMENT

CHARACTERIZING THE DEVELOPMENT OF NEUROIMMUNE PROTEINS IN THE HUMAN PRIMARY VISUAL CORTEX

By EWALINA JEYANESAN, B.Sc.

A Thesis Submitted to the School of Graduate Studies

in Partial Fulfillment of the Requirements for the Degree Master of Science

McMaster University

© Copyright by Ewalina Jeyanesan, August 2020

MASTER OF SCIENCE (2020) McMaster University

(Neuroscience) Hamilton, Ontario

TITLE: Characterizing the development of neuroimmune proteins in the human primary visual cortex

AUTHOR: Ewalina Jeyanesan, B.Sc. (McGill University)

SUPERVISOR: Dr. Kathryn M. Murphy

NUMBER OF PAGES: xi, 178

Lay Abstract

The human brain develops across the lifespan. This ability of the brain to change and adapt to the environment is called *plasticity* and it is essential for normal brain functions, such as processing visual information. Immune proteins play important roles in the visual cortex- the brain region responsible for visual information processing. They help establish brain circuits in early development and regulate ongoing neural processes important to brain plasticity. In my thesis, I measure the expression of neuroimmune proteins to unpack their developmental patterns in the human visual cortex. I found that these proteins have fluctuating levels across development, with many displaying heightened expression levels in early childhood. Additionally, I found eight common trajectory patterns that were shared between the proteins. These findings enable a better understanding of how regulators of human brain development mature.

Abstract

Neuroimmune proteins are involved in a wide array of biological functions throughout brain development. Importantly, these molecular mechanisms regulate the activity-dependent sculpting of neural circuits during the critical period. Abnormal expression of these molecular mechanisms, especially in early development, is linked to the emergence of neurodevelopmental disorders. Despite having central roles in both normal and pathological conditions, very little is known about the lifespan expression of neuroimmune proteins in the human cortex. As studies exploring the relationship between inflammation and disease tend to rely on animal models, unpacking immune lifespan trajectories in the human brain will be essential for translational research. Furthermore, it will aid the development of timely and effective therapeutic interventions for neurodevelopmental disorders. In my thesis, I characterize the development of 72 neuroimmune proteins in 30 postmortem tissue samples of the human primary visual cortex. These samples cover the lifespan from 20 days to 79 years. I compare the developmental profiles of these immune markers to those of well-studied classic neural proteins including glutamatergic, GABAergic and other synaptic plasticity-related markers. Using a data-driven approach, I found that the 72 neuroimmune proteins share approximately eight developmental patterns, most of which undulate across the lifespan. Furthermore, I used unsupervised hierarchical clustering to show that the development of neuroimmune proteins in the human visual cortex varies from that of classic neural proteins. These findings facilitate a deeper understanding of human cortical development through two classes of proteins involved in brain development and plasticity.

Acknowledgements

To begin, I would like to thank Dr. Kathryn Murphy for her guidance these past two years. Dr. Murphy brought an unwavering enthusiasm for neuroscience to my mentorship, and for that, I will be forever grateful. A big thank you to Dr. Ram Mishra and Dr. Jane Foster for their feedback and instruction as members of my supervisory committee. Thank you to Keon Arbabi and Dezi Ahuja for welcoming me to the lab and for being great friends. Thank you to Brendan Kumagai for introducing me to the life-changing world of R Markdowns. Thank you to Ms. Sandra Murphy for answering my never-ending list of questions and for the genuine interest you show in student success. Thank you to Dr. Jay Olson for providing an unparalleled example of how to be a great mentor to fellow students.

I would also like to thank Tyurina and Deanna for their steadfast belief in me. Thank you to Godwin for being on my side these past 21 years. And finally, to Amma and Appa... even in a world with approximately 6,500 languages there are no adequate words to express how grateful I am for your love. For you, a simple “thank you” will never be enough.

Table of Contents

List of Figures

Chapter 2

List of Tables

Chapter 2

List of Abbreviations

2A	GluN subunit 2A
2B	GluN subunit 2B
AD	Alzheimer's Disease
AMPAR	α-amino-3-hydroxy-5-methyl-4-isoxazolepropionic acid receptor
ASD	Autism Spectrum Disorder
AU	approximately unbiased p-value
Axl	tyrosine-protein kinase receptor UFO
BBB	blood brain barrier
BCA	bicinchinchoic acid
BD	binocularly deprived
C1q	complement component 1q
CB1	cannabinoid receptor 1
CDKL5	cyclin-dependent kinase-like 5
CI	confidence interval
CNS	central nervous system
MCSF	macrophage colony-stimulating factor 1
DNA	deoxyribonucleic acid
EGF R	epidermal growth factor receptor
E:I	excitatory: inhibitory
ELISA	enzyme-linked immunosorbent assay
ErbB3	receptor tyrosine-protein kinase erbB-3
FDR	false discovery rate
Flt-3L	fms-related tyrosine kinase 3 ligand
GABA	gamma-aminobutyric acid
GAD	glutamate decarboxylase
GDNF	glial cell line-derived neurotrophic factor
GDF-15	growth differentiation factor 15
GFAP	glial fibrillary acidic protein
GluA	glutamate receptor ionotropic AMPA receptor
GluN	glutamate receptor ionotropic NMDA receptor
GO	Gene Ontology
gp130	Glycoprotein 130
HFMD	hand foot and mouth disease
HGF	hepatocyte growth factor
HOM	homogenate
HVEM	hepatitis viral entry mediator
ICAM-1	intercellular adhesion molecule 1
IEA	inferred from electronic annotation
IL2Rg	interleukin-2 receptor subunit gamma
IL	interleukin
IQR	interquartile range

LGN	lateral geniculate nucleus
LIF	leukemia inhibitory factor
LIMPII	lysosome membrane protein 2
LOD	lower limit of detection
LOESS	locally estimated scatterplot smoothing
LTD	long-term potentiation
LTP	long-term depression
LYVE-1	lymphatic vessel endothelial hyaluronic acid receptor 1
MAX	maximum / upper limit of detection
MBP	myelin basic protein
MCSF	macrophage colony-stimulating factor 1
MD	monocular deprivation
ME	monocular enucleation
MeCP2	methyl-CpG binding protein 2
MHC	major histocompatibility complex
MIA	maternal immune activation
mEPSC	miniature excitatory postsynaptic current
mIPSC	miniature inhibitory postsynaptic current
MS	multiple sclerosis
mRNA	messenger ribonucleic acid
Narp	neuronal activity-regulated pentraxin
NMDAR	N-methyl-D-aspartate receptor
NrCAM	neuronal cell adhesion molecule
ODC	ocular dominance column
ODP	ocular dominance plasticity
PDGF	platelet derived growth factor
PirB	paired-immunoglobulin–like receptor B
PLAUR	urokinase receptor
PMI	postmortem interval
polyI:C	polyinosinic:polycytidylic acid
PSD-95	postsynaptic density protein 95
RGC	retinal ganglion cells
RSKC	robust and sparse k-means clustering
SNP	single nucleotide polymorphisms
STRINGdb	Search Tool for the Retrieval of Interacting proteins database
TGFα	transforming growth factor alpha
TIMP	tissue inhibitors of metalloproteinases
TNFα	tumor necrosis factor-α
TNFR II	tumor necrosis factor receptor 2
Tyro3	tyrosine-protein kinase receptor
V1C	primary visual cortex
VEP	visual evoked potentials
VGAT	vesicular inhibitory amino acid transporter
WSS	within-cluster sum of square

Declaration of Academic Achievement

Chapter 2 of my thesis is a research article currently in preparation for submission to Frontiers Neuroscience, a peer-reviewed open access journal. This work was a collaboration between and myself and Dr. Kathryn Murphy. I was the lead on designing the study, analyzing and interpreting the data, and drafting the manuscript. Some of the data acquisition was completed by Dr. Caitlin Siu, Dr. Justin Balsor, Dr. Simon Beshara, Dr. Joshua Pinto and Dr. Kate Williams. Dr. Justin Balsor, Keon Arbabi and Brendan Kumagai assisted with certain data preparation and data visualization steps.

Chapter 1. General Introduction

The term *neuroimmune* refers to the interaction between the nervous system and the immune system. Communication between these two systems is bidirectional (Reardon et al., 2018) and the study of these interactions is termed neuroimmunology (Nutma et al., 2019). Proteins traditionally found in the immune system have important roles in brain, where they regulate many neural functions, including visual information processing (Boulanger, 2009). In addition to their roles in the healthy brain, immune proteins are implicated in a wide range of neurodevelopmental disorders (Garay & McAllister, 2010). Despite their involvement in both development and disease, very little is known about the lifespan expression profiles of immune proteins in the human brain. Studies exploring the links between inflammation, aging and disease rely heavily on animal models. Therefore, unpacking the lifespan trajectories of these immune proteins is essential for translational research and for identifying molecular targets for treating neurodevelopmental disorders.

The influence of peripheral inflammation on the central nervous system (CNS), and the crosstalk between neurons and glial cells are two examples of neuroimmune activity. In my thesis, a third branch of neuroimmune interactions will be assessed. Specifically, I explore the expression of immune proteins in the brain (i.e. neuroimmune proteins) and their involvement in brain functions like development and plasticity. I create a database detailing the developmental trajectories of 72 neuroimmune proteins in the human primary visual cortex (V1C). Furthermore, I compare their trajectories to the lifespan expression patterns of classic neural proteins known to regulate critical period plasticity.

1.1 Critical period plasticity and neuroimmune proteins

1.1.1 The critical period

The critical period is a time in development when the brain is especially sensitive to external factors. While genetics plays an important role in determining the initial structure and connectivity of neural circuits, environmental factors are also key players (Hensch, 2004). Abnormal experience during the critical period can have enduring, irreversible, negative effects throughout the lifespan. The study of critical periods was pioneered by Hubel and Wiesel in the 1960s. Originally, completing their work in kittens, Hubel and Wiesel found that monocular deprivation (MD), a process through which one eye is occluded, produced profound changes in the cat's visual system properties (Hubel & Wiesel, 1963, Wiesel & Hubel, 1963a; Wiesel & Hubel, 1963b). Using single unit recordings, they found that after MD kittens had a decreased number of cells in the lateral geniculate nucleus (LGN) that received input from the deprived eye (Wiesel & Hubel, 1963a). Interestingly they found that this decrease was greatest in the kitten with no visual experience - i.e. one eye sutured from birth (Wiesel & Hubel, 1963a). The atrophy was less in kittens with previous visual experience, and no such atrophy corresponding to the deprived eye was observed when the adult cat was monocularly deprived (Wiesel & Hubel, 1963a). They subsequently measured cellular responses in the cat visual cortex and found that the kittens visually deprived since birth had more cells that preferentially responded to the open eye (Wiesel & Hubel, 1963b). Once again, they found that this preference for the open eye was absent in adult cats that underwent MD. They remark that there is a “pronounced difference between kittens and adults in susceptibility to

deprivation" (Wiesel & Hubel, 1963b). The work by Hubel and Wiesel was the initial indication that there are time sensitive windows where the brain is susceptible to influence by visual experience.

1.1.2 Ocular dominance columns and plasticity

Hubel and Wiesel's work also laid the foundation for the study of ocular dominance columns (ODCs). These refer to striated patterns of neurons in the visual cortex that preferentially respond to one eye over the other (Katz & Crowley, 2002). Once again, Hubel and Wiesel's studies in monocularly deprived kittens revealed that selective receptive field properties were present in visually inexperienced kittens (Hubel & Wiesel, 1963). Consequently, Hubel and Wiesel theorized that there must be a genetic component that orchestrates the responses of neurons in the absence of visual experience (Hubel & Wiesel, 1963). In later experiments, injections of radioactive chemicals into the left eye of a Rhesus monkey, made it possible to visualize these striated patterns in the visual cortex (Wiesel et al., 1974). Using this autoradiography technique, they later showed that monocularly deprived macaque monkeys had larger bands corresponding to the open eye, while the bands corresponding to the deprived eye had shrunk (Hubel et al., 1977). Importantly, these changes in band width were not observed when occluding the eye of an adult macaque monkey; providing further evidence that there are periods of time (i.e. a critical period) when the functional architecture of the visual cortex is susceptible to alterations based on visual experience, or lack thereof (Hubel et al., 1977). In later studies, LeVay et al. (1978) showed that the striated pattern was evident in adult cats, but not in kittens of around one to two weeks of age. Instead, LeVay et al. (1978)

observed one continuous band in kittens. Experiments by Crair et al. (1998) looking at binocularly deprived (BD) cats demonstrated that while these cortical maps were innate (as they developed in kittens whose eyes had not yet opened), visual experience was required for the modification of neural responses to the contralateral and ipsilateral eye.

Critical periods have since been assessed in the visual cortex of cats, non-human primates, mice, and other animal models by numerous researchers (Espinosa & Stryker, 2012). Using a combination of methods such as eye patching, cataracts to occlude the eyes, and more recently, gene knockout methods, we have been able to selectively disturb normal binocular vision and determine the molecular mechanisms that regulate the critical period for ocular dominance plasticity (ODP). Key players include proteins integral to excitatory and inhibitory transmission as well as the regulation of experience-dependent cortical plasticity.

Glutamate decarboxylase 65 (GAD65), creates the on-demand supply of gamma-aminobutyric acid (GABA) through the decarboxylation of glutamate, and has been linked to the opening of the critical period for ODP (Iwai et al., 2003). Hensch et al. (1998) showed that in GAD65 knockout mice, cells do not show preference for the open eye after brief MD during the critical period for ODP. Rather cells continued to respond preferentially to the contralateral eye (Hensch et al., 1998). Next, they supplied the knockout mice with the benzodiazepine agonist, diazepam which reinstated the ocular dominance shift in monocularly deprived mutant mice (Hensch et al., 1998). It was later found that the diazepam infusion did not need to coincide with the entire deprivation

period, rather brief GABAergic transmission at the beginning of MD was required to facilitate ODP (Iwai et al., 2003).

Similarly, $GABA_A$ receptor subunits have also been studied in the context of ODP. The $GABA_A$ subunit is responsible for the binding of GABA to the receptor (Smith & Olsen, 1995). Fagiolini et al. (2004) studied knock out mice for the three $GABA_A$ subunits: α1, α2 and α3. Using a series of knockin experiments, they selectively targeted the benzodiazepine binding site on each of the three receptor subunits separately. Fagiolini et al. (2004) observed that while the α1 subunit was required to drive visual cortical plasticity, the other two were not.

Glutamatergic receptors have also been implicated in the regulation of synaptic plasticity and the opening and closing of the critical period for ODP. For example, increases in the level of postsynaptic scaffolding protein 95 (PSD-95) are necessary for the closing of the critical period, as it facilitates the maturation of synapses (Huang et al., 2015). The glutamate receptor 2 (GluA2) subunit, on the other hand, has been implicated in the opening of the critical period (Rumpel et al., 1998). In fact, the critical period for ODP is divided into stages. The process begins with a decrease in response to the deprived eye followed by an increase in response to the open eye - with minor increases in deprived eye responses as well (Espinosa & Stryker, 2012). Finally, if the deprived eye is opened during the critical period, responses are recovered (Kaneko, Hanover, et al., 2008). Each of these stages are governed by different sets of molecular mechanisms. Loss of GluA2 (Heynen et al., 2003) and an increase in the immature glutamate receptor ionotropic NMDA 2B subunit (GluN2B) accompanies the weakening of responses to the

deprived eye (Chen & Bear, 2007). An increase in GluA2 (Lambo & Turrigiano, 2013) and decrease in the mature glutamate receptor ionotropic NMDA 2A subunit (GluN2A) is associated with the strengthening of responses to the open eye (Smith et al., 2009). These molecular mechanisms also contribute to regulating ODP in the healthy brain. For example, visual experience during the critical period drives the loss of GluN2B (Philpot, et al., 2001) and an increase of GluN2A, which combined reduce ODP (Quinlan et al., 1999). This 2A:2B subunit balance is considered a regulator of metaplasticity in the visual cortex (Philpot et al., 2007).

1.1.3 Neuroimmune proteins and plasticity during the critical period

Neuroimmune proteins also play important roles in the regulation of the critical period for ODP. Multiple studies have found that the major histocompatibility complex (MHC) family of molecules restrict ODP (Espinosa & Stryker, 2012). These molecules have important roles in the detection of antigens as part of the immune system (Wieczorek et al., 2017). They function by binding fragments of pathogens and displaying them on the cell surface to trigger responses by T-cells (Wieczorek et al., 2017). In the nervous system, paired-immunoglobulin–like receptor B (PirB) is a receptor for the MHC class I molecules widely implicated in activity-dependent synaptic plasticity (Shatz, 2009). Syken et al. (2006) used a mutant mouse in which four exons encoding the transmembrane portion and part of intracellular component of the PirB receptor were removed. This mutation made PirB unable to signal across the plasma membrane (Syken et al. 2006). Syken et al. (2006) found that the mutated mice had enhanced ODP after monocular enucleation (ME) and MD. Interestingly, they observed this enhancement in

adult mice also, suggesting that PirB is required to limit experience-dependent plasticity, not just within the critical period, but also beyond it (Syken et al., 2006). Following this discovery, Datwani et al. (2009) examined ODP after the deletion of 2 members of the MHC family of molecules: H2-K^b and H2-D^b. They too found that the deletion was sufficient to enhance ODP in the mouse visual system after both MD and ME (Datwani et al., 2009).

Tumor necrosis factor-α (TNFα) is a proinflammatory cytokine that also has important roles in ODP, particularly in the strengthening of responses to the open eye. Using TNFα knockout mice it was possible to dissociate the first and second stages of ODP (Kaneko, Stellwagen, et al., 2008). First, researchers monocularly deprived mutant mice by lid suture for a brief period during the peak of the critical period. When optical imaging was used to measure responses to both eyes, researchers found that there was a decrease in the ocular dominance shift (Kaneko, Stellwagen, et al., 2008). As mentioned previously, the ocular dominance shift occurs in two distinct stages. First, with a decrease in deprived-eye responses, which is followed by an increase in open-eye responses (Espinosa & Stryker, 2012). Kaneko, Stellwagen, et al. (2008) found that while TNFα knockout mice showed decreases in response to the deprived eye, the expected increase in response to the open eye were not observed. This revealed a role for TNFα in strengthening the responses to the open eye following MD. Taken together these findings suggest pleiotropic roles for neuroimmune markers in ODP, as some promote plasticity (i.e. TNFα) while others act as a break on ODP (i.e. proteins in the MHC family of proteins).

1.2 Neuroimmune proteins and brain development

1.2.1 Neuroimmune proteins in the central nervous system

The brain was traditionally considered to be an immune-privileged site, where the blood brain barrier (BBB) prevented peripheral immune proteins from entering the CNS. Only in the event of insult, such as during brain injury or disease when the integrity of the BBB is compromised, were immune proteins thought to crossover to the CNS (Forrester et al., 2018; Galea et al., 2007; Zlokovic, 2008). The current understanding of neuroimmune interactions is much more complex, as recent studies have unveiled the expression of immune markers by the healthy brain. From a functional perspective, the immune system and the nervous system have much in common (McAllister & Water, 2009). For example, they both detect and respond to external cues through the release of secretory molecules to distant targets, and both immune and neurons are capable of forming synapses (Kioussis & Pachnis, 2009). With their many functional similarities it is comprehensible that the proteins that carry out these common functions are present in both systems. Due to their dual roles, classic immune markers are considered pleiotropic. Notably, they do not simply perform immune functions in the brain. Rather inflammatory markers are developmentally regulated and modulate nervous system development (Garay & McAllister, 2010). In fact, a wide range of immune proteins from both the innate and adaptive immune systems can be found in the human brain. These include cytokines, members of the complement system, and the MHC family of molecules (Boulanger, 2009). These classic immune proteins are associated with a range of neural processes, such as the experience-dependant refinement of cortical circuits, determining

the number of synapses, the proliferation and survival of neuronal and glial cells, axon guidance and synapse formation, to name a few (Stolp, 2013).

1.2.2 Developmental roles for neuroimmune proteins

The Shatz's laboratory demonstrated that the healthy CNS expresses immune proteins, and that their expression levels are regulated by neural activity. In their study, spontaneous neuronal activity in the fetal cat visual system was blocked using an intracranial infusion of tetrodotoxin (TTX) (Corriveau et al., 1998). A subsequent messenger ribonucleic acid (mRNA) screen was performed to determine genes in the LGN that were differentially expressed in response to this activity blockade. This experiment surprisingly revealed that the MHC class I mRNA was downregulated. Subsequent studies looking at MHC molecules have revealed that neuronal expression of MHC molecules is linked to activity-dependent plasticity (Shatz, 2009). In the mouse dorsal LGN, during normal development, few cells receive input from the ipsilateral eye, while cells that receive input from the contralateral eye are more numerous (Kerschensteiner & Guido, 2017). Studies in the mouse visual cortex have revealed that knocking out MHC class I gene expression results in the incomplete development of connections between the retina and its target cells in the dorsal LGN (Huh et al., 2000). Specifically, the number of ipsilateral projections were high, compared to wild type mice (Huh et al., 2000). This shows that MHC class I molecules are necessary in the refinement of connections in the brain.

Subsequent studies have elucidated the role of other neuroimmune proteins in synapse elimination and refinement. In early development, neurons in the brain form

numerous connections; many more than actually necessary (Vonhoff & Keshishian, 2017). Synapses are subsequently pruned in an activity-dependent manner (Vonhoff & Keshishian, 2017). This process is fundamental to the development and maturation of the nervous system. In addition to MHC molecules, members of the complement cascade also play roles in synapse refinement (Schafer & Stevens, 2010). In one study, retinal ganglion cells (RGC) were cultured either alone or with a feeding layer of immature astrocytes, and a gene profiling approach was used to detect differentially expressed mRNA (Stevens et al., 2007). The researchers found that complement component 1q (C1q) mRNA was upregulated in RGC (i.e. neuronal expression) that were cultured with astrocytes (Stevens et al., 2007). C1q is the activating protein in the classical complement cascade, which is part of our innate immune system (Bohlson et al., 2014). C1q works to detect foreign antigens and also promotes the phagocytosis of apoptotic cells (Bohlson et al., 2014). Stevens et al. (2007) show that C1q is localized to the synapses during the developmental period for synapse pruning, and that using mechanisms similar to their immune response, C1q targets CNS synapses for elimination in the retinogeniculate pathway.

Immune proteins called pentraxins also play roles in synapse elimination and synapse formation (Boulanger, 2009). Increases in the pentraxin neuronal activity-regulated pentraxin (Narp) has been linked to increases in the number of excitatory synapses (Boulanger, 2009; O'Brien et al., 1999). On the other end of the spectrum, pentraxins also play roles in synapse elimination in the visual system of mice, as

knocking out neuronal pentraxins delays the maturation and refinement of glutamatergic synapses (Bjartmar et al., 2006).

Neuroimmune proteins interact and modulate the activity of classic neural proteins involved in the brain's communication activities. MHC class I molecules on neurons for instance, regulate the density of GABAergic and glutamatergic synapses, and the frequency of both miniature excitatory postsynaptic currents (mEPSC) and miniature inhibitory postsynaptic currents (mIPSC) in the visual cortex (Elmer and McAllister, 2012). Due to the differential effects of MHC and its receptors on glutamatergic and GABAergic receptors, the excitatory: inhibitory (E:I) balance is also modulated by MHC expression levels (Glynn et al., 2011).

Moreover, excitatory α-amino-3-hydroxy-5-methyl-4-isoxazolepropionic acid receptors (AMPAR) in the brain are susceptible to regulation by multiple immune proteins. For example, the release of TNFα by glial cells has been implicated in synaptic scaling (Boulanger, 2009). The TNF family of proteins is involved in many physiological functions in the immune system including the swelling and lysis of cells, embryo development, and mediating both acute and chronic inflammation (Chu, 2013). In terms of synaptic plasticity, exogenous TNFα has been shown to increase the number of AMPARs present on the cell surface of hippocampal neurons, this in turn increases the frequency of postsynaptic currents (Beattie et al., 2002). When hippocampal cell cultures were exposed to concentrations of TNFα, a two-fold increase in the number of surface AMPARs was observed (Beattie et al., 2002). To test if the synaptic strength is modified by the addition of TNFα, Beattie et al. (2002) compared the levels of AMPARs detected

in the synapses of both TNFα treated and untreated cultures. They found that the treated cultures had a much higher proportion of detectable AMPAR and that the frequency of mEPSC increased. Applying a TNFα antagonist however resulted in less frequent mEPSC with smaller amplitude and a smaller amount of cell surface AMPARs were detected (Beattie et al., 2002). To determine the endogenous source of TNFα, the researchers applied an astrocyte -condition media to the hippocampal neurons and found an increase in AMPARs and an increase in the mean frequency of mEPSC, similar to that observed when applying exogenous TNFα (Beattie et al., 2002). This suggested that glial cells were the endogenous source of TNFα that facilitated synaptic scaling (Beattie et al., 2002).

The effects of TNFα on AMPARs has been linked to homeostatic synaptic scaling in response to activity (Stellwagen & Malenka, 2006). Mice hippocampal slices from TNFα knockout mice were measured for long-term potentiation (LTP) and long-term depression (LTD) changes and were found to be normal (Stellwagen & Malenka, 2006). The authors interpret these results as evidence that TNFα is not mandatory for rapid, long-term plasticity (Stellwagen & Malenka, 2006). Nonetheless, when cell cultures were treated with TTX in order to block activity, an increase in the levels of surface AMPARs was observed, similar to that when incubated with TNFα (Stellwagen & Malenka, 2006). They found that adding an TNFα antagonist prevented the accumulation of AMPARs to the cell surface upon chronic TTX exposure (Stellwagen & Malenka, 2006). Moreover, the addition of the antagonist prevented the normal increase in mEPSC, and decrease in mIPSC, associated with chronic activity blockade (Stellwagen & Malenka, 2006). Taken

together these results suggests that TNFα is required for activity-dependent homeostatic synaptic scaling. Moreover, Stellwagen and Malenka (2006) found that TNFα released from glial cells were responsible for this synaptic scaling, as knocking out glial TNFα prevented the changes in postsynaptic currents and surface levels of AMPARs. TNFα preferentially increases the expression of AMPARs that lack the GluA2 subunit as the levels of GluA2 did not change upon treatment with TNFα, while the levels of glutamate receptor 1 (GluA1) increased two-fold (Stellwagen et al., 2005). Calcium permeable (i.e. GluA2 lacking AMPARs) have been implicated in the induction of synaptic plasticity (Man, 2011) and strengthened excitatory neocortical synapses (Wright & Vissel, 2012). Thus, the selective trafficking of AMPARs without GluA2, in response to TNFα, indicates increased synaptic plasticity and strength. TNFα can also regulate the number of surface-$GABA_A$ receptors (responsible for fast inhibitory transmission) in hippocampal cells, as exposure to exogenous TNFα resulted in fewer surface $GABA_A$ receptors and reduced inhibitory signalling (Stellwagen et al., 2005). In fact, Stellwagen et al. (2005) observed that the amount of endocytosed $GABA_A$ receptors increased by nearly two-fold upon treatment with TNFα.

In addition to the roles mentioned above, neuroimmune proteins are also implicated in progenitor cell differentiation, neurogenesis and astrogenesis, the recruitment of microglia into the developing brain, and neural cell migration (Bilbo & Schwarz, 2012). Neuroimmune proteins are developmentally regulated and consequently are expressed at varying levels throughout the lifespan to modulate brain development.

1.3 The roles of neuroimmune proteins in disorders and disease

1.3.1 Inflammation in neurodevelopmental disorders

Due to the extensive involvement of neuroimmune proteins in healthy brain development, the abnormal expression of these molecular markers may underlie pathological conditions. For instance, neurodevelopmental disorders such as Rett syndrome and Autism spectrum disorder (ASD) have been linked to elevated levels of inflammation. Rett syndrome is a neurodevelopmental disorder with a known genetic basis as the majority of cases are caused by mutations to the X-linked methyl-CpG binding protein 2 (MECP2) gene (Leonard et al., 2016). The MeCP2 protein is a nuclear protein (Leoncini et al., 2015) that was originally described as a transcription repressor that binds to methylated deoxyribonucleic acid (DNA) (Ip et al., 2018). Today the MeCP2 protein is known to exert both enhancing and inhibiting effects on gene expression and can use micro-RNA to regulate post-transcriptional expression levels of genes (Ip et al., 2018). Cyclin-dependent kinase-like 5 (CDKL5) is a protein involved in mediating the phosphorylation of MeCP2 (Leoncini et al., 2015). Less commonly, mutations in the CDKL5 gene also underlie Rett syndrome (Leoncini et al., 2015). Individuals with this disorder are predominantly female as MECP2 mutations in males usually result in death within 2 years of age (Ip et al., 2018). Individuals initially follow normal patterns of development but then display regression and subsequent impairments of cognitive, motor and verbal abilities (Ip et al., 2018). In addition to these classic features, individuals with Rett syndrome also show impaired visual processing. For example, at the level of the eye, these individuals have refractive errors (Saunders et al.,

1995). Studies of pattern-reversal visual evoked potentials (VEP) in heterozygous MeCP2 mutant mice, as well as 34 females with Rett syndrome, have found a decrease in VEP amplitude at later stages of the disorder (LeBlanc et al., 2015). Moreover, these individuals showed low visual spatial acuity when presented with a high spatial frequency stimulus (LeBlanc et al., 2015). Another study examined the visual acuity of 42 female participants with Rett syndrome, these individuals between 2 ½ years to 47 years old, showed acuity levels similar to unaffected infants 12 to 24 months of age (Tetzchner et al., 1996). Animal studies linking peripheral inflammation and Rett syndrome have found that many immune proteins are differentially expressed in Rett (Derecki et al., 2012). This is also true in humans, for example, an increase in the plasma levels of T helper 2 related cytokines were observed in MECP2-Rett (Leoncini et al., 2015). These cytokines facilitate protective immune responses, and yet contribute to diseases of chronic inflammation such as asthma (Walker & McKenzie, 2017).

In contrast to Rett syndrome, ASD does not have a single, known genetic basis. Rather it is a complex disorder that is linked to a large number of genes and environmental factors (Lord et al., 2020). Features of ASD include restricted interests, repetitive behaviors, and impaired communication skills (Goines & Water, 2010). Abnormalities in cytokine expression, immunoglobulins, dysregulation of inflammation, and altered cellular activation have been reported in individuals with ASD (Goines & Water, 2010). One study found higher levels of chemokine expression in the blood plasma of 80 children with ASD (Ashwood et al., 2011). Furthermore, the increased chemokine levels were accompanied by greater aberrant behavior scores and greater

impairments in visual reception, fine motor skills and expressive language (Ashwood et al., 2011).

1.3.2 Neuroimmune proteins in neuropsychiatric disorders

Similar to ASD, neuropsychiatric disorders are complex and cannot be explained by a single genetic mutation or environmental cause (Garay & McAllister, 2010). Just as neurodevelopmental disorders present visual impairment, individuals with neuropsychiatric disorders also experience visual perception changes. One commonly studied disorder with visual impairments is schizophrenia. This neuropsychiatric disorder is characterized by both positive symptoms such as hallucinations and delusions, as well as negative symptoms, such as impaired speech and cognitive abilities (Patel et al., 2014). In addition, some schizophrenic individuals experience abnormal vision, with impairments in contrast sensitivity, facial emotion recognition, perceptual organization and motion processing (Silverstein et al., 2015). Moreover, impaired synaptic transmission (Frankle et al., 2003) and impaired LTP mechanisms in the human visual cortex have been reported in schizophrenic individuals (Çavuş et al., 2012). These findings suggest that the visual cortex may be affected in neuropsychiatric disorders.

Studies exploring the biological basis for neuropsychiatric disease and mood disorders have drawn parallels between systemic infection and pathological conditions. Both are associated with elevated levels of cytokine production in the brain and have similar behavioural outcomes such as sleep disturbances and loss of appetite (Bilbo & Schwarz, 2012). The similarities between the response to acute illness and to

neuropsychiatric disease provides evidence that psychiatric disorders may be caused by a dysregulation of neuroimmune mechanisms.

Importantly, there is evidence that neuropsychiatric diseases are developmental in origin. In this line of work, studies looking at maternal immune activation (MIA) have linked increased prenatal levels of cytokines to abnormal fetal development (Bilbo & Schwarz, 2012). The most common model used to assess MIA is exposure to immunostimulant polycytidylic acid (polyI:C), a double stranded RNA molecule that mimics viral infection, and amongst other things, results in an increase in cytokine levels (Minakova & Warner, 2018). In mouse models, knockout of the pleiotropic cytokine interleukin-6 (IL-6) prevents behavioural changes seen in the adult offspring of wild type mice (Smith et al., 2007). Specifically, the prepulse inhibition, social interaction, and open-field behavior of adult offspring was comparable to offspring of wild controls (Smith et al., 2007). Importantly, MIA rodent models illustrate that early exposure to immunostimulants have enduring effects into adulthood (Garay et al., 2013; Minakova & Warner, 2018). MIA has neurobiological effects in addition to behavioural ones. Notably there are changes in the number of synapses, excitatory and inhibitory transmission, and structural impairments of presynaptic inputs in adult offspring (Coiro et al., 2015). Furthermore, Winter et al. (2009) show that a single dose of polyI:C is sufficient to induce changes in the baseline levels of neurotransmitters, including an increase in dopamine, and a decrease in serotonin in the adult offspring.

According to the neurodevelopmental theory of schizophrenia the etiology of the disorder is rooted in genetic and environmental factors that impact brain development

before reaching an adult-like state (Fatemi & Folsom, 2009). A two-hit model is sometimes used to explain schizophrenia, where a prenatal genetic or environmental "first hit" disrupts neural circuitry and confers vulnerability to a second hit that occurs later in life during adolescence (Maynard et al., 2001). Importantly, neither insult alone is sufficient to induce schizophrenia (Maynard et al., 2001). In this context, viral infections during prenatal development, including exposure to retroviruses (Karlsson et al., 2001), herpes simplex virus (Buka et al., 2001), and influenza (Mednick et al., 1988) are associated with the emergence of schizophrenia in later life (Fatemi & Folsom, 2009). In fact, the link between maternal influenza virus and schizophrenia in humans is one of the main motivators for using a viral mimic (i.e. polyI:C) to study MIA (Bilbo & Schwarz, 2012). Interestingly, primary sensory areas, such as the V1C, are densely vascularized (Schmid et al., 2019). Consequently, these regions are vulnerable to viral infection during illness when there is severe inflammation, and cytokines can induce damage and increase the BBB permeability (Bilbo & Schwarz, 2012; Yarlagadda et al., 2009).

1.3.3 Neuroimmune proteins in age-related disorders

Finally, inflammation has also been studied in the context of aging and age-related diseases. Aging is the main risk factor for most neurodegenerative disorders like Alzheimer's disease (AD) (Hou et al., 2019). Many molecular mechanisms that underlie the normal aging process also underlie neurodegenerative disorders; this includes inflammation (Franceschi et al., 2018). According to the inflammaging model, aging in the brain is a chronic, progressive increase in proinflammatory state (Franceschi et al., 2000). Immune responses are considered stressors in this model, which argues that over

time the capacity of the brain to deal with such stressors is reduced (Franceschi et al., 2000). Consequently, disorders of the brain can be considered cases of neuroprogression in which accelerated aging is taking place (Franceschi et al., 2018; Perna et al., 2016). For example, synapse loss is linked to AD and studies have found that the release of soluble factors, such as TNFα and IL-6 by microglia induce loss of synapses (Rajendran & Paolicelli, 2018).

In fact, accelerated aging and inflammation have also been linked with neuropsychiatric disorders like schizophrenia. In their review, Nguyen et al. (2017) report that in studies of schizophrenia, markers of synaptic functions are most frequently differentially related to age. Other studies find that illness duration is associated with higher levels of inflammatory markers in serum samples (Ganguli et al., 1994). Overall, as neuroimmune proteins are spatially and temporally regulated, with specific functions during development, abnormal increases in their expression in early development may underlie the deficits and behavioural abnormalities seen in neurological disorders.

1.4 Study Rationale, Objective and Specific Aims

Rationale: Neuroimmune proteins are involved in the plasticity and development of the human visual cortex (Boulanger, 2009). Nonetheless, very little is known about the lifespan expression patterns of neuroimmune proteins in the human brain. Unpacking the developmental trajectories of these molecular mechanisms will facilitate the translation of neuroinflammation, aging, and disease-related findings from animal models to humans. Furthermore, this information will increase our understanding of how the human visual cortex develops and will help identify periods of heightened immune expression that can be targeted for treatment of neurodevelopmental disorders.

Objective: To unpack the neurobiological development of the human V1C by characterizing the lifespan trajectories of neuroimmune proteins.

Specific Aims:

1. Measure the expression of a collection of neuroimmune proteins in the human V1C using a multiplex ELISA and determine the number of trajectory patterns displayed by these proteins using unsupervised hierarchical clustering.
2. Use known classic visual plasticity markers, such as glutamatergic and GABAergic receptor proteins, as guides to identify candidate plasticity processes for neuroimmune proteins.
3. Compare the lifespan profiles of classic plasticity markers and neuroimmune mechanisms to determine whether the profile of human visual cortex development varies between different classes of proteins.

Approach: I take a data-driven approach to unpacking the development of neuroimmune proteins. This study falls in the realm of discovery research (opposed to hypothesis testing) and aims to provide novel insights about neuroimmune expression at different periods of the lifespan. As a data-driven study, a wide range of unsupervised clustering and data mining tools are used in my thesis to unpack the neurobiological development of the visual cortex.

Chapter 2. Characterizing the development of neuroimmune proteins in the human primary visual cortex

2.1 Introduction

Neuroimmune proteins participate in the refinement of cortical circuits during the critical period for experience-dependent plasticity (Boulanger, 2009). Abnormal development of these mechanisms confers risk for neurodevelopmental disorders including neuropsychiatric disease (Bilbo & Schwarz, 2012; Garay & McAllister, 2010). While neuroimmune proteins are involved in numerous developmental processes, very little is known about their lifespan expression patterns. This is especially true for early developmental stages that overlap with the critical periods for cortical plasticity. Unpacking neuroimmune lifespan trajectories in the human cortex will enable translational research and allow us to apply insights from animal models to our understanding of inflammation and aging in the human brain. Moreover, characterizing neuroimmune trajectories will be instrumental in determining therapeutic targets for neurodevelopmental and neuropsychiatric disorders. While many brain regions have been linked to such disorders, the visual cortex is one of the most well-studied models for cortical plasticity (Smith et al., 2019). In our lab, we have previously used the visual cortex as a model to explore classic neurobiological mechanisms (i.e. glutamatergic and GABAergic receptors subunits) during the critical period (Pinto et al., 2010, Siu et al., 2015, Siu et al., 2017). In this study, we use the visual cortex, an exemplary model for neurodevelopment and plasticity, to unpack the lifespan expression patterns of a set of neuroimmune proteins using a data-driven approach.

Although the brain was originally considered to be an immune-privileged site, it is now understood that immune proteins are expressed by the healthy human brain. In

addition to their immunological roles, many classes of immune molecules, including the MHC family of proteins, toll-like receptors, cytokines, and chemokines, contribute to neural processes throughout brain development (Boulanger, 2009). Studies in the cat visual system have shown that the class I MHC molecules are required for activity-dependent formation of synapses (Corriveau et al., 1998). Similarly, the proinflammatory cytokine TNFα regulates synaptic scaling (Stellwagen et al., 2005; Stellwagen & Malenka, 2006), while cell adhesion molecules like down syndrome cell adhesion molecule (Dscam) and neuron cell adhesion molecule (NrCAM) regulate axon guidance, synapse formation and dendritic spine morphology in early development (Boulanger, 2009; Mohan et al., 2018). MD studies in mice provide evidence that ODP is regulated by immune activity, as the period of strengthening of synapses corresponding to the open eye are extended in the absence of immune proteins like PiRB (Garay & McAllister, 2010). Importantly, neuroimmune proteins do not function in isolation, rather they interact with classic plasticity mechanisms like glutamatergic and GABAergic receptor proteins and regulate the E: I balance in the visual cortex (Lin et al., 2008; Stellwagen et al., 2005; Stellwagen & Malenka, 2006). These classic neural mechanisms have well-known roles in regulating the critical period for visual experience-dependent plasticity. Recent studies by Pinto et al. (2010) and Siu et al. (2017) have shown that at the protein level, both glutamatergic receptor subunits and GABAergic receptor subunits have prolonged development in the human V1C and that their trajectories are not completely monotonic. Nonetheless, very little is known about the lifespan trajectories of

neuroimmune proteins that function alongside these excitatory and inhibitory markers in the visual cortex.

Due to the extensive involvement of neuroimmune proteins in brain development, abnormalities associated with these molecular mechanisms have been linked to the emergence of neurodevelopmental disorders (Garay & McAllister, 2010). According to the inflammaging model, aging can be described as an increase in proinflammatory state (Franceschi et al., 2000*).* Consequently, immune proteins are considered to be central players in brain disorders, where early increases in inflammatory state are thought to disturb cortical connectivity and function. Importantly, many brain pathologies, including neurodevelopmental disorders present visual perceptual impairment. Amblyopia, for example, is a neurodevelopmental disorder that stems from abnormal binocular experience during infancy and early childhood (Lunghi et al., 2018). While a clear genetic basis for amblyopia has not been identified, abnormalities in visual experience during the critical period have perceptual deficits including reduced visual acuity and impaired binocular vision (Lunghi et al., 2018). Similarly, neurological disorders with known a genetic basis such as Rhett syndrome also display compromised visual resolution acuity (Tetzchner et al., 1996). Interestingly, abnormalities in vision are also present in more complex, polygenic disorders such as schizophrenia and Bipolar disorder. In fact, slowed binocular rivalry rate has been described as an endophenotype for bipolar disorder (Law et al., 2017). Additionally, thinning of cell layers in the retina have been detected in individuals with bipolar disorder (Garcia-Martin et al., 2019). On the other

hand, a host of literature has connected visual impairments to schizophrenia. Specifically, impaired synaptic transmission (Frankle et al., 2003) and impaired long-term potentiation in the human V1C have been reported in schizophrenic individuals (Çavuş et al., 2012). While many brain regions are impacted in neurodevelopmental and neuropsychiatric disorders, the visual cortex is the region best understood in terms of cortical plasticity (Smith et al., 2019). In this study we will use a data-driven approach to unpack the development of the visual cortex, a well-studied model for neurodevelopment and plasticity. In conjunction with immunoassay methods, unsupervised clustering methods, and data mining tools will be used to profile the development of neuroimmune proteins in the human brain and compare their trajectories to those of classic markers of visual cortical plasticity.

2.2 Materials and Methods

Tissue samples

The study design was approved by the Hamilton Integrated Research Ethics Board. The post-mortem tissue samples employed in this study were obtained from the Brain and Tissue Bank for Developmental Disorders at the University of Maryland (Baltimore, MD, USA). A total of 30 samples covering the lifespan from 20 days to 79 years were used (**Table 1**). Tissue donors had no history of brain disorders and the cause of death was of minimal trauma. Samples were taken from the posterior pole of the left hemisphere and included the superior and inferior portions of the calcarine fissure, corresponding to the human V1C. Sample post-mortem intervals (PMI) are less than 23hrs. Upon collection the samples were sectioned coronally at 1cm intervals, flash frozen, and stored at -80 ℃ at the Brain and Tissue Bank.

Sample preparation

A small piece of tissue (50–100 mg) was cut from the calcarine fissure of each frozen block of human V1 sample, and suspended in a cold homogenization buffer (2X Lysis Buffer RayBiotech - that was diluted to 1X with dH_20 and included a protease inhibitor tablet), and completely homogenized using a high-throughput FastPrep-24 Tissue and Cell Homogenizer (MP Biomedicals). The homogenized sample was then filtered through a pluriStrainer Mini 100µm filter. The filtered homogenate (100µm) was transferred into a chilled cryovial.

Table 1. Cases used in the study.

Age Bin	Age (Years)	Sex	Post-mortem Interval (Hrs)
Neonates	0.05	M	9
Neonates	0.24	F	23
Neonates	0.26	M	12
Neonates	0.27	M	16
Neonates	0.33	M	22
Neonates	0.33	M	23
Infants	0.36	M	16
Infants	0.37	F	11
Infants	0.75	M	10
Young Children	1.34	M	21
Young Children	2.16	F	21
Young Children	2.21	F	11
Young Children	3.34	F	11
Young Children	4.56	M	15
Young Children	4.71	M	17
Older Children	5.39	M	17
Older Children	8.14	F	20
Older Children	8.59	F	20
Older Children	9.13	F	20
Teens	12.45	M	22
Teens	13.27	M	5
Teens	15.22	M	16
Teens	19.21	F	16
Young Adults	22.98	M	4
Young Adults	32.61	M	13
Young Adults	50.43	M	8
Young Adults	53.90	F	5
Older Adults	69.30	M	12
Older Adults	71.91	F	9
Older Adults	79.50	F	14

Measure and equate protein concentrations

Bicinchoninic acid (BCA) assay guidelines (Pierce, Rockford, IL, USA) were used to determine the total protein concentration in each tissue preparation. The samples were compared to a set of protein standards (0.25, 0.5, 1.0, 2.0 mg/ml) (BSA protein standards, Bio-Rad Laboratories). Each of the four protein standards were pipetted into separate wells of a 96-well microplate to establish experimenter pipetting variability. Next, a small amount of each sample (3µl) was added to separate wells. This process was repeated three times for each sample and each protein standard. Next, we added 300µl of the BCA solution to each well and the plate was incubated at 45°C for 45 min to activate the reaction. The colorimetric change was quantified by scanning the plate in the iMark Microplate Absorbance Reader (Bio-Rad Laboratories, Hercules, CA, USA).

The protein concentration of each standard was plotted against the net light absorbance. A line of best fit was used to determine the strength of the relationship between protein concentration and absorbance. If a minimum correlation of 0.99 was not achieved the assay was repeated. The average absorbance of each sample was calculated using all runs. We determined the total protein concentration by dividing the absorbance by the slope of the linear function and adding any linear shift (y-intercept) in the function. The concentration for each protein was then recorded and the vials were stored at -20°C.

Antibody array

We used a multiplexed sandwich enzyme-linked immunosorbent assay (ELISA) (RayBiotech Quantibody Human Cytokine Array 4000, User Manual) based quantitative array platform for detecting and quantifying a set of 200 cytokines, chemokines, growth

factors and other inhibitory factors. Once the tissue samples were prepared, they were outsourced to RayBiotech for protein quantification. To summarize the major steps, a series of glass slides with capture antibodies bound to the surface were used to run the ELISA. An individual glass slide consists of 16 wells; therefore, 16 samples can be processed on a single glass slide simultaneously. Each antibody is arrayed in quadruplicate in an individual well. The glass slide is left to reach room temperature. Next, the sample diluent (100µl) is added to each well and incubated at room temperature for 30 minutes to block slides. Subsequently, 100µl of sample or a standard protein cocktail are added to each well and incubated at room temperature for 1-2 hours. This is followed by incubation with a biotinylated antibody cocktail (i.e. the detection antibody) at room temperature for 1-2 hours. Finally, incubation with Cy3 equivalent dye labeled streptavidin occurs for 1 hour. Fluorescence was detected using a laser scanner equipped with Cy3 wavelength. The RayBiotech QAnalyzer Tool converts the detected fluorescence to concentration values in pg/ml. **Figure 1** outlines the tissue preparation and protein quantification workflow.

Data selection

An upper (MAX) and a lower limit of detection (LOD) were reported for each of the 200 neuroimmune proteins in the ELISA. These values indicate concentrations that can be reliably measured using the array platform. Only proteins with a minimum of 10 measurements between the LOD and MAX values were used in this study (**Figure 2**). Upon applying the quality cut-off 72 neuroimmune proteins were selected.

© Shutterstock
© 2020 MP Biomedicals
© genengnews Vol.34, No.9
© RayBiotech Q4000 User Manual
© 2020 LI-COR Inc.
© Odyssey Scanner User Manual

Sample Preparation Workflow

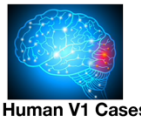

30 Human V1 Cases:
20 days to 79 years

Sample Homogenization:
FastPrep-24

Neuroimmune Proteins

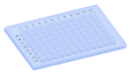

BCA Assay

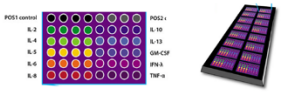

RayBiotech Glass Slide:
Antibodies arrayed in quadruplicate,
16 samples per slide

Incubation Steps:
Sample, Detection Antibody,
Cy3 equivalent dye

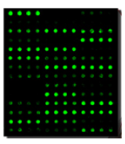

Detect 200 protein concentrations:
Laser scanner + RayBiotech
Q-analyzer software

Classic Plasticity Markers

Synaptoneurosome
Preparation

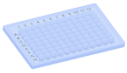

BCA Assay

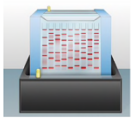

Electrophoresis:
Samples run multiple times

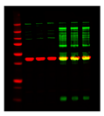

Band Visualization:
Odyssey Scanner

Band Analysis:
Odyssey Scanner +
Densitometry

Figure 1. Tissue sample preparation and protein quantification workflow. Tissue samples were obtained from 30 human V1C cases covering the lifespan from 20 days to 79 years. The samples were homogenized using a FastPrep-24 tissue homogenizer. Synaptoneurosome preparations were performed for the measurement of classic plasticity markers. This step was not carried out when preparing tissue for neuroimmune protein detection. BCA assay was completed to equate the total protein concentration in each of the samples. To measure the neuroimmune proteins, samples were outsourced to RayBiotech for quantification using a multiplex ELISA. Samples were processed on a glass slide and each antibody was arrayed in quadruplicate. Samples were incubated with detection antibodies and a fluorescent dye. Fluorescence was detected using a laser scanner. Computational software (RayBiotech Q-analyzer) was used to convert the fluorescence measurements to concentrations in pg/ml. Western blot techniques were used to measure the expression of classic plasticity markers. Multiple tissue samples from each case were run on a gel. Bands were scanned using an Odyssey scanner and densitometry was used to analyze bands. Expression levels were reported relative to a control sample. Average expression values were computed across all runs.

Note: Images used in the above workflow were obtained from external sources. The FastPrep-24 image was obtained from the MP Biomedicals product page. The RayBiotech glass slide image was adapted from a genengnews *article about the product. The RayBiotech incubation steps and protein detection images were obtained from the Quantibody Human Cytokine Array 4000 User Manual. The band visualization image was obtained from the Li-Cor Inc. webpage. The Odyssey scanner image was obtained from the product user manual. The remaining images are stock images from Shutterstock. All sources are cited with URLs in the reference list.*

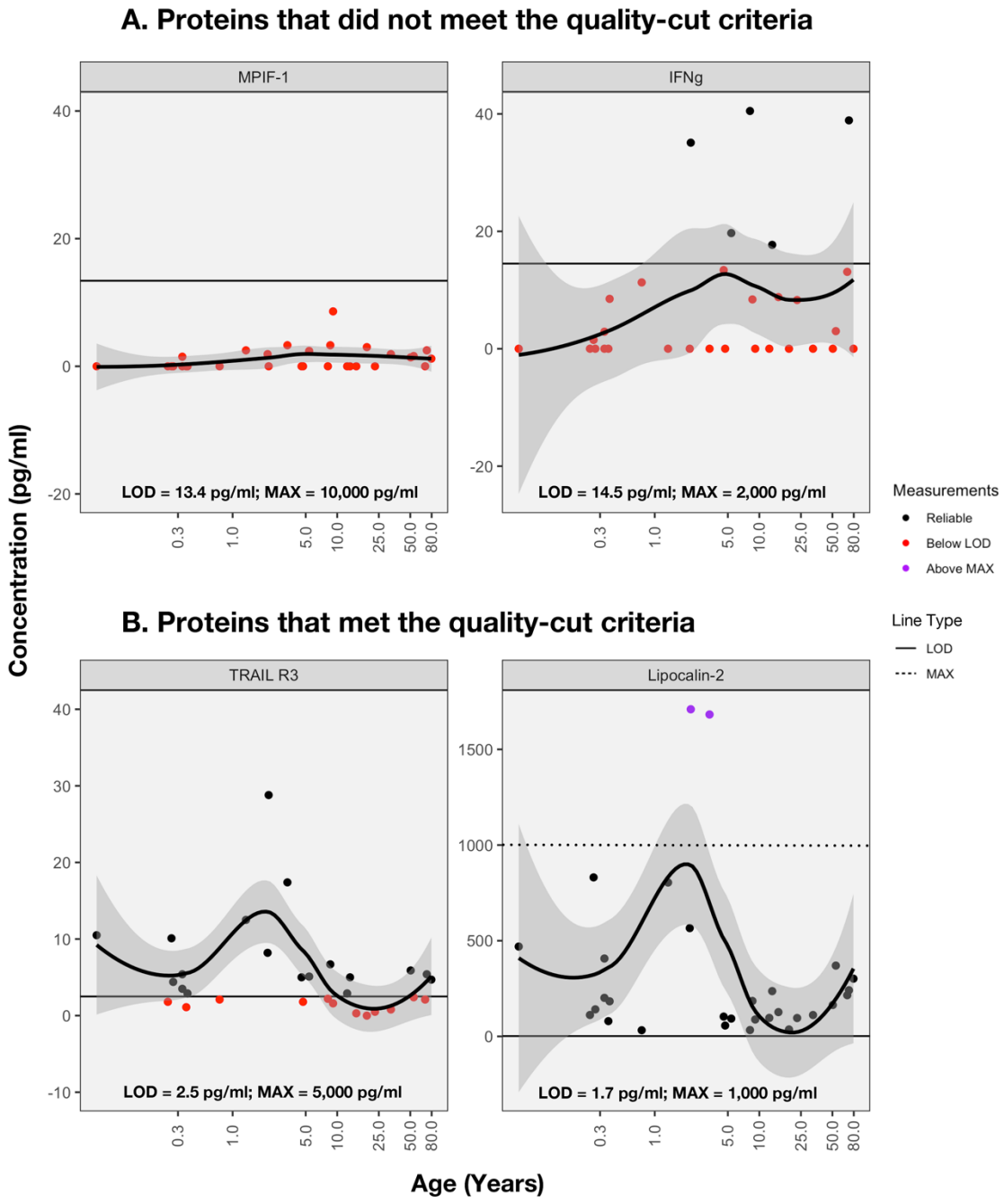
A. Proteins that did not meet the quality-cut criteria
MPIF-1
IFNg
LOD = 13.4 pg/ml; MAX = 10,000 pg/ml
LOD = 14.5 pg/ml; MAX = 2,000 pg/ml
B. Proteins that met the quality-cut criteria
TRAIL R3
Lipocalin-2
LOD = 2.5 pg/ml; MAX = 5,000 pg/ml
LOD = 1.7 pg/ml; MAX = 1,000 pg/ml
Concentration (pg/ml)
Age (Years)
Measurements
Reliable
Below LOD
Above MAX
Line Type
LOD
MAX

Figure 2. Neuroimmune data selection: examples of unreliable protein measurements and selected proteins. Neuroimmune proteins were quantified using a multiplex ELISA which reports an upper and lower limit of detection for each protein. The lower limit is the LOD and is represented by a solid black line. Red dots represent values that fall beneath this threshold. The upper limit is the MAX value and is represented by a dashed line. Purple dots represent values above this threshold. Black dots represent values between these thresholds and indicate reliable expression. Proteins selected for further analyses have a minimum of 10 measurements that fall into this range. **(A)** Examples of proteins that do not meet the quality-cut algorithm: the LOD score for MPIF-1 is 13.4pg/ml, all values fall below this threshold. Similarly, only five measurements corresponding to IFNg fall in the reliable range (14.5 - 2,000 pg/ml). Consequently, these proteins are removed from further analyses. **(B)** Examples of selected proteins: TRAIL R3 contains 18 measurements that fall in the reliable range (2.5 - 5000 pg/ml). Similarly, Lipocalin-2 contains 28 measurements in the reliable range (1.7 - 1000 pg/ml), with two measurements above the MAX threshold. These proteins meet the quality-cut criteria and were selected for further analyses.

Value substitutions

A few of the 72 neuroimmune proteins contained measurements that fall outside of the LOD-MAX range. We defined three rules for substituting these values. First, concentrations greater than the protein MAX were identified and rounded down to the MAX value. In dealing with protein concentrations below the LOD, two scenarios must be considered. First, expression below the LOD may reflect an absence of protein, but it may also indicate an error in the detection of the protein. We rationalized that if the protein was truly not present during a particular stage of the lifespan then neighbouring cases would also have low expression (i.e. below the LOD). Therefore, we organized the data by increasing sample age. Next, we calculated an average concentration using the measurement identified as being less than the LOD and the concentrations of four neighbouring cases (two older, two younger). If the average concentration of all five cases was also less than the LOD, we substituted the measurement with a value of 0.1 pg/ml (the smallest decimal place in our data set). If the average concentration of these five cases was above the LOD, we assigned the protein LOD as the concentration for that sample.

Plasticity marker data

In addition to the neuroimmune data, a set of lifespan expression profiles for 21 classic neural plasticity markers including glutamatergic, GABAergic, structural, and myelin-related proteins were analyzed in this study. This data was published previously by Siu (2017) in her thesis. The proteins were measured in human V1C tissues from the same 30 samples used in quantifying the expression of neuroimmune proteins. However,

these plasticity markers were measured using the semi-quantitative western blot method, as opposed to the quantitative ELISA approach. Consequently, all plasticity marker expression values are reported relative to a control sample consisting of a mixture of all 30 tissue samples. Band visualization was carried out using the Odyssey Scanner (Li-Cor Biosciences) and densitometry was used for band analysis.

Importantly, each synaptic plasticity marker was quantified more than once in a given case and the average expression across all runs was calculated. While most proteins were quantified in a synaptoneurosome tissue preparation - used for the enrichment of synaptic proteins (Murphy et al., 2014; Siu et al., 2018), PSD-95 and gephyrin were measured in both homogenate and synaptoneurosome preparations. Consequently, this data set consists of 23 different lifespan expression profiles for 21 unique proteins. There are no LOD or MAX values associated with the western blots, as a result, all detected values were used. If a particular protein was not measured in a case, leading to missing values in the data set, the values were imputed using the predictive mean matching method to create a full data set. In this method, cases with no missing values are used as the pool from which a value is drawn to fill the missing data (Little, 1988; Rubin, 1986). I ran the imputation algorithm five times for robustness and used the average imputed value to create the final imputed data set. In total, 95 protein trajectories, corresponding to 93 unique proteins, were analyzed in this study (**Table 2**).

Table 2. Protein used in the study: names, short forms and gene symbols.

Protein Target (Short form where applicable)*	Protein Names (in Full)	Gene Symbol
ALCAM	CD166 antigen	ALCAM
Angiogenin	Angiogenin	ANG
Axl	Tyrosine-protein kinase receptor UFO	AXL
bFGF	Basic fibroblast growth factor 2	FGF2
Cathepsin S	Cathepsin S	CTSS
CB1	Cannabinoid receptor 1	CNR1
CD14	Monocyte differentiation antigen CD14	CD14
CEACAM-1	Carcinoembryonic antigen-related cell adhesion molecule 1	CEACAM1
Classic-MBP	Classic Myelin basic protein	MBP
Contactin-2	Contactin-2	CNTN2
CXCL16	C-X-C motif chemokine 16	CXCL16
Drebrin	Drebrin	DBN1
Dtk	Tyrosine-protein kinase receptor TYRO3	TYRO3
EG-VEGF	Prokineticin-1	PROK1
EGF R	Epidermal growth factor receptor	EGFR
ErbB3	Receptor tyrosine-protein kinase erbB-3	ERBB3
Fas	Tumor necrosis factor receptor superfamily member 6	FAS
Fcg RIIBC	Low affinity immunoglobulin gamma Fc region receptor II-b	FCGR2B
Flt-3L	Fms-related tyrosine kinase 3 ligand	FLT3LG
$GABA_A\alpha1$	Gamma-aminobutyric acid receptor subunit alpha-1	GABRA1
$GABA_A\alpha2$	Gamma-aminobutyric acid receptor subunit alpha-2	GABRA2
$GABA_A\alpha3$	Gamma-aminobutyric acid receptor subunit alpha-3	GABRA3
Gad65	Glutamate decarboxylase 2	GAD2
Gad67	Glutamate decarboxylase 1	GAD1
GDF-15	Growth/differentiation factor 15	GDF15
GDNF	Glial cell line-derived neurotrophic factor	GDNF
Gephyrin	Gephyrin	GPHN
GFAP	Glial fibrillary acidic protein	GFAP
GluA2	Glutamate receptor 2	GRIA2

GluN1	Glutamate receptor ionotropic, NMDA 1	GRIN1
GluN2A	Glutamate receptor ionotropic, NMDA 2A	GRIN2A
GluN2B	Glutamate receptor ionotropic, NMDA 2B	GRIN2B
Golli-MBP	Golli Myelin basic protein	MBP
gp130	Glycoprotein 130	IL6ST
HCC-1	C-C motif chemokine 14	CCL14
HGF	Hepatocyte growth factor	HGF
HVEM	Herpes virus entry mediator A / Tumor necrosis factor receptor superfamily member 14	TNFRSF14
I-TAC	C-X-C motif chemokine 11	CXCL11
ICAM-1	Intercellular adhesion molecule 1	ICAM1
ICAM-2	Intercellular adhesion molecule 2	ICAM2
IGFBP-1	Insulin-like growth factor-binding protein 1	IGFBP1
IGFBP-2	Insulin-like growth factor-binding protein 2	IGFBP2
IGFBP-6	Insulin-like growth factor-binding protein 6	IGFBP6
IL-1α	Interleukin-1 alpha	IL1A
IL-1Ra	Interleukin-1 receptor antagonist protein	IL1RN
IL-2 Rβ	Interleukin-2 receptor subunit beta	IL2RB
IL-2 Rg	Cytokine receptor common subunit gamma	IL2RG
IL-4	Interleukin-4	IL4
IL-6R	Interleukin-6 receptor subunit alpha	IL6R
IL-8	Interleukin-8	CXCL8
IL-9	Interleukin-9	IL9
IL-11	Interleukin-11	IL11
IL-13 R1	Interleukin-13 receptor subunit alpha-1	IL13RA1
IL-13 R2	Interleukin-13 receptor subunit alpha-2	IL13RA2
IL-16	Pro-interleukin-16	IL16
Integrin-β3	Integrin beta-3	ITGB3
LIF	Leukemia inhibitory factor	LIF
LIMPII	Lysosome membrane protein 2	SCARB2
Lipocalin-2	Neutrophil gelatinase-associated lipocalin	LCN2
LYVE-1	Lymphatic vessel endothelial hyaluronic acid receptor 1	LYVE1
MCP-1	C-C motif chemokine 2	CCL2
MCSF	Macrophage colony-stimulating factor 1	CSF1
MCSF R	Macrophage colony-stimulating factor 1 receptor	CSF1R

MICA	MHC class I polypeptide-related sequence A	MICA
NAP-2	Platelet basic protein	PPBP
NrCAM	Neuronal cell adhesion molecule	NRCAM
OPN	Osteopontin	SPP1
PARC	C-C motif chemokine 18	CCL18
PDGF-AA	Platelet-derived growth factor subunit A	PDGFA
PDGF-AB	Platelet-derived growth factor subunit AB	PDGFAB
PDGF-BB	Platelet-derived growth factor subunit B	PDGFB
PECAM-1	Platelet endothelial cell adhesion molecule	PECAM1
PF4	Platelet factor 4	PF4
PSD-95	Disks large homolog 4	DLG4
RANTES	C-C motif chemokine 5	CCL5
Resistin	Resistin	RETN
SCF R	Mast/stem cell growth factor receptor Kit	KIT
Siglec-5	Sialic acid-binding Ig-like lectin 5	SIGLEC5
Synapsin	Synapsin-1	SYN1
Synaptophysin	Synaptophysin	SYP
TGFα	Protransforming growth factor alpha	TGFA
TGFβ1	Human TGF-beta 1 cDNA	TGFB1
TIMP-1	Metalloproteinase inhibitor 1	TIMP1
TIMP-2	Metalloproteinase inhibitor 2	TIMP2
TNF RI	Tumor necrosis factor receptor 1 / Tumor necrosis factor receptor superfamily member 1A	TNFRSF1A
TNF RII	Tumor necrosis factor receptor 2 / Tumor necrosis factor receptor superfamily member 1B	TNFRSF1B
TNFα	Tumor necrosis factor	TNF
TRAIL R3	Tumor necrosis factor receptor superfamily member 10C	TNFRSF10C
Trappin-2	Elafin	PI3
Ube3A	Ubiquitin-protein ligase E3A	UBE3A
uPAR	Urokinase plasminogen activator surface receptor	PLAUR
VEGF R1	Vascular endothelial growth factor receptor 1	FLT1
VGAT	Vesicular inhibitory amino acid transporter	SLC32A1

* Due to the variation in protein name lengths, short forms are used to refer to the proteins in the figures found in my thesis. The protein target names for neuroimmune proteins are derived from the RayBiotech multiplex ELISA data sheets. For the classic plasticity markers, short forms commonly found in literature have been used. The protein names (in full), and gene symbol are derived from the RayBiotech multiplex ELISA data sheets and the UniProt database. Additionally, "HOM" will be used in my thesis to differentiate proteins measured in homogenate preparation from those measured in synaptoneurosome preparations.

Age bins

Cases are grouped into age bins: Neonates are < 0.3 years old; Infants are between 0.3 - 1 year old; Young Children are between 1 - 4 years old; Older Children are between 5 - 11 years old; Teens are between 12 - 20 years old; Young Adults are between 21 - 55 years old; and finally Older Adults are > 55 years old.

Visualizing protein lifespan trajectories

Protein concentration values were log2 transformed in order to normalize the distribution of the data. Many proteins are present at concentrations less than 1.0pg/ml, therefore a constant of 1.0 was added to each measurement to prevent obtaining negative values upon log2 normalization. To bring all protein trajectories to the same scale, concentrations were z-scored on a protein basis. Next, a locally estimated scatterplot smoothing (LOESS) curve was fitted to each protein and the 95% confidence interval (CI) was calculated. **Figure 3** outlines the steps taken to transform protein concentrations in pg/ml to z-scored protein levels and protein trajectories.

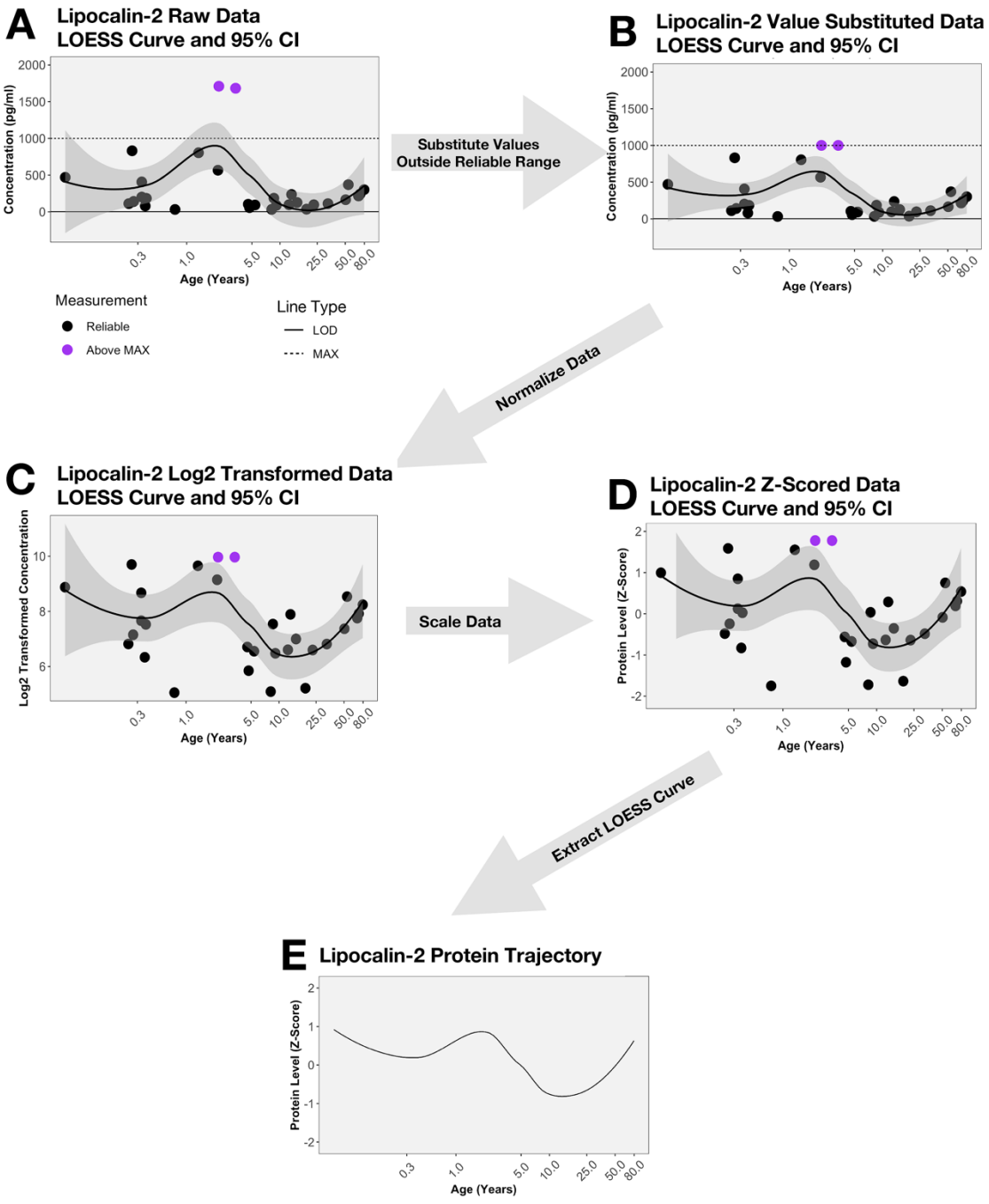
A
Lipocalin-2 Raw Data
LOESS Curve and 95% CI
Concentration (pg/ml)
Age (Years)
Measurement
Reliable
Above MAX
Line Type
LOD
MAX
Substitute Values
Outside Reliable Range
B
Lipocalin-2 Value Substituted Data
LOESS Curve and 95% CI
Normalize Data
C
Lipocalin-2 Log2 Transformed Data
LOESS Curve and 95% CI
Log2 Transformed Concentration
Scale Data
D
Lipocalin-2 Z-Scored Data
LOESS Curve and 95% CI
Protein Level (Z-Score)
Extract LOESS Curve
E
Lipocalin-2 Protein Trajectory

Figure 3. Neuroimmune data preparation workflow. Raw expression values corresponding to the 72 selected neuroimmune proteins were subjected to a series of transformations in preparation of the analyses. Here, Lipocalin-2 is provided as a workflow example. **(A)** Concentration values were determined to lie either within or outside of the reliable detection range. This range is visualized as a dashed line to represent the MAX threshold and a solid line to represent the LOD. Purple dots represent values above the MAX threshold for Lipocalin-2. Black dots represent points in the reliable range. **(B)** Measurements that fall outside of the reliable detection range were substituted. The two Lipocalin-2 measurements above the MAX threshold are rounded down to the MAX value. **(C)** Log2 transformation is used to normalize the data. **(D)** Log2 expression values were z-scored to bring all protein expression values to the same scale. **(E)** LOESS curves applied to the z-score values are used as the protein lifespan trajectory.

Clustering protein trajectories

To determine the number of different lifespan trajectories in the human V1C, protein trajectories were clustered according to their similarity. The optimal number of clusters was determined using calculations of the total within-cluster sum of squares (WSS) for a range of cluster numbers. WSS is a measure of compactness in clustering, where a smaller WSS indicates greater compactness within clusters (Kassambara, 2017). The total WSS was calculated for a range of cluster numbers and plotted as a connected scatterplot. The bend in the plot was used as the optimal number of clusters as it indicates the point where a balance is achieved between forming too few clusters with minimal compactness and forming too many clusters with a small number of constituent proteins in each (Kassambara, 2017).

Next, protein trajectories were grouped together using ward.D2 hierarchical clustering and a dendrogram was produced. Ward.D2 is an agglomerative clustering method in which each object to be clustered is initially considered to be its own cluster (Kassambara, 2017). At each iterative step, the proteins with the smallest Euclidean distance are grouped together. This process is repeated until the desired number of clusters (as determined using the total WSS) is obtained. Approximately unbiased p-values were calculated for the clusters using a multistep-multiscale bootstrap algorithm. Ward.D2 clustering has one main assumption: that the clusters are roughly spherical (Johnson & Wichern, 2007). A common approach to preparing data for clustering is to normalize the data, as we have done. This promotes the formation of spherical clusters and helps prevent elongated clusters in high-dimensional space. Using z-scored values

ensures that clusters are not formed based on magnitude of expression but rather on lifespan patterns, as all protein values will be on the same scale.

We find that ward.D2 is also less likely to form widely unequal clusters, where multiple clusters consist of only one protein and the rest are grouped together into a large cluster. This is actually beneficial in our study as we want to group proteins together by their similarity and do not want to obtain large clusters with minimal compactness.

Protein trajectories were clustered together in three different data sets. First, using the 72 neuroimmune proteins alone, then on the 23 classic plasticity marker trajectories alone, and finally, on a combined data set of all 95 protein trajectories. Clustering results from the neuroimmune data set and the plasticity marker data set were labelled from "A" to "H", or "1" to "5" respectively, based on the order of the ward.D2 dendrogram. Clusters resulting from the combined data set including both neuroimmune and plasticity markers were ordered using the SynGO database [Last Version Update: 2018-07-31], which annotated genes with their known synaptic functions (Koopmans et al., 2019). Clusters were labelled from "I" to "VIII" in order of decreasing number of proteins with synaptic functions as indicated by SynGO. Protein trajectories in a cluster were averaged together to create an average curve for each cluster.

Trajectory similarity measure

Fréchet distances were used as a separate metric to assess the degree of similarity between pairs of trajectories in a cluster and to compare trajectories mapped to different clusters. In calculating Fréchet distances the "sum" method was used, in which multiple distances are computed between all points along the two trajectories. Finally, these

distances are summed to produce a final distance score. Two identical trajectories would obtain a Fréchet distance of zero. Estimation statistics were calculated on the Fréchet distances obtained from proteins in the same cluster to determine if the level of heterogeneity across clusters is comparable. Estimation statistics were also applied to Fréchet distances between proteins of varying clusters to determine whether the degree of similarity within a cluster was greater (as expected) than the similarity between proteins in different clusters.

Gene Ontology enrichment

To determine the enriched molecular functions, cellular components and biological processes associated with groups of proteins in this study, a gene enrichment analysis was performed using gProfiler, an interface for the Gene Ontology (GO) database [gProfiler Version: e100_eg47_p14_7733820; Last GO Version Update: 2020-06-01] (Ashburner et al., 2000; Mi et al., 2019; The Gene Ontology Consortium, 2019). Genes corresponding to the proteins assessed in this study were first determined. The reference list for this analysis consisted of all Homosapien genes in the GO database with at least one annotation. Some annotations made by gProfiler are derived from silico curation methods called “Inferred from Electronic Annotation” (IEA) codes (Raudvere et al., 2019). It is accepted that experimental, computational and manually curated evidence are more reliable when annotating genes than IEA codes (Raudvere et al., 2019). Consequently, IEA based annotations were not used in this analysis. I used the g:SCS algorithm to test for statistical significance (Raudvere et al., 2019). This method was specifically designed for GO terms that exist in a hierarchy and are thus unsuited to

common methods for correcting for multiple comparisons like the false discovery rate (FDR) and Bonferroni correction (Raudvere et al., 2019).

In addition to revealing enriched terms, the GO analysis indicates which proteins in the data set map onto each of the enriched terms. Using this information, we calculated the proportion of proteins in a cluster that map onto a single term. Next, we calculated the overall proportion of proteins in the entire data set that map onto that term. A binomial test was used to determine whether the proportion in a cluster varied from the expected proportion based on the entire data set. Using the formula (1-pvalue) * k we calculated a score to reflect the probability that a term is differentially represented in a cluster. Here, k = -1 if the cluster proportion was less than the overall proportion and k = 1 if the cluster proportion was greater than the overall proportion.

Identify candidate plasticity processes

Next, two parallel approaches were taken to evaluate the similarity between neuroimmune and classic plasticity marker development (**Figure 4**). First, Fréchet distances were computed between these protein trajectories *while maintaining cluster designation*. In other words, neuroimmune clusters were compared to classic plasticity marker clusters. This allowed me to identify groups of proteins that were highly similar to one another. Taking advantage of the fact that classic neural proteins have known expression and function in the visual cortex, I was able to use them as guides to understand neuroimmune function and development.

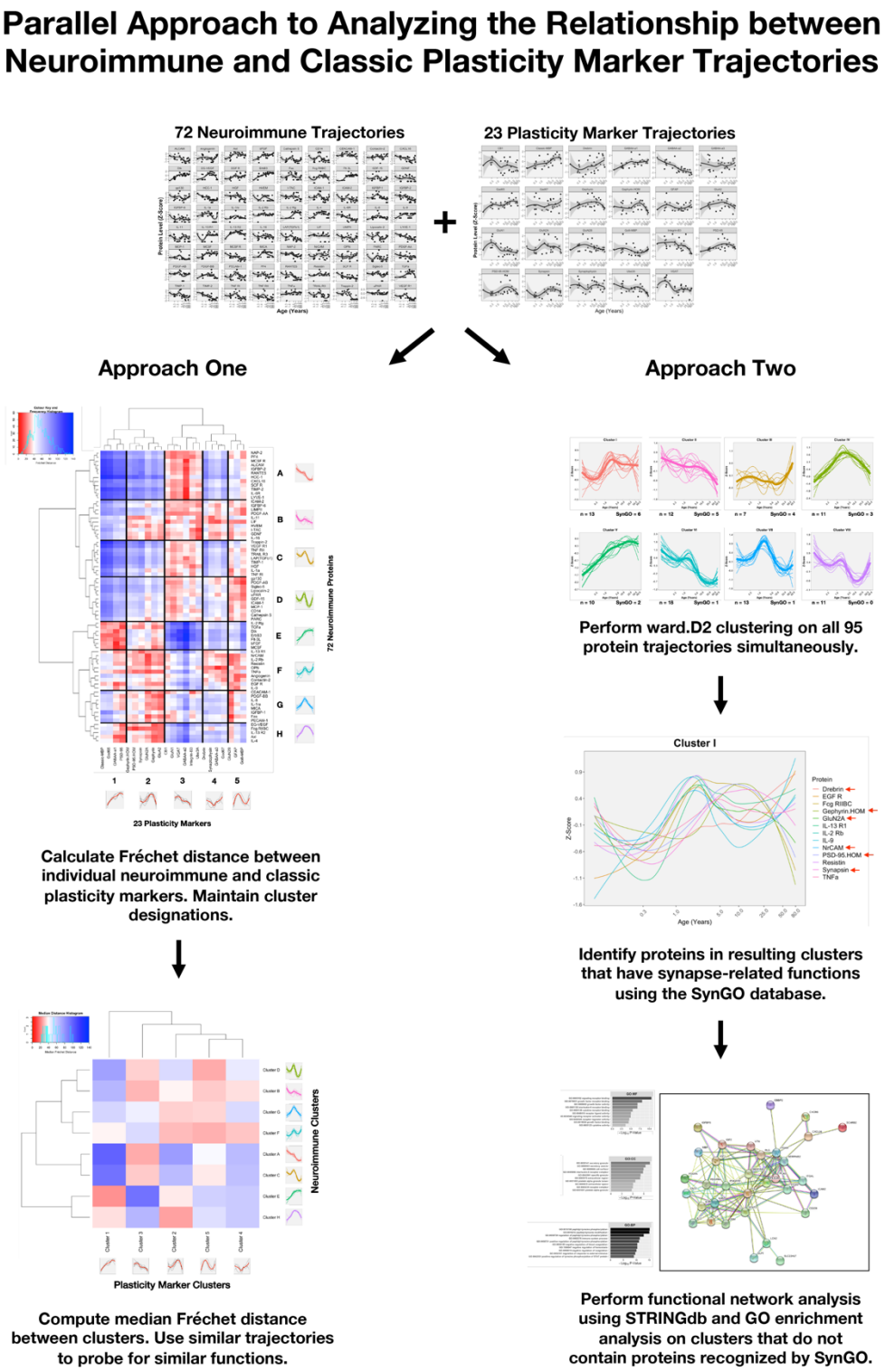
Parallel Approach to Analyzing the Relationship between Neuroimmune and Classic Plasticity Marker Trajectories
72 Neuroimmune Trajectories
23 Plasticity Marker Trajectories
Approach One
Approach Two
72 Neuroimmune Proteins
23 Plasticity Markers
Calculate Fréchet distance between individual neuroimmune and classic plasticity markers. Maintain cluster designations.
Neuroimmune Clusters
Plasticity Marker Clusters
Compute median Fréchet distance between clusters. Use similar trajectories to probe for similar functions.
Perform ward.D2 clustering on all 95 protein trajectories simultaneously.
Cluster I
Identify proteins in resulting clusters that have synapse-related functions using the SynGO database.
Perform functional network analysis using STRINGdb and GO enrichment analysis on clusters that do not contain proteins recognized by SynGO.

Figure 4. Parallel approach to comparing neuroimmune and classic plasticity marker trajectories. To unpack the relationship between neuroimmune protein trajectories and their involvement in brain plasticity and development, a set of classic plasticity markers (ex. glutamatergic and GABAergic receptor subunits) were used as guides to identify candidate neural functions for the immune proteins. Two parallel approaches were taken in this analysis. The first approach involved calculating Fréchet distances between individual neuroimmune and classic plasticity markers. These proteins were organized by their respective cluster designations (i.e. eight neuroimmune clusters and five plasticity marker clusters) to allow the calculation of a median Fréchet distance between the two clustering results. Clusters that have similar trajectories were analyzed further using literature reviews to determine if similar trajectories were indicative of similar functions. Comparatively, the second approach ignores previous cluster designations. Instead all neuroimmune and classic plasticity markers were grouped together and ward.D2 clustering was carried out on the combined data set. Resulting clusters were annotated to highlight proteins with known synapse-related functions using the SynGO database. Neuroimmune proteins that cluster with these synapse-related proteins were identified as candidate plasticity mechanisms in the human V1C. In the event that a cluster contained no synapse-related proteins, STRINGdb was used to create a functional network using those proteins and a GO enrichment analysis was performed on that network to identify the biological functions that the proteins are generally associated with.

The second approach differs from the first in that it ignores previous cluster designations. Instead, I combined the two collections of proteins to create a data set of 95 protein trajectories (i.e. 72 neuroimmune and 23 classic plasticity markers). Next, I performed ward.D2 hierarchical clustering on the combined data set. Using this approach, I identified proteins from both data sets that share similar developmental trajectories. For each of the resulting clusters, I determined the number of proteins that have synapse-related functions. As described previously, the SynGO database was used for this analysis. In the event that a cluster was comprised only of neuroimmune proteins, I performed a functional network analysis on that cluster using the Search Tool for the Retrieval of Interacting proteins database (**STRINGdb**) [Version: 11.0; Last Version Update: 2019-01-19] (Szklarczyk et al., 2018). An integrated cluster network was created by adding predicted functional partners, in increments of one, to the first shell. The enriched molecular functions, cellular components and biological processes for this integrated network were determined using the GO database as described previously. However, as this second GO enrichment analysis was conducted on a functional network comprised of proteins not included in my original data, I did not test for differential representation of terms against the entire data set.

Viral receptors

A list of human viral receptors mediating entry into cells was downloaded from UniProt [Last Version Update: 2020-03] using the keyword "Host cell receptor for virus entry (KW-1183)" (The UniProt Consortium, 2019). The resulting list was used to select for viral receptors in our data set and their LOESS curves were graphed to compare the

lifespan trajectories. The supplemental file "Multimedia component 1" from Qi et al. (2020) was used to annotate these genes with their associated viral families, specific viruses, and to check for links between viral receptors trajectory and their function.

Clustering of samples

Robust and sparse k-means clustering (RSKC) was used to cluster cases together based on their protein expression. RSKC is well suited for clustering our cases as our data is high-dimensional in nature and contains many more variables (i.e. proteins) than observations (i.e. samples) (Kondo et al., 2016). In addition, RSKC is able to simultaneously perform clustering, detect outliers, and determine noise variables (Kondo et al., 2016). Consequently, RSKC assigns protein weights in accordance with the protein's contribution to forming the case clusters (Kondo et al., 2016). Here, proteins with lower weights are treated as noise variables. The age of the cases was not supplied to the clustering algorithm, rather a matrix with solely protein expression values was included. Post-clustering, the median age of each cluster and the 25th and 75th percentile were calculated. Clusters were ordered based on their median age and box plots of the cluster median, 25th and 75th percentiles were graphed to show the progression of cluster ages. This analysis was performed separately on the neuroimmune and plasticity marker data. The clustering results from the neuroimmune RSKC and plasticity marker RSKC were compared using the Jaccard similarity measure. To briefly explain this calculation, let the neuroimmune RSKC results be called "A" and the plasticity marker RSKC results be called "B". Using these results, three values were determined (Ramey, 2012; Wiwie et al., 2015): N1- the number of observation pairs that cluster together in both A and B;

N2- the number of observation pairs that cluster together in A, but not in B; and
N3- the number of observation pairs of cases that cluster together in B, but not A. The Jaccard similarity coefficient of clusters is calculated as: $J = N1 / (N1 + N2 + N3)$.

Jaccard coefficients can also be calculated for each cluster by treating the clusters as individual data sets. For this analysis, each case was given a binary value to indicate its presence (i.e. 1) or absence (i.e. 0) in a cluster (Saiz, 2016). This was done for both neuroimmune and plasticity RSKC results, such that each case had two binary values for each cluster. Then on a cluster-by-cluster basis, I calculated the number of cases that had the same cluster designation in both clustering results (Glen, 2016). I divided this number by the total number of cases assigned to that cluster in either of the clustering results (Glen, 2016).

Finally, a human V1C neuroimmune developmental profile was created using the RSKC weighted expression values for each individual case. To obtain these weighted expression values, the weight assigned by RSKC for each protein was multiplied by each of the protein's expression values. Next, the weighted expression values associated with an individual case were summed. These scores were plotted, and a LOESS curve was fit to the data points to reveal trends.

Coding

The data preparation steps, and all results presented in this study, were performed and generated in the R programming language (R Core Team, 2020) using the integrated development environment RStudio (RStudio Team, 2020).

Contribution to methods

Tissue preparation and protein quantification

The immune protein expression was measured in 30 homogenate tissue samples prepared by Dr. Kathryn Murphy, Dr. Justin Balsor and Steve Mancini. The samples were sent to RayBiotech Inc. for processing on their multiplex ELISA (RayBiotech Quantibody Human Cytokine Array 4000). The company sent back a series of files with expression values (in pg/ml) for 200 neuroimmune proteins in each of the 30 samples.

Classic plasticity markers were measured in a combination of both homogenate and synaptoneurosome samples. These tissue samples were prepared by Dr. Kathryn Murphy, Dr. Kate Williams, Dr. Joshua Pinto, Dr. Simon Beshara, Dr. Caitlin Siu and Dr. Justin Balsor. They also performed western blots to detect protein expression and generated the plasticity marker data set used in the study.

Data selection, value substitution and transformation

Dr. Kathryn Murphy and I defined the rule for selecting neuroimmune proteins to be used in this study from the collection of 200 markers assayed in the multiplex ELISA. The pipeline for processing the neuroimmune expression data was created by myself, Keon Arbabi and Dr. Kathryn Murphy. This includes defining rules for substituting values outside of the reliable detection range. In terms of the classic plasticity marker data set, I imputed the missing values using the predictive mean matching method.

Analyses

I completed the regression analysis by fitting LOESS curves to protein expression in both the neuroimmune and classic neuroplasticity marker data sets. The unsupervised

hierarchical clustering results reported in this thesis were generated by me. All Fréchet distance analyses (both within and between clusters) reported in this thesis were also completed by me. I performed the GO enrichment analysis on the 72 neuroimmune proteins and the SynGO analysis in this study. Furthermore, I conducted the STRINGdb analysis, the RSKC analyses on the tissue samples, as well as the evaluation of RSKC cluster similarity.

Keon Arbabi helped determine which hierarchical clustering method to use in the study. Moreover, a modified version of his code was used to create GO enrichment bar graphs (Figure 12). Dr. Justin Balsor's code for analyzing the RSKC results was modified and used in my thesis. Brendan Kumagai helped apply whiskers to my RSKC age progression box plots (Figure 26, Figure 28), and he created the code for visualizing my RSKC similarity results (Figure 29). Brendan provided the code for conducting binomial tests on my GO enrichment results to compute probability values (Figure 14). He also suggested edits to my data preparation code to make it shorter and more efficient. Dr. Kathryn Murphy helped determine the viral receptors to be analyzed in the study and provided general instruction throughout.

2.3 Results

Lifespan profiles of 72 neuroimmune proteins

To determine how a set of 72 cytokines, chemokines, growth factors and other immune factors develop across the lifespan, we used a multiplex ELISA to measure protein concentration in human V1C tissue samples covering the lifespan from 20 days to 79 years. We z-scored the expression, applied LOESS regression and determined the 95% CI (**Figure 5**). This analysis revealed a dynamic range of developmental patterns. For example, receptor tyrosine-protein kinase erbB-3 (ErbB3), a protein implicated in cancer (Kiavue et al., 2019) and suicide (Mahar et al., 2017), shows increasing protein levels across the lifespan. In contrast, lymphatic vessel endothelial hyaluronic acid receptor 1 (LYVE-1), a regulator of cell growth implicated in multiple sclerosis (MS) (Chaitanya et al., 2013), shows a steady decrease across the lifespan. The majority of developmental patterns, however, cannot be described as a simple increase or decrease in expression. Rather, numerous proteins display undulating patterns, where protein levels follow a series of increases and decreases throughout development. Importantly, these undulating patterns are not all the same. For example, both glycoprotein 130 (gp130) - a pleiotropic cytokine involved in the cardiovascular, nervous and immune systems (White & Stephens, 2011), and glial cell line-derived neurotrophic factor (GDNF) - a protein involved in the development and maintenance of neurons (Airaksinen & Saarma, 2002) show undulating patterns. However, gp130 displays increasing expression into aging, while GDNF expression levels decrease into aging.

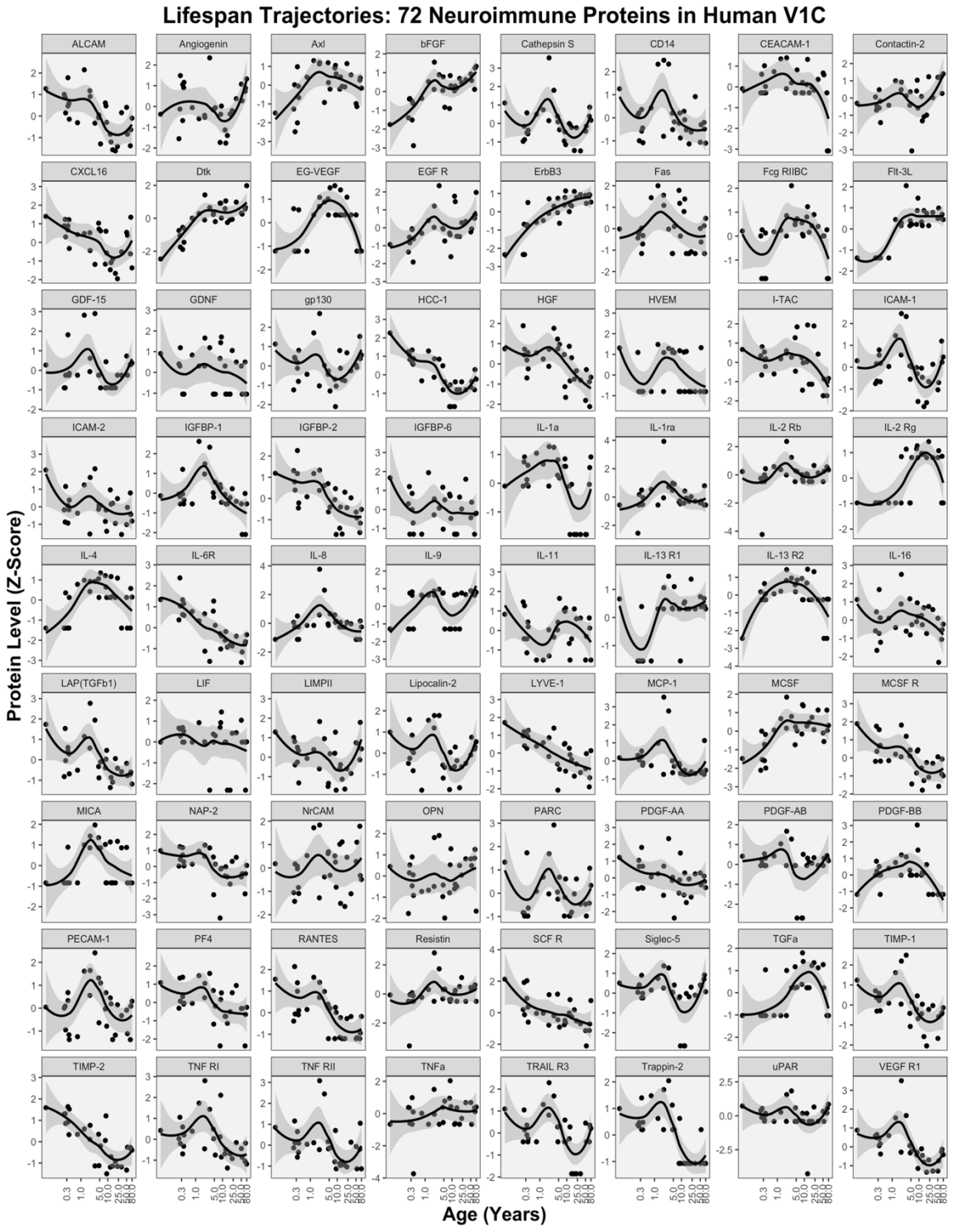
Lifespan Trajectories: 72 Neuroimmune Proteins in Human V1C
Protein Level (Z-Score)
Age (Years)
ALCAM
Angiogenin
Axl
bFGF
Cathepsin S
CD14
CEACAM-1
Contactin-2
CXCL16
Dtk
EG-VEGF
EGF R
ErbB3
Fas
Fcg RIIBC
Flt-3L
GDF-15
GDNF
gp130
HCC-1
HGF
HVEM
I-TAC
ICAM-1
ICAM-2
IGFBP-1
IGFBP-2
IGFBP-6
IL-1a
IL-1ra
IL-2 Rb
IL-2 Rg
IL-4
IL-6R
IL-8
IL-9
IL-11
IL-13 R1
IL-13 R2
IL-16
LAP(TGFb1)
LIF
LIMPII
Lipocalin-2
LYVE-1
MCP-1
MCSF
MCSF R
MICA
NAP-2
NrCAM
OPN
PARC
PDGF-AA
PDGF-AB
PDGF-BB
PECAM-1
PF4
RANTES
Resistin
SCF R
Siglec-5
TGFa
TIMP-1
TIMP-2
TNF RI
TNF RII
TNFa
TRAIL R3
Trappin-2
uPAR
VEGF R1

Figure 5. Lifespan trajectories of 72 neuroimmune proteins in the human V1C. Stamp collection of the lifespan trajectories of a set of 72 cytokines, chemokines, growth factors and other inflammatory factors. Trajectories were determined by fitting LOESS regression curves to the z-scored expression values. Age is plotted on a logarithmic scale. Black dots indicate the z-scored data points. Solid black lines represent the lifespan trajectory as revealed by LOESS regression. Grey bands indicate the 95% CI.

On the other hand, tissue inhibitor matrix metalloproteinase 1 (TIMP-1) and tumor necrosis factor receptor 2 (TNF RII) show very similar trajectories. TIMP-1 is a metalloproteinase inhibitor with important roles in tumor invasion, development of metastatic disease, cell proliferation, and anti-apoptotic function (Song et al., 2016). TNF RII is a TNFα receptor that has modulatory roles in immune function and is thought to be involved in CNS inflammatory diseases like autoimmune encephalomyelitis (Yang et al., 2018). Both these proteins start with high expression during the beginning of the neonatal period at ~0.05 years and decrease in expression throughout infancy (0.33 – 1 year old), with a subsequent local peak in expression in early childhood at ~ 2 years of age. Both proteins switch to declining patterns throughout late childhood (5 - 11 years), adolescence (12 - 20 years) and into early adulthood (23 - 28 years), at which point their expression levels increase once again into aging. In summary, neuroimmune proteins show a dynamic range of undulating expression patterns in the human V1C. Importantly, we do not find one common trajectory or 72 unique trajectories for these proteins. Instead, there are a number of common patterns shared by this collection of biological mechanisms.

Grouping neuroimmune proteins and identifying number of trajectory types

To study the number of different trajectories displayed by the 72 neuroimmune proteins in the human V1C, we performed ward.D2 hierarchical clustering on the protein trajectories. We determined the optimal number of clusters by calculating the total within-sum of squares for a range of different cluster numbers. Next, we plotted these values as a scatter plot and identified that the bend in the resulting curve occurs at 8 ± 2

clusters, which represents the optimal number of clusters (**Figure 6**). Ward.D2 hierarchical clustering of the 72 neuroimmune proteins revealed 8 clusters of varying size (**Figure 7**). An approximately unbiased p-value (AU) was calculated as a preliminary step to indicate cluster validity (Cluster A: n = 12, AU = 0.32; Cluster B: n = 10, AU = 0.43; Cluster C: n = 9, AU = 0.72; Cluster D: n = 11, AU = 0.85; Cluster E: n = 7, AU = 0.65; Cluster F: n= 10, AU = 0.73, Cluster G: n = 8, AU = 0.80; Cluster H: n = 5, AU = 0.73). The smallest cluster contained five proteins, while the largest cluster contained 12 proteins. Taking protein trajectories that group together, we calculated an average curve to represent each cluster's lifespan profile. We did not find any clusters that were strictly linear, rather all clusters display a non-linear, undulating pattern across the lifespan. Descriptively, the clusters that most closely resemble a linear pattern are Cluster A and Cluster E. While Cluster A is generally decreasing across the lifespan, there is a small increase in protein levels that begins around 28 years of age and continues into aging. In contrast, Cluster E generally increases across the lifespan, but protein levels begin to plateau in early childhood through adolescence before decreasing slightly into aging. Overall, neuroimmune lifespan profiles seem to follow numerous non-linear patterns.

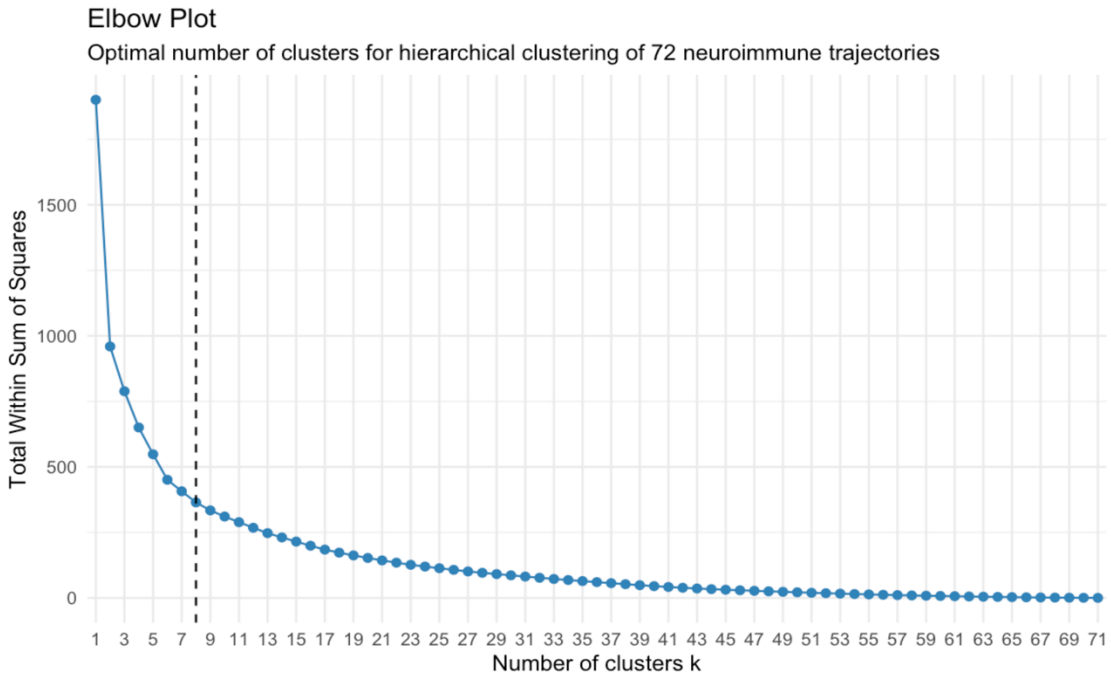
Elbow Plot
Optimal number of clusters for hierarchical clustering of 72 neuroimmune trajectories
Total Within Sum of Squares
1500
1000
500
0
1 3 5 7 9 11 13 15 17 19 21 23 25 27 29 31 33 35 37 39 41 43 45 47 49 51 53 55 57 59 61 63 65 67 69 71
Number of clusters k

Figure 6. Total Within Sum of Square calculations for determining the optimal number of neuroimmune protein trajectory clusters. WSS values (a measure of the compactness of clusters) corresponding to the hierarchical clustering of 72 neuroimmune lifespan trajectories. A range of cluster numbers were assessed from one to 71. The x-axis indicates the number of clusters and the y-axis indicates the total WSS for that cluster number. The WSS values decrease as the number of clusters increases. The bend in the curve indicates the point at which a balance is reached between minimizing the WSS and creating too many clusters. Here, the elbow method for determining the optimal number of clusters reveals a bend at 8 ± 2 clusters.

A. Ward.D2 Hierarchical Clustering Dendrogram: 72 Neuroimmune Proteins

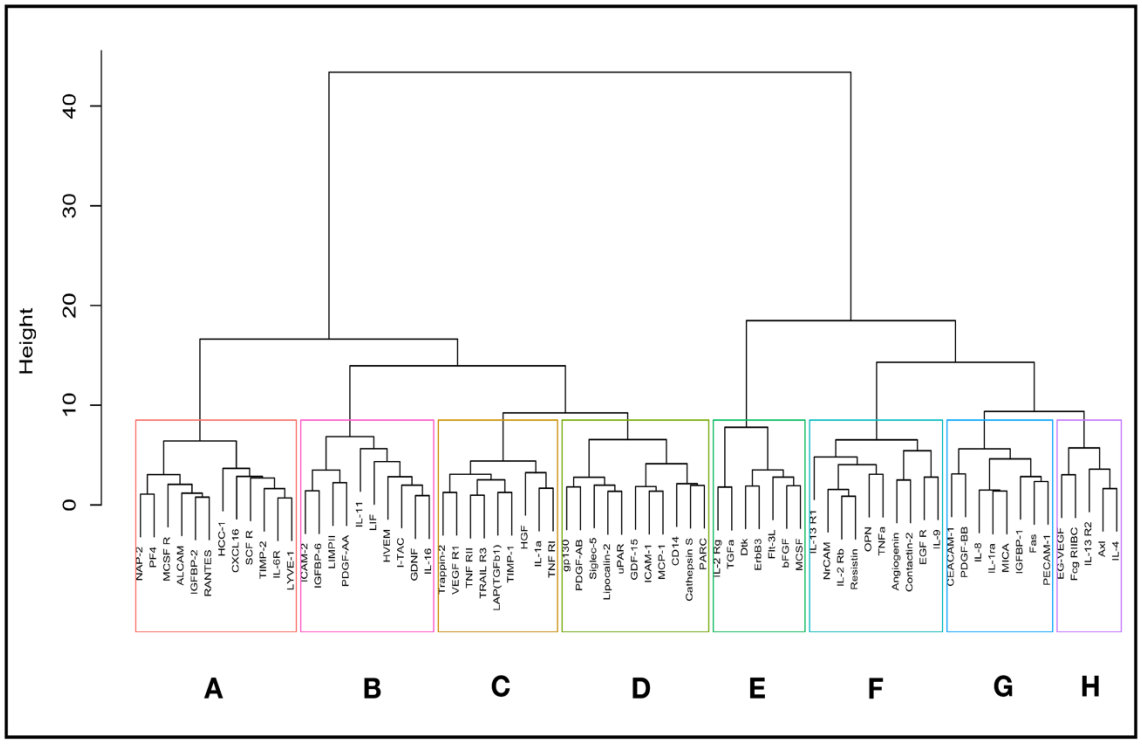

B. Ward.D2 Hierarchical Clustering: Average LOESS Curves

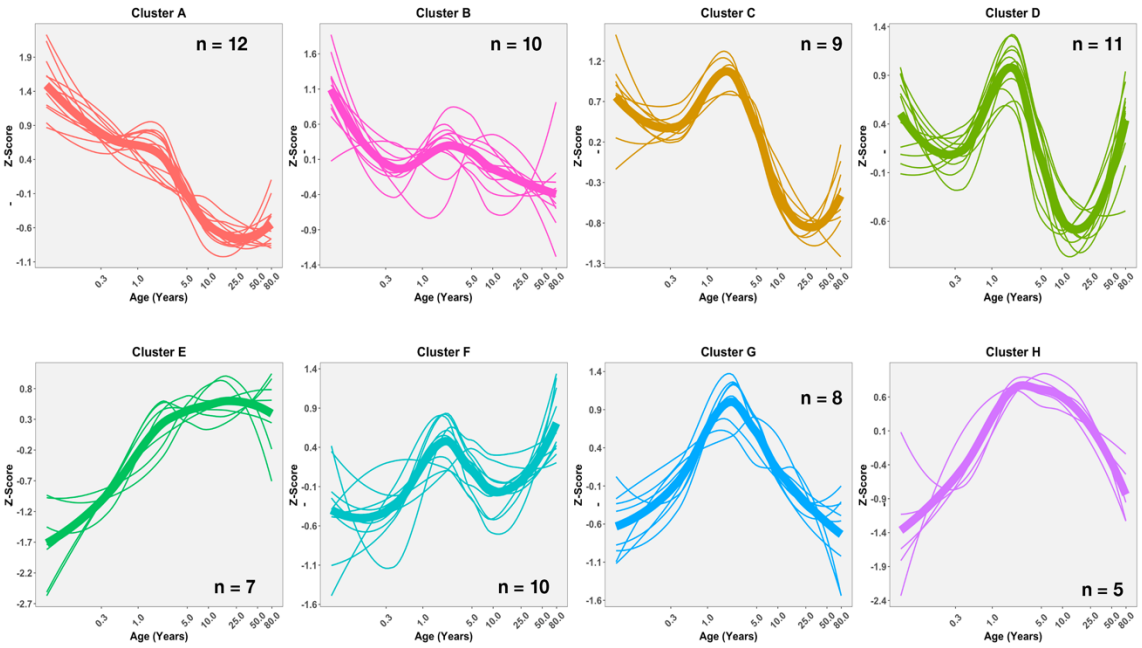

Figure 7. Ward. D2 hierarchical clustering of neuroimmune protein trajectories. Hierarchical relationships and cluster designations for 72 neuroimmune proteins. **(A)** Hierarchical clustering dendrogram, in which the height is a reflection of the proximity between the trajectories, with smaller values indicating a closer relationship. Here, the eight clusters are identified by coloured boxes. The dendrogram is cut at a height of ~ 9 and the clusters are labelled “A” through “H” in order from left to right on the dendrogram. **(B)** Average curves for the eight identified clusters. Age is plotted on a logarithmic scale, and protein levels (z-score) are shown. Thick lines represent the average curves, while the thin lines indicate individual protein trajectories. The number of proteins (n) in each cluster are indicated on the plots, this number ranges from 5 to 12.

Evaluate within-cluster and between cluster trajectory similarities

We evaluated the within-cluster similarities by calculating the pairwise Fréchet distances between the protein trajectories in a cluster (**Figure 8**). A lower Fréchet score indicates a greater level of similarity. Across all eight clusters, 306 intracluster Fréchet distances were calculated with an overall median distance of ~17.3. Median (Mdn) values were also assessed for each cluster (Cluster A Mdn = 13.1; Cluster B Mdn = 20.2; Cluster C Mdn = 14.9; Cluster D Mdn = 17.1; Cluster E Mdn = 17.4; Cluster F Mdn = 21.9; Cluster G Mdn = 17.9; Cluster H Mdn = 17.5). Next, we subtracted the overall median distance from each cluster median to get a median difference score (Δ). For each comparison we used estimation statistics to produce a bootstrap CI for the difference score. If the bootstrapped CI overlap or are really close to zero, the overall median and cluster medians can be considered similar. The analysis revealed however, that only Cluster C: Δ= -2.4 [95CI -5.5, +0.1]; Cluster D: -0.2 [95CI -2.8, +2.0]; Cluster E: +0.2 [95CI -4.4, +8.3]; Cluster G: +0.6, [95CI -1.9, +3.3]; and Cluster H: +0.3 [95CI -4.5, +5.3]; have comparable levels of intracluster variance. Comparatively, Cluster A: -4.2, [95CI -6.2, -2.4] has an intracluster median that is well below the overall median, indicating that it is more compact than the other clusters. In contrast, Cluster B: +2.9 [95CI +1.1, +7.1] and Cluster F: +4.6 [95CI +2.3, +7.3] have median Fréchet scores that are greater than the overall median and the bootstrap CIs do not overlap with zero. Therefore, according to the Fréchet distance metric, the proteins in clusters B and F are more heterogeneous compared to the other clusters.

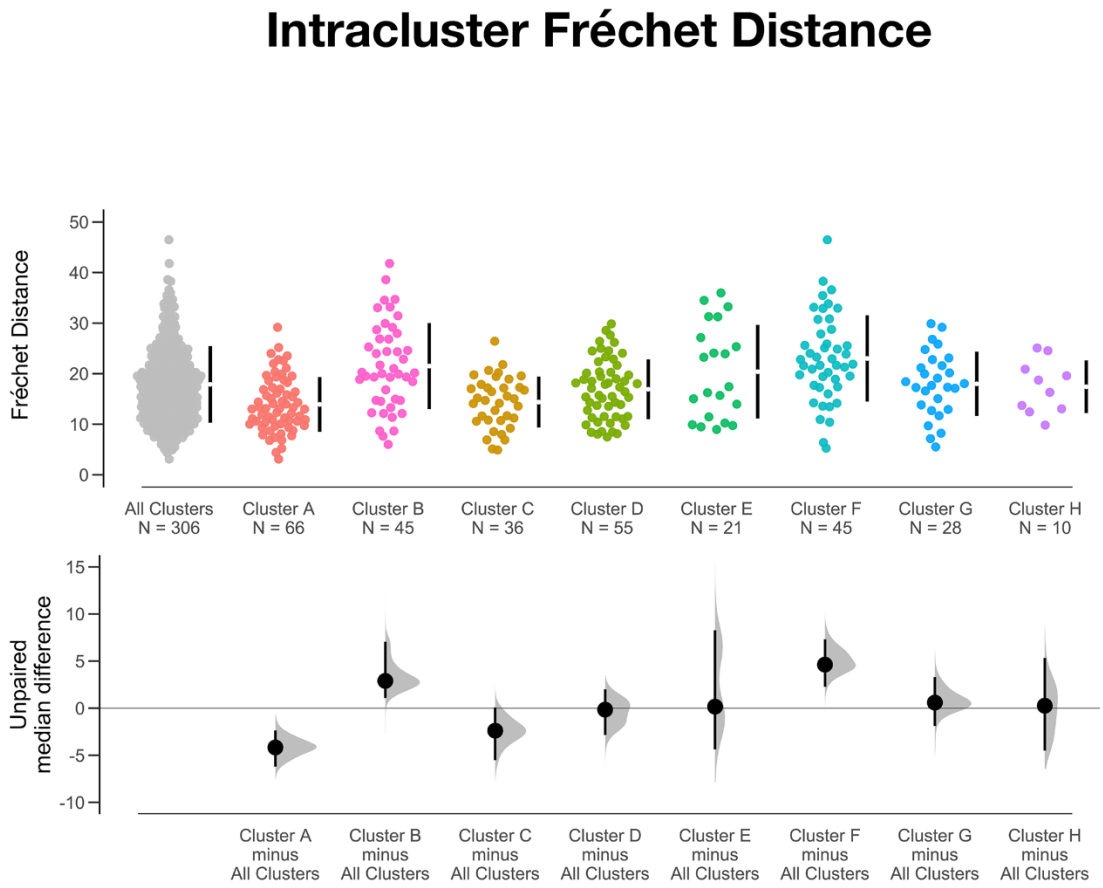
Intracluster Fréchet Distance
Fréchet Distance
50
40
30
20
10
0
All Clusters N = 306
Cluster A N = 66
Cluster B N = 45
Cluster C N = 36
Cluster D N = 55
Cluster E N = 21
Cluster F N = 45
Cluster G N = 28
Cluster H N = 10
Unpaired median difference
15
10
5
0
-5
-10
Cluster A minus All Clusters
Cluster B minus All Clusters
Cluster C minus All Clusters
Cluster D minus All Clusters
Cluster E minus All Clusters
Cluster F minus All Clusters
Cluster G minus All Clusters
Cluster H minus All Clusters

Figure 8. Fréchet distance metric for measuring intracluster similarity. Pairwise Fréchet distances between proteins trajectories in the same cluster. The swarm plot indicates the individual pairwise Fréchet distances. Here a total of nine categories are represented. The first category is the collection of all pairwise intracluster Fréchet distances. Each subsequent category corresponds to one of the eight clusters. Estimation statistics were used to determine if the cluster medians varied significantly from the overall median. Cluster A: -4.2, [95CI -6.2, -2.4] has a lower median Fréchet distance than the overall median, suggesting that it is a more compact cluster. The Cluster B: +2.9 [95CI +1.1, +7.1] and Cluster F: +4.6 [95CI +2.3, +7.3] medians are greater than the overall median Fréchet distance, revealing that these clusters are slightly more heterogenous, and that the proteins in these clusters share a lower degree of similarity when compared to other clusters. The remaining clusters all have comparable intracluster similarities as indicated by the 95% CI for unpaired median difference scores overlapping zero.

Fréchet distances were also used to compare the degree of similarity between clusters. Pairwise Fréchet distances were computed between all 72 proteins and the results were visualized as a heatmap (**Figure 9**). The median Fréchet distance protein *excluding self-comparisons* is ~38.9. The median Fréchet distance *excluding all intracluster comparisons* is ~42.9, which is more than double the magnitude obtained when analyzing intracluster distances. Consequently, it appears that the proteins within a cluster have greater similarity to each other than proteins grouped in other clusters. To assess this, we used estimation statistics to examine whether the intracluster median is less than the intercluster median. The median difference score: -25.6, [95CI -27.4, -23.9] reveals that the intracluster median is smaller than the intercluster median (**Figure 10**).

Next, we completed pairwise comparisons between protein in the same cluster and proteins in different clusters to determine how similar the clusters are to one another (**Figure 11**). We found that comparatively, the first four clusters are similar to each other, and that they vary from the last four clusters. This is especially evident when comparing Cluster A's intracluster distances with the Fréchet distances between Cluster A proteins and proteins in the next three clusters. While none of the 95% CI intervals overlap with zero, the median difference scores are all less than 23 (Cluster B: +20.8 [95CI +16.9, +23.4]; Cluster C: +11.5 [95CI +9.0, +15.2]; Cluster D: +22.2 [95CI +20.2, +24.8]). On the other hand, median difference scores between Cluster A and the last four clusters are all above 47 (Cluster E: +96.7 [95CI +92.5, +100.0]; Cluster F: +54.3 [95CI +51.5, +57.6]; Cluster G: +47.5 [95CI +42.9, +50.3]; Cluster H: +71.8 [95CI +67.5, +76.3]). This shows that while none of the clusters are completely similar to each other, the first

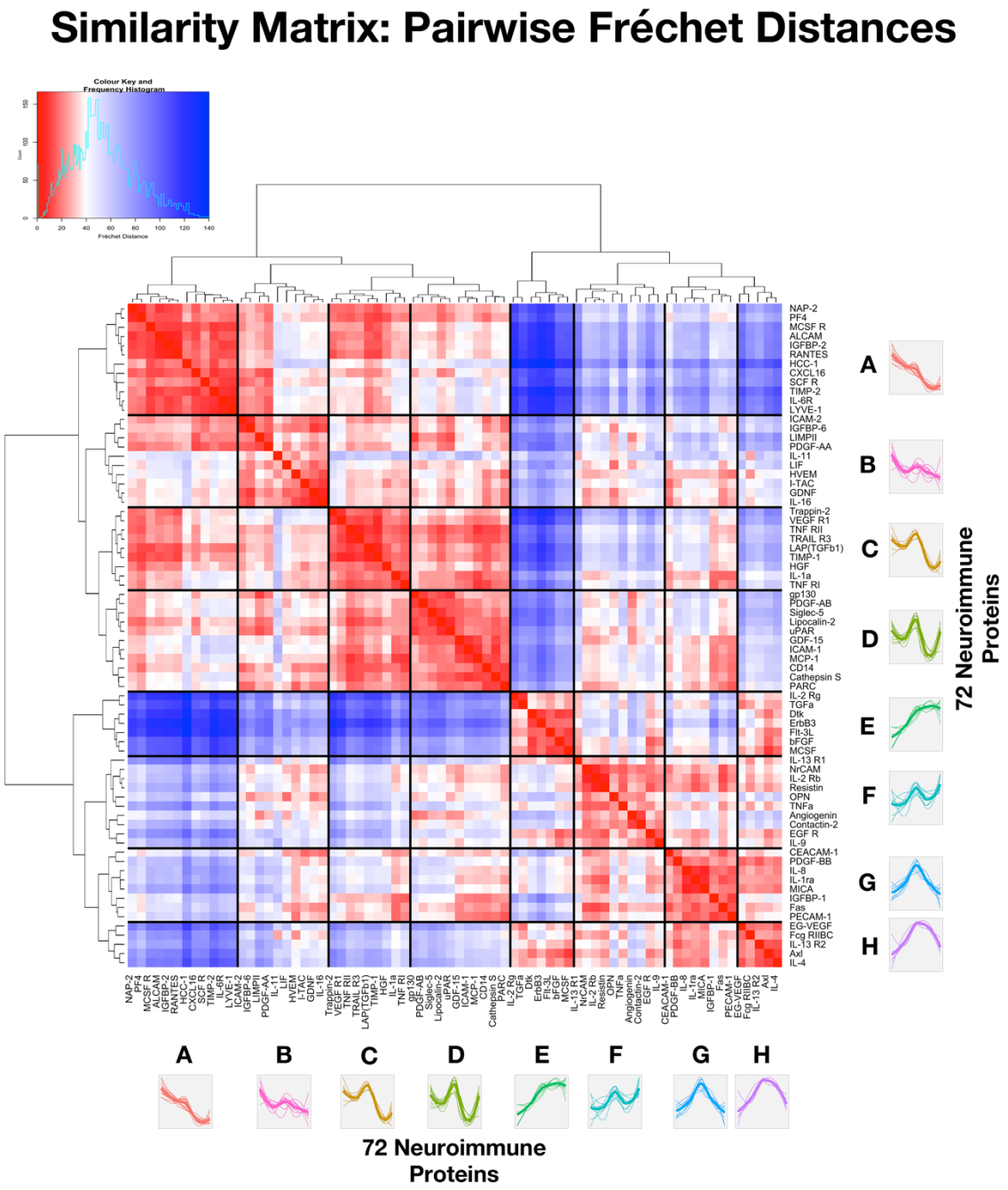
Similarity Matrix: Pairwise Fréchet Distances
Colour Key and Frequency Histogram
Count
Fréchet Distance
NAP-2
PF4
MCSF R
ALCAM
IGFBP-2
RANTES
HCC-1
CXCL16
SCF R
TIMP-2
IL-6R
LYVE-1
ICAM-2
IGFBP-6
LIMPII
PDGF-AA
IL-11
LIF
HVEM
I-TAC
GDNF
IL-16
Trappin-2
VEGF R1
TNF RII
TRAIL R3
LAP(TGFb1)
TIMP-1
HGF
IL-1a
TNF RI
gp130
PDGF-AB
Siglec-5
Lipocalin-2
uPAR
GDF-15
ICAM-1
MCP-1
CD14
Cathepsin S
PARC
IL-2 Rg
TGFa
Dtk
ErbB3
Flt-3L
bFGF
MCSF
IL-13 R1
NrCAM
IL-2 Rb
Resistin
OPN
TNFa
Angiogenin
Contactin-2
EGF R
IL-9
CEACAM-1
PDGF-BB
IL-8
IL-1ra
MICA
IGFBP-1
Fas
PECAM-1
EG-VEGF
Fcg RIIBC
IL-13 R2
Axl
IL-4
A
B
C
D
E
F
G
H
72 Neuroimmune Proteins
72 Neuroimmune Proteins

Figure 9. Pairwise Fréchet distance matrix for measuring similarity between clusters. Pairwise Fréchet distances between all combinations of the 72 neuroimmune trajectories. A total of 5184 distances have been calculated and the proteins are organized according to their ward.D2 cluster designation. The clusters and their average trajectories have been labelled on the figure. The Fréchet distances range from 8.1 to 134.6, *excluding intracluster comparisons,* and the median Fréchet distance *excluding intracluster comparisons* is ~42.9. Red cells correspond to smaller Fréchet distances and indicate a greater degree of similarity, while larger Fréchet distances are coloured blue and indicate lower levels of similarity. As both intra- and intercluster Fréchet distances are plotted on this heatmap, the white cells represent values between 38-39, which is the median Fréchet distance when considering the pool of both intracluster and intercluster Fréchet distances (without protein self-comparisons). Overall, a high degree of similarity can be seen within the clusters. Additionally, the first four clusters seem to be closely related to each other, while the last four clusters are closely related to one another.

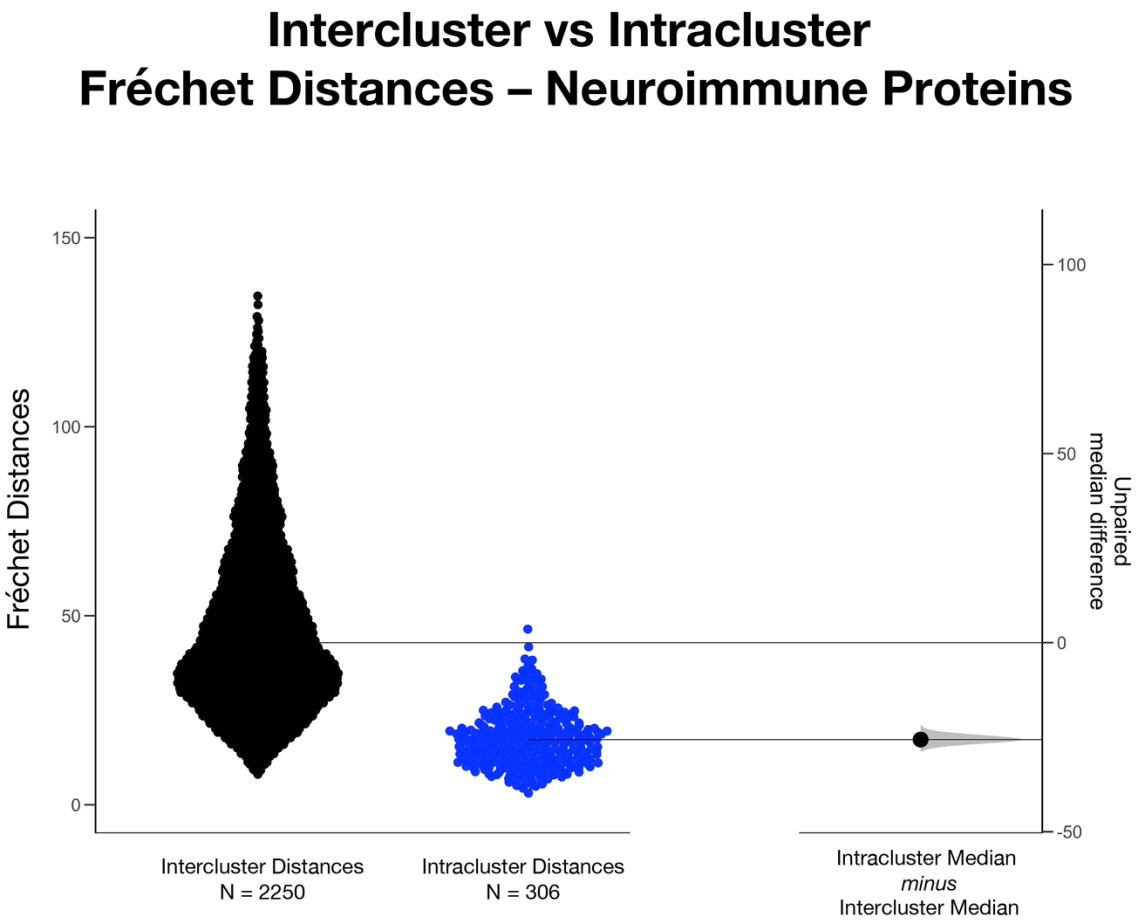
Intercluster vs Intracluster
Fréchet Distances – Neuroimmune Proteins
Fréchet Distances
150
100
50
0
100
50
0
-50
Unpaired
median difference
Intercluster Distances
N = 2250
Intracluster Distances
N = 306
Intracluster Median
minus
Intercluster Median

Figure 10. Median difference between intercluster and intracluster Fréchet distances. The black dots in the swarm plot indicate the Fréchet distances between the 72 neuroimmune proteins in varying clusters (i.e. intercluster distances). The Fréchet distances between proteins in the same cluster, with the exception of protein self-comparisons, is indicated by the collection of blue dots. The Fréchet distances themselves can be seen on the y-axis on the left. The median intercluster Fréchet distance is 42.9, while the median intercluster distance is 17.3. The difference between the median value of these two sets of Fréchet distances is plotted on the second y-axis on the right. Estimation statistics was used to compute a bootstrap interval for the difference (-25.6, [95CI -27.4, -23.9]).

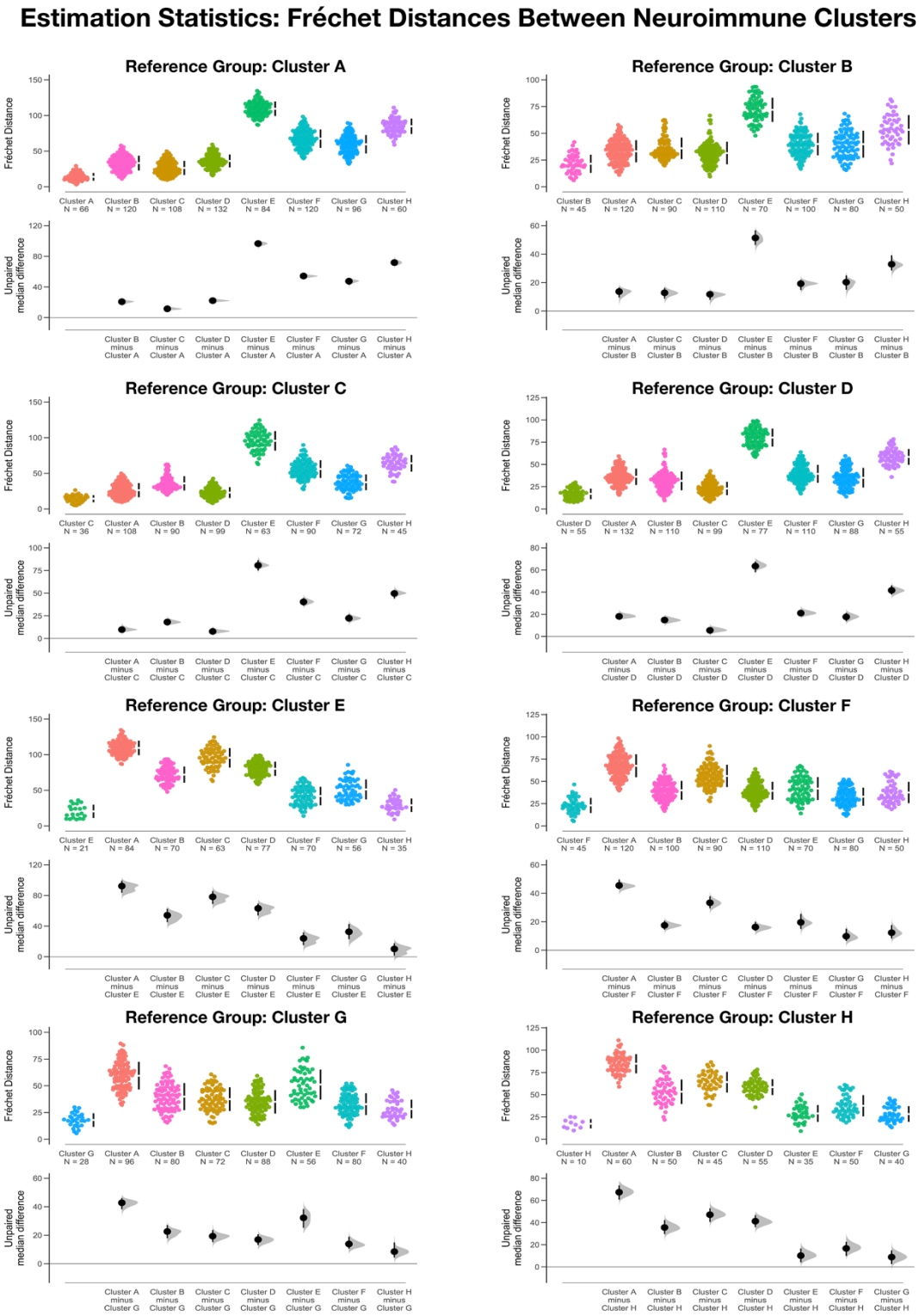
Estimation Statistics: Fréchet Distances Between Neuroimmune Clusters
Reference Group: Cluster A
Reference Group: Cluster B
Reference Group: Cluster C
Reference Group: Cluster D
Reference Group: Cluster E
Reference Group: Cluster F
Reference Group: Cluster G
Reference Group: Cluster H
Fréchet Distance
Unpaired median difference

Figure 11. Estimation statistics for measuring trajectory similarity between clusters. Swarm plots of intracluster Fréchet scores and pairwise Fréchet distances between proteins in different clusters. This stamp collection of estimation plots includes eight graphs, corresponding to the eight clusters. In an individual plot the first category corresponds to the reference group: Fréchet distances between proteins in the same cluster. Subsequent categories indicate the Fréchet distances between proteins in the reference cluster and each of the seven other clusters (i.e. test clusters). An unpaired median difference score (test cluster median *minus* reference cluster median) is indicated along with bootstrapped CIs for each median difference score. Here we find that all 56 bootstrapped 95% CIs lie outside the zero range, indicating that no two clusters have great similarity between their trajectory patterns.

four clusters share a greater degree of similarity and display different patterns from the last four clusters.

The last four clusters also share a greater degree of similarity with one another. This is represented by the median difference between the Cluster H intracluster Fréchet scores and the distances between Cluster H proteins and all other clusters. The median difference scores between Cluster H and the first four clusters is above 35 (Cluster A: +67.4, [95CI +60.8, +73.5]; Cluster B: +35.5 [95CI +29.6, +42.1]; Cluster C: + 47.1 [95CI +40.6, +52.9]; Cluster D: +41.2 [95CI +35.6, +46.7]). In contrast, the difference scores between Cluster H and the last three clusters in less than 17 (Cluster E: +10.1, [95CI +4.1, +16.6]; Cluster F: +16.7 [95CI +9.9, +22.6]; Cluster G: +8.8 [95CI +2.6, +14.9]).

As expected, Cluster A and Cluster E show the greatest variation from each other based on their opposing lifespan patterns. The median intracluster Fréchet distances corresponding to Cluster A is ~ 13.1. In contrast, the median distance between Cluster A's proteins and the proteins in Cluster E is ~ 109.8. Consequently, there is a difference of ~ 96.7 between these median scores. In comparison, the maximum difference when comparing the intracluster Fréchet distances is ~ 8.8. Therefore, the maximum differences of intra- and intercluster Fréchet scores vary by an order of magnitude. Furthermore, as seen in Figure 11, each cluster's median intracluster Fréchet distance lies outside the bootstrapped CI for comparisons with other clusters. These results suggest that ward.D2 clustering successfully groups together proteins with similar trajectories and places protein trajectories with lower levels of similarity into different groups.

Functional enrichment analysis for neuroimmune proteins

Next, a GO enrichment analysis was performed to determine the enriched molecular functions, cellular components, and biological processes associated with the 72 neuroimmune proteins. One of the proteins in our data set, platelet derived growth factor (PDGF)-AB, is a heterodimer and is not encoded by a single gene. Consequently, it was not recognized by the enrichment platform and was removed from this analysis (n = 71). Nonetheless, the two PDGF-AB subunits: PDGF-A and PDGF-B, are also part of our collection of 72 neuroimmune proteins (as homodimers) and these were included in the GO analysis. We performed gene enrichment on all 71 neuroimmune proteins encoded by a single gene and determined the top 25 terms in each GO category (**Figure 12**).

Some of the topmost enriched molecular functions are signalling receptor binding ($p < 0.001$), receptor regulator activity ($p < 0.001$) and cytokine activity ($p < 0.001$). Of the remaining terms, multiple are associated with growth factor-related functions including growth factor binding ($p < 0.001$) and growth factor activity ($p < 0.001$). This is unsurprising as our collection of proteins are either cytokines, chemokines, growth factors or other immune receptors, involved in signalling to initiate an immune response.

The various enriched cellular components are the extracellular region ($p < 0.001$), cell surface ($p < 0.001$) and receptor complexes ($p < 0.001$). Cellular components with a lower (yet significant) level of enrichment include the intrinsic components of the plasma membrane ($p < 0.001$) and secretory granules ($p < 0.001$).

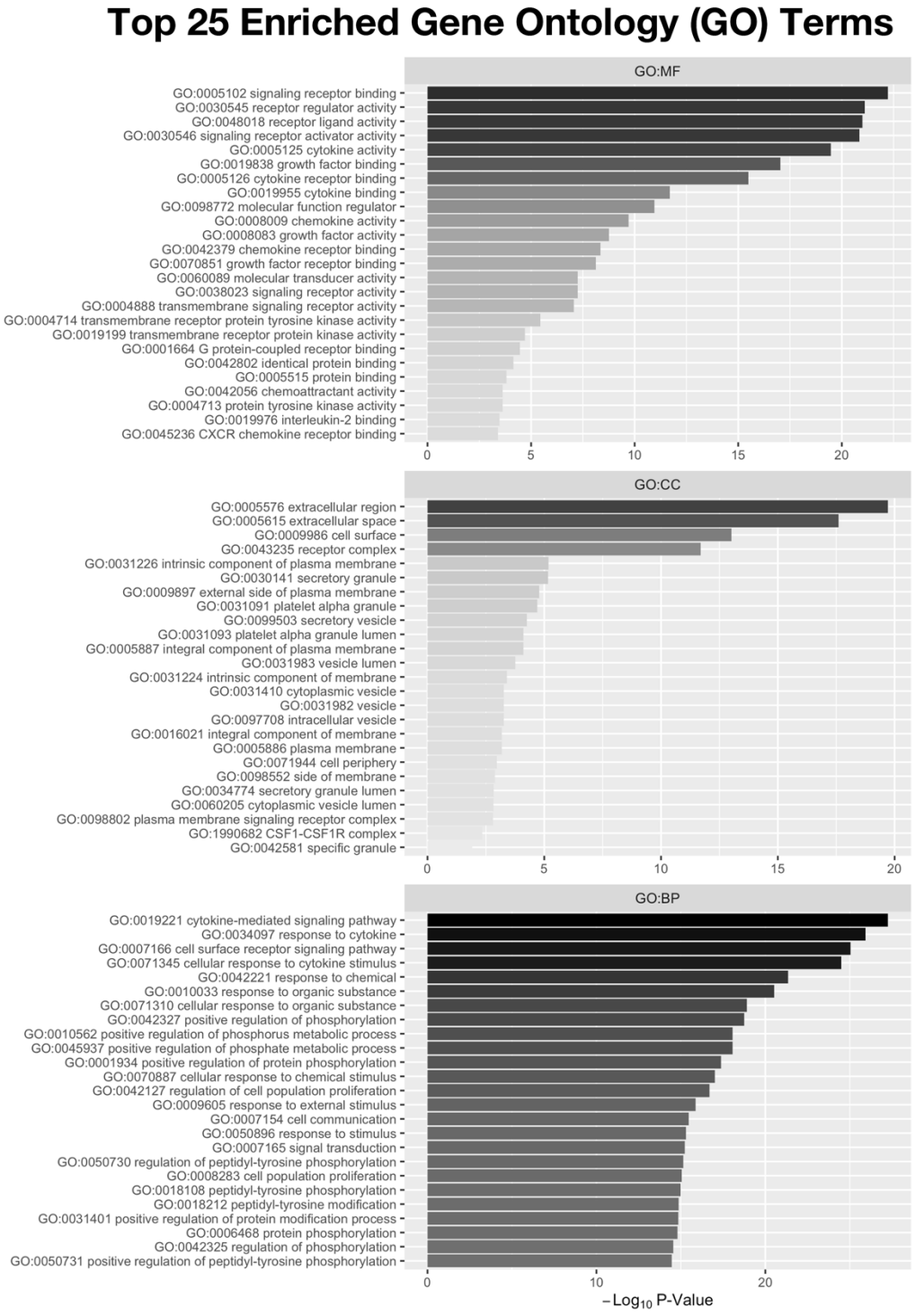
Top 25 Enriched Gene Ontology (GO) Terms
GO:MF
GO:0005102 signaling receptor binding
GO:0030545 receptor regulator activity
GO:0048018 receptor ligand activity
GO:0030546 signaling receptor activator activity
GO:0005125 cytokine activity
GO:0019838 growth factor binding
GO:0005126 cytokine receptor binding
GO:0019955 cytokine binding
GO:0098772 molecular function regulator
GO:0008009 chemokine activity
GO:0008083 growth factor activity
GO:0042379 chemokine receptor binding
GO:0070851 growth factor receptor binding
GO:0060089 molecular transducer activity
GO:0038023 signaling receptor activity
GO:0004888 transmembrane signaling receptor activity
GO:0004714 transmembrane receptor protein tyrosine kinase activity
GO:0019199 transmembrane receptor protein kinase activity
GO:0001664 G protein-coupled receptor binding
GO:0042802 identical protein binding
GO:0005515 protein binding
GO:0042056 chemoattractant activity
GO:0004713 protein tyrosine kinase activity
GO:0019976 interleukin-2 binding
GO:0045236 CXCR chemokine receptor binding
0
5
10
15
20
GO:CC
GO:0005576 extracellular region
GO:0005615 extracellular space
GO:0009986 cell surface
GO:0043235 receptor complex
GO:0031226 intrinsic component of plasma membrane
GO:0030141 secretory granule
GO:0009897 external side of plasma membrane
GO:0031091 platelet alpha granule
GO:0099503 secretory vesicle
GO:0031093 platelet alpha granule lumen
GO:0005887 integral component of plasma membrane
GO:0031983 vesicle lumen
GO:0031224 intrinsic component of membrane
GO:0031410 cytoplasmic vesicle
GO:0031982 vesicle
GO:0097708 intracellular vesicle
GO:0016021 integral component of membrane
GO:0005886 plasma membrane
GO:0071944 cell periphery
GO:0098552 side of membrane
GO:0034774 secretory granule lumen
GO:0060205 cytoplasmic vesicle lumen
GO:0098802 plasma membrane signaling receptor complex
GO:1990682 CSF1-CSF1R complex
GO:0042581 specific granule
0
5
10
15
20
GO:BP
GO:0019221 cytokine-mediated signaling pathway
GO:0034097 response to cytokine
GO:0007166 cell surface receptor signaling pathway
GO:0071345 cellular response to cytokine stimulus
GO:0042221 response to chemical
GO:0010033 response to organic substance
GO:0071310 cellular response to organic substance
GO:0042327 positive regulation of phosphorylation
GO:0010562 positive regulation of phosphorus metabolic process
GO:0045937 positive regulation of phosphate metabolic process
GO:0001934 positive regulation of protein phosphorylation
GO:0070887 cellular response to chemical stimulus
GO:0042127 regulation of cell population proliferation
GO:0009605 response to external stimulus
GO:0007154 cell communication
GO:0050896 response to stimulus
GO:0007165 signal transduction
GO:0050730 regulation of peptidyl-tyrosine phosphorylation
GO:0008283 cell population proliferation
GO:0018108 peptidyl-tyrosine phosphorylation
GO:0018212 peptidyl-tyrosine modification
GO:0031401 positive regulation of protein modification process
GO:0006468 protein phosphorylation
GO:0042325 regulation of phosphorylation
GO:0050731 positive regulation of peptidyl-tyrosine phosphorylation
0
10
20
−Log10 P-Value

Figure 12. Enriched Gene Ontology (GO) Terms. Top 25 enriched terms in three GO categories: molecular functions (MF), cellular components (CC), and biological processes (BP). GO analyses were performed on 71 proteins recognized by the gProfiler and GO enrichment tools. P-values were -log transformed and are indicated on the x-axis. GO term names, including the GO term ID, are indicated on the y-axis. Terms have been sorted from top to bottom in order of increasing p-value. Smaller p-values (i.e. larger -log(p-values)) are coloured black, while larger p-values are filled with a translucent grey shade. Note that all terms listed meet the threshold for statistical significance ($p < 0.05$).

These results are expected as immune proteins may be released as secretory molecules to initiate an immune response, while immune receptors are often expressed on the surface of cells to bind and detect foreign antigens (Nicholson, 2016). Additionally, the sample preparation used on our tissue samples filtered for membrane proteins, thus the enriched cellular components coincide with known properties of immune and membrane proteins (Nicholson, 2016).

Finally, the 71 neuroimmune proteins are enriched for biological processes such as the cytokine-mediated signalling pathway ($p < 0.001$), response to cytokines ($p < 0.001$) and cell surface signalling pathways ($p < 0.001$). Many of the remaining enriched biological functions have to do with some form of phosphorylation which is a common signalling mechanism that regulates the immune system (Sadreev et al., 2014). To investigate whether a GO term is disproportionately represented in a particular cluster, we mapped each protein to the 75 terms across all three GO categories (**Figure 13**). We calculated the proportion of proteins in each cluster that map onto the GO terms. Next, a binomial test was used to produce a probability score [i.e. $P(x) = (1 - \text{p-value}) * k$]. This value was used to indicate whether the cluster proportion truly varies from the overall proportion of proteins that map onto a term. Here, negative probability values (i.e. $k = -1$) indicate cluster proportions that are less than the overall proportion. Comparatively, positive values (i.e. $k = 1$) indicate proportions that are greater than the overall proportion (**Figure 14**).

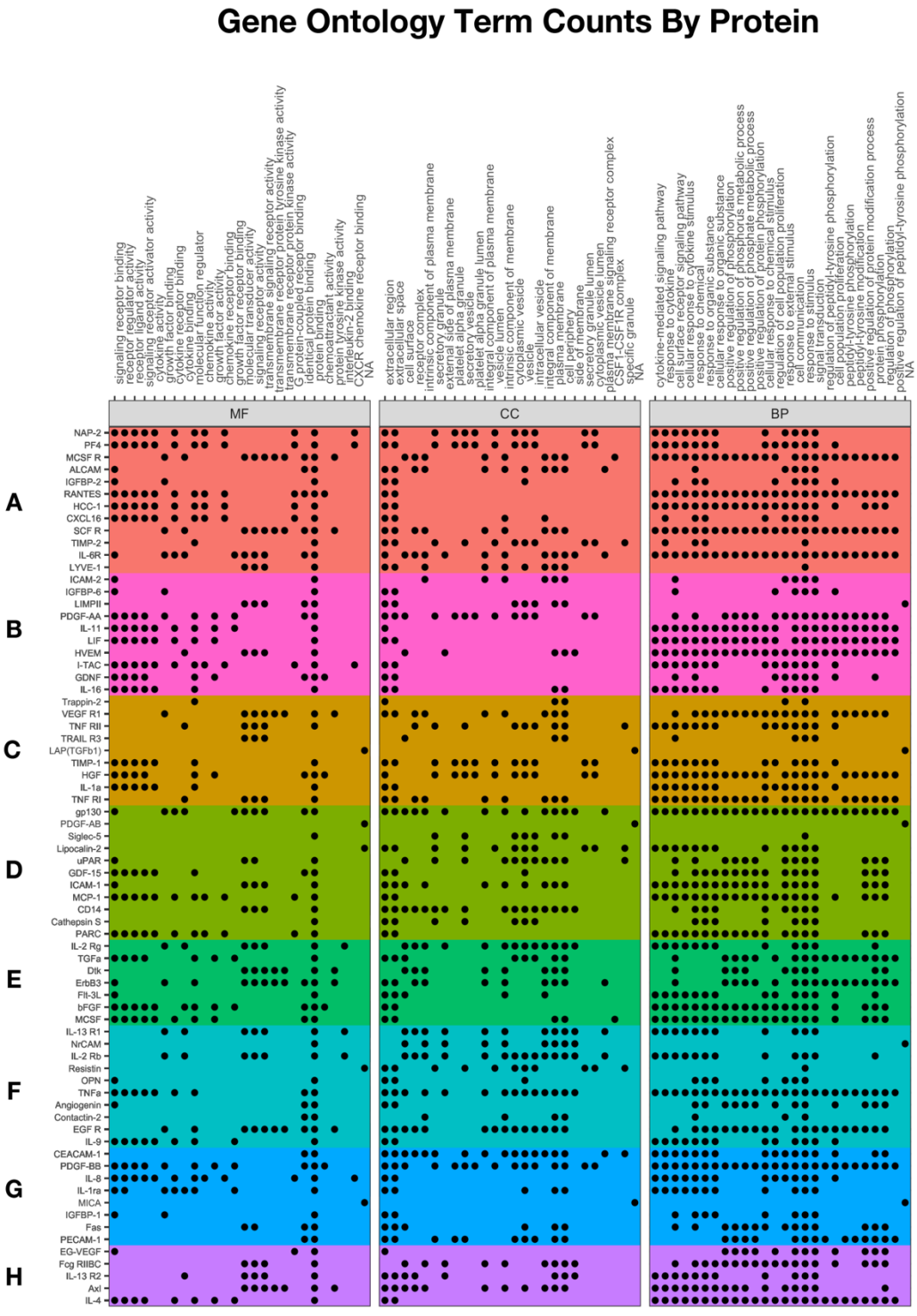
Gene Ontology Term Counts By Protein
MF
CC
BP
signaling receptor binding
receptor regulator activity
receptor ligand activity
signaling receptor activator activity
cytokine activity
growth factor binding
cytokine receptor binding
molecular function regulator
chemokine activity
growth factor activity
chemokine receptor binding
growth factor receptor binding
protein tyrosine kinase activity
signaling receptor activity
transmembrane signaling receptor activity
transmembrane receptor protein tyrosine kinase activity
transmembrane receptor protein kinase activity
cytokine receptor binding
identical protein binding
protein binding
chemoattractant activity
protein tyrosine kinase activity
molecular transducer activity
CXCR chemokine receptor binding
NA
extracellular region
extracellular space
cell surface
receptor complex
intrinsic component of plasma membrane
secretory granule
external side of plasma membrane
platelet alpha granule
secretory vesicle
platelet alpha granule lumen
integral component of plasma membrane
vesicle lumen
intrinsic component of membrane
cytoplasmic vesicle
vesicle
intracellular vesicle
integral component of membrane
plasma membrane
cell periphery
side of membrane
secretory granule lumen
cytoplasmic vesicle lumen
plasma membrane signaling receptor complex
CSF1-CSF1R complex
specific granule
NA
cytokine-mediated signaling pathway
response to cytokine
cell surface receptor signaling pathway
cellular response to cytokine stimulus
response to chemical
response to organic substance
cellular response to organic substance
positive regulation of phosphorylation
positive regulation of phosphorus metabolic process
positive regulation of phosphate metabolic process
positive regulation of protein phosphorylation
cellular response to chemical stimulus
regulation of cell population proliferation
response to external stimulus
cell communication
response to stimulus
signal transduction
regulation of peptidyl-tyrosine phosphorylation
cell population proliferation
peptidyl-tyrosine phosphorylation
protein tyrosine phosphorylation
positive regulation of protein modification process
protein phosphorylation
regulation of phosphorylation
positive regulation of phosphorylation
positive regulation of peptidyl-tyrosine phosphorylation
NA
A
NAP-2
PF4
MCSF R
ALCAM
IGFBP-2
RANTES
HCC-1
CXCL16
SCF R
TIMP-2
IL-6R
LYVE-1
B
ICAM-2
IGFBP-6
LIMPII
PDGF-AA
IL-11
LIF
HVEM
I-TAC
GDNF
IL-16
C
Trappin-2
VEGF R1
TNF RII
TRAIL R3
LAP(TGFb1)
TIMP-1
HGF
IL-1a
TNF RI
D
gp130
PDGF-AB
Siglec-5
Lipocalin-2
uPAR
GDF-15
ICAM-1
MCP-1
CD14
Cathepsin S
PARC
E
IL-2 Rg
TGFa
Dtk
ErbB3
Flt-3L
bFGF
MCSF
F
IL-13 R1
NrCAM
IL-2 Rb
Resistin
OPN
TNFa
Angiogenin
Contactin-2
EGF R
IL-9
G
CEACAM-1
PDGF-BB
IL-8
IL-1ra
MICA
IGFBP-1
Fas
PECAM-1
H
EG-VEGF
Fcg RIIBC
IL-13 R2
Axl
IL-4

Figure 13. Gene Ontology term counts by protein. Count of the number of proteins in each cluster that map onto the top 25 terms from each of the three GO categories: molecular functions (MF), cellular components (CC), and biological processes (BP). Proteins are organized by their order in the ward.D2 clustering dendrogram. Each cluster has been coloured differently for visualization purposes. The terms are organized from left to right in order of increasing p-value. The three GO categories are illustrated in separate plots.

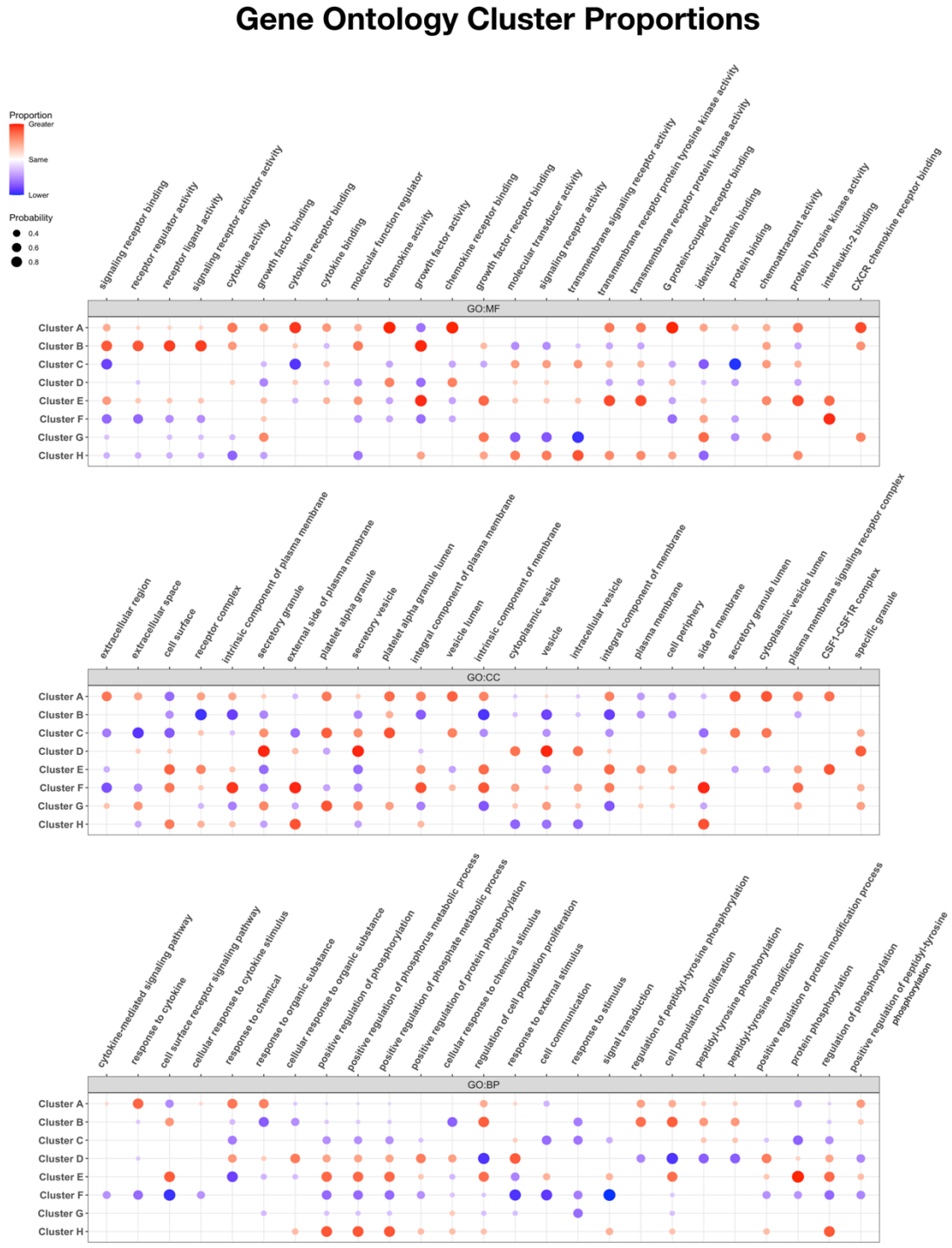
Gene Ontology Cluster Proportions
Proportion
Greater
Same
Lower
Probability
0.4
0.6
0.8
GO:MF
signaling receptor binding
receptor regulator activity
receptor ligand activity
signaling receptor activator activity
cytokine activity
growth factor binding
cytokine receptor binding
cytokine binding
molecular function regulator
chemokine activity
growth factor activity
chemokine receptor binding
growth factor receptor binding
molecular transducer activity
signaling receptor activity
transmembrane signaling receptor activity
transmembrane receptor protein tyrosine kinase activity
transmembrane receptor protein kinase activity
G protein-coupled receptor binding
identical protein binding
protein binding
chemoattractant activity
protein tyrosine kinase activity
interleukin-2 binding
CXCR chemokine receptor binding
Cluster A
Cluster B
Cluster C
Cluster D
Cluster E
Cluster F
Cluster G
Cluster H
GO:CC
extracellular region
extracellular space
cell surface
receptor complex
intrinsic component of plasma membrane
secretory granule
external side of plasma membrane
platelet alpha granule
secretory vesicle
platelet alpha granule lumen
integral component of plasma membrane
vesicle lumen
intrinsic component of membrane
cytoplasmic vesicle
vesicle
intracellular vesicle
integral component of membrane
plasma membrane
cell periphery
side of membrane
secretory granule lumen
cytoplasmic vesicle lumen
plasma membrane signaling receptor complex
CSF1-CSF1R complex
specific granule
GO:BP
cytokine-mediated signaling pathway
response to cytokine
cell surface receptor signaling pathway
cellular response to cytokine stimulus
response to chemical
response to organic substance
cellular response to organic substance
positive regulation of phosphorylation
positive regulation of phosphorus metabolic process
positive regulation of phosphate metabolic process
positive regulation of protein phosphorylation
cellular response to chemical stimulus
regulation of cell population proliferation
response to external stimulus
cell communication
response to stimulus
signal transduction
regulation of peptidyl-tyrosine phosphorylation
cell population proliferation
peptidyl-tyrosine phosphorylation
peptidyl-tyrosine modification
positive regulation of protein modification process
protein phosphorylation
regulation of phosphorylation
positive regulation of peptidyl-tyrosine phosphorylation

Figure 14. Gene Ontology cluster proportions and probability scores. Bubble chart indicating the probability that enriched GO terms are represented in clusters at proportions that differ from the overall proportion across all clusters. The expected value indicates the fraction of all 71 proteins that map onto the term. Red dots indicate cluster proportions that are greater than the overall proportion, blue dots indicate cluster proportions that are less than the overall proportion. In cases where there is no difference between the overall proportion and the cluster proportion the bubble chart is left blank. The size of the dots indicates the probability that the cluster proportion is truly different from the overall proportion. Smaller dots, corresponding to smaller probabilities, are given a more translucent color. GO terms are organized in order of increasing p-value as illustrated in Figure 12. Each of the three GO categories (i.e. MF, CC, and BP) are presented in its own plot.

By focusing on probabilities greater than 0.95, we find that Cluster A, which decreases in expression until early adulthood before increasing into aging, contains a larger than expected proportion of proteins related to three functions: chemokine activity (P(x) = 0.99), chemokine receptor binding (P(x) = 0.99) and G-coupled receptor binding (P(x) = 0.98). Cluster B, which has high levels of expression in early development (~0.05 years) and subsequently fluctuates across the lifespan, has a higher than expected proportion of proteins with growth factor activity (P(x) = 0.95). Proteins that continually increase into adulthood in Cluster E are related to protein phosphorylation (P(x) = 0.98). Importantly, these proportions should be considered trends rather than concrete relationships as the small cluster sizes do not provide adequate power for meaningful significance testing upon correction for multiple comparisons.

Furthermore, the analysis did not reveal a one-to-one relationship between trajectory and function. For instance, proteins with similar trajectories had opposing associations with GO terms. For example, as determined by the Fréchet distances, Cluster G and Cluster H have similar protein trajectories. Both display lower levels of expression during the neonatal period (< 0.3 years) and in older adults (55+ years old), with a peak in expression occurring in early childhood at approximately 2-3 years. Nonetheless, these clusters show opposing relationships with transmembrane signalling receptor activity. Cluster G contains no proteins that map onto this term, whereas 30% of all 71 terms map onto transmembrane signalling receptor activity. Therefore, there is a difference in proportion of -30% (p = 0.06, P(x) = -0.94). Cluster H on the other hand contains a greater proportion (60%, p = 0.18, P(x) = 0.82) of proteins that map onto this term. In this

analysis, we also found that clusters with widely different average trajectory patterns had greater than expected proportions for the same term. For example, clusters B (P(x) = 0.95) and E (P(x) = 0.93) both have a high proportion of proteins that map onto growth factor activity. While both clusters exhibit undulating patterns, Cluster B generally decreases across the lifespan, while Cluster E generally increases across the lifespan. Altogether these results suggest that an individual trajectory does not represent involvement in a particular molecular function. Rather, there seems to be a dynamic relationship between protein trajectory and function.

Classic neural plasticity marker trajectories and clusters

Neuroimmune proteins are known to have reciprocal relationships with classic neural plasticity markers like glutamatergic and GABAergic receptor proteins which regulate synaptic plasticity in the human VIC. Here, we used plasticity markers as a guide to identify candidate plasticity processes for our neuroimmune proteins. Note that two proteins in this data set (i.e. PSD-95 and gephyrin) were measured in both homogenate and synaptoneurosome sample preparations. First, we used the WSS (**Figure 15**) and ward.D2 hierarchical clustering (**Figure 16**) methods to determine that the 23 trajectories segregate into five unique clusters. The clusters were of varying size, from three to six proteins in each cluster. AU values were calculated as a preliminary measure of the cluster integrity (Plasticity Cluster 1: n = 4, AU = 0.87; Plasticity Cluster 2: n = 6, AU = 0.90; Plasticity Cluster 3: n = 6, AU = 0.74; Plasticity Cluster 4: n = 4, AU = 0.97; Plasticity Cluster 5: n = 3, AU = 0.87).

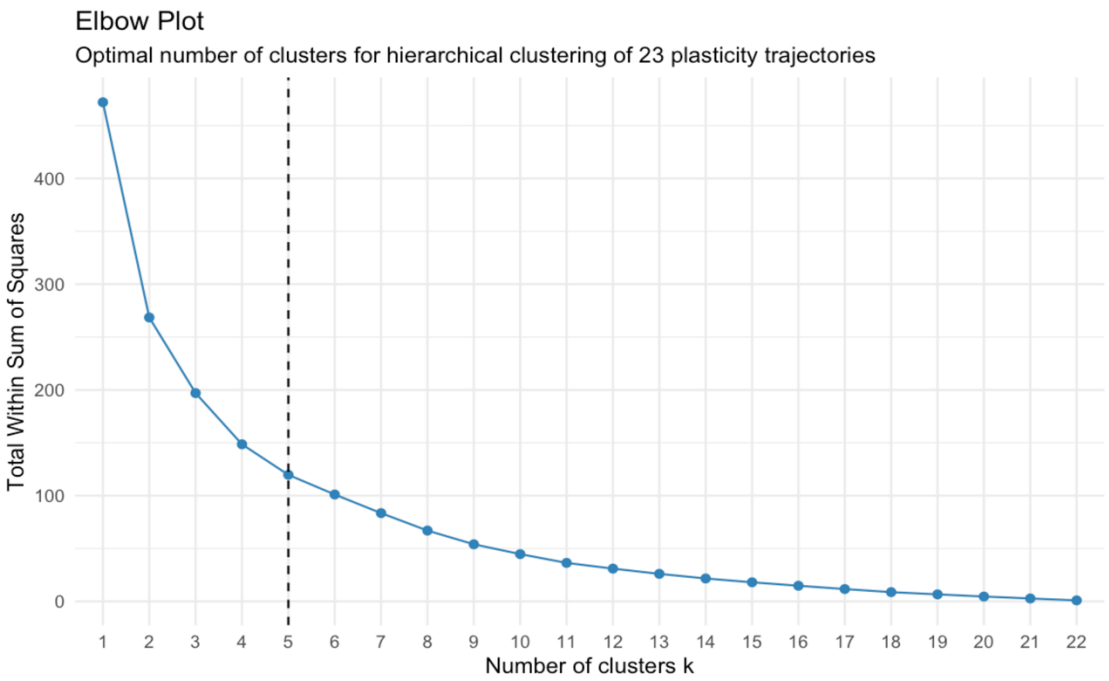
Elbow Plot
Optimal number of clusters for hierarchical clustering of 23 plasticity trajectories
Total Within Sum of Squares
0
100
200
300
400
1 2 3 4 5 6 7 8 9 10 11 12 13 14 15 16 17 18 19 20 21 22
Number of clusters k

Figure 15. Total Within Sum of Square calculations for determining the optimal number of plasticity trajectory clusters. WSS values (a measure of the compactness of clusters) corresponding to the hierarchical clustering of 23 plasticity marker lifespan trajectories. A range of cluster numbers were assessed from one to 22. The x-axis indicates the number of clusters and the y-axis indicates the total WSS for that cluster number. The WSS values decrease as the number of clusters increases. The bend in the curve indicates the point at which a balance is reached between minimizing the WSS and creating too many clusters. Here, the elbow-method for determining the optimal number of clusters reveals a bend at 5 ± 1 clusters.

A. Ward.D2 Hierarchical Clustering Dendrogram: 23 Plasticity Marker Trajectories

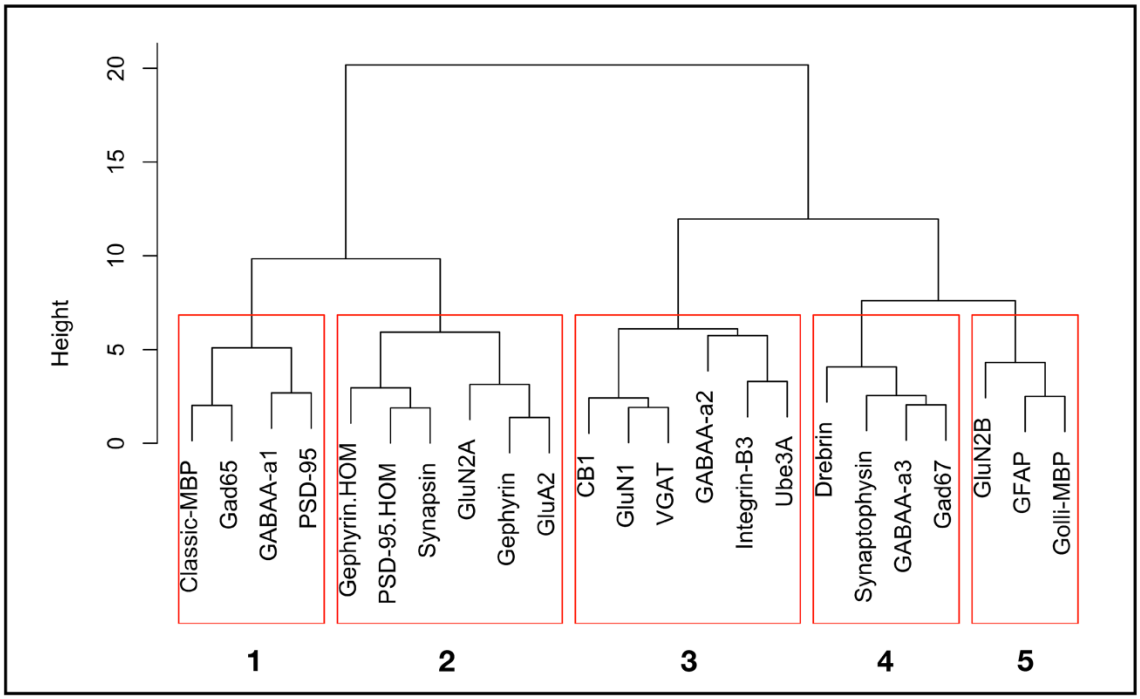

B. Ward.D2 Hierarchical Clustering: Average LOESS Curves

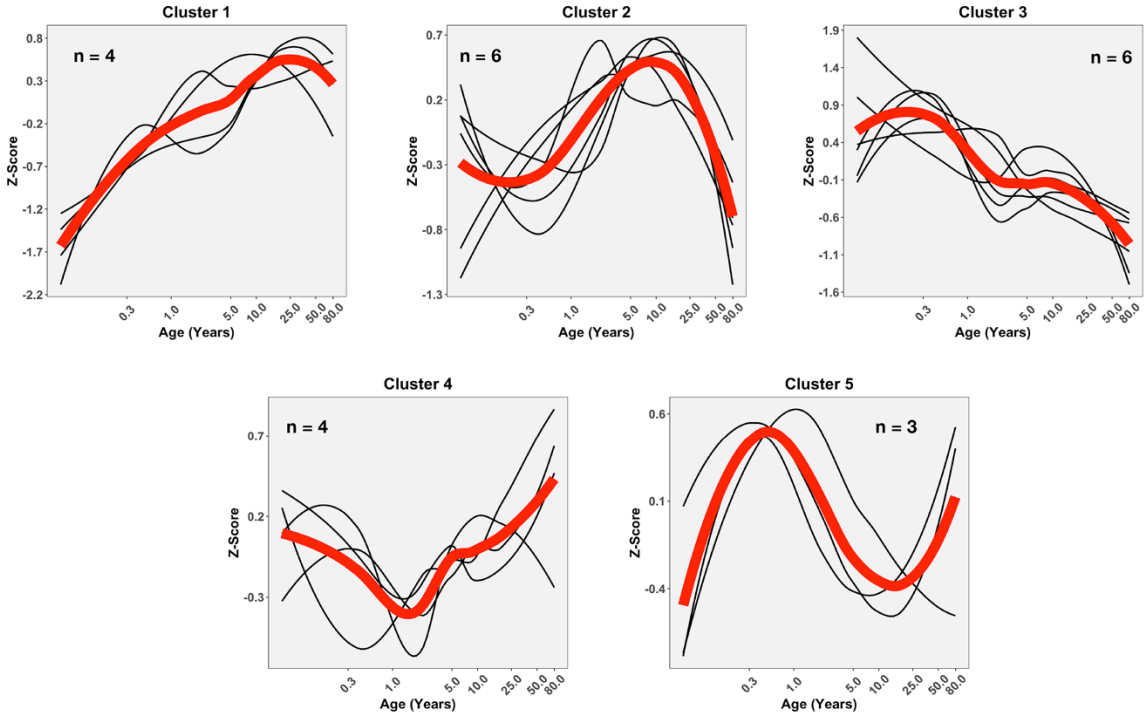

Figure 16. Ward. D2 hierarchical clustering of neuroplasticity marker trajectories. Hierarchical relationships and cluster designations for 23 classic visual cortical plasticity trajectories. **(A)** Hierarchical clustering dendrogram, in which the height is a reflection of the proximity between the trajectories, with smaller values indicating a closer relationship. Here, the eight clusters are identified by coloured boxes. The dendrogram is cut at a height of ~ 7 and the clusters are labelled "1" through "5" in order from left to right on the dendrogram. **(B)** Average curves for the five identified clusters. Age is plotted on a logarithmic scale, and protein levels (z-score) are shown. Thick lines represent the average curves, while the thin lines indicate individual protein trajectories. The number of proteins (n) in each cluster are indicated, this number ranges from three to six.

Similar to the neuroimmune Fréchet analysis, intracluster distances (Mdn = 20.1) were compared to intercluster distances (Mdn = 40.9). The median difference: -20.8, [95CI -24.4, -16.3] indicates that the intracluster median is much smaller than the intercluster median (**Figure 17**). This illustrates that ward.D2 is successful in grouping proteins with similar trajectories together.

Approach One: Comparison of neuroimmune and plasticity marker trajectories

Subsequently, two parallel approaches were carried out to compare the development of these plasticity markers with the neuroimmune proteins. In the first approach, we calculated the Fréchet distances between the 72 neuroimmune proteins and the 23 plasticity marker trajectories to determine if any lifespan patterns are unique to either of these protein classes (**Figure 18**). In this analysis the proteins were organized according to their cluster designations. More specifically, immune proteins were organized into their eight clusters and the plasticity markers were organized into their five clusters. We found that the Fréchet distances range from ~4.7 to ~126.3, and that the median Fréchet distance is ~42.8. Interestingly, the range of Fréchet values when comparing synaptic and neuroimmune trajectories is smaller than the range obtained when comparing the neuroimmune proteins to one another. To recap, the range of Fréchet distances for neuroimmune trajectory comparisons between clusters was ~8.1 to ~134.6 with a median distance of ~42.9. This suggests that neuroimmune proteins show great variation amongst their own lifespan patterns, and that the degree of similarity between neuroimmune trajectories in varying clusters is similar to their relationship with the classic plasticity marker trajectories explored in this study.

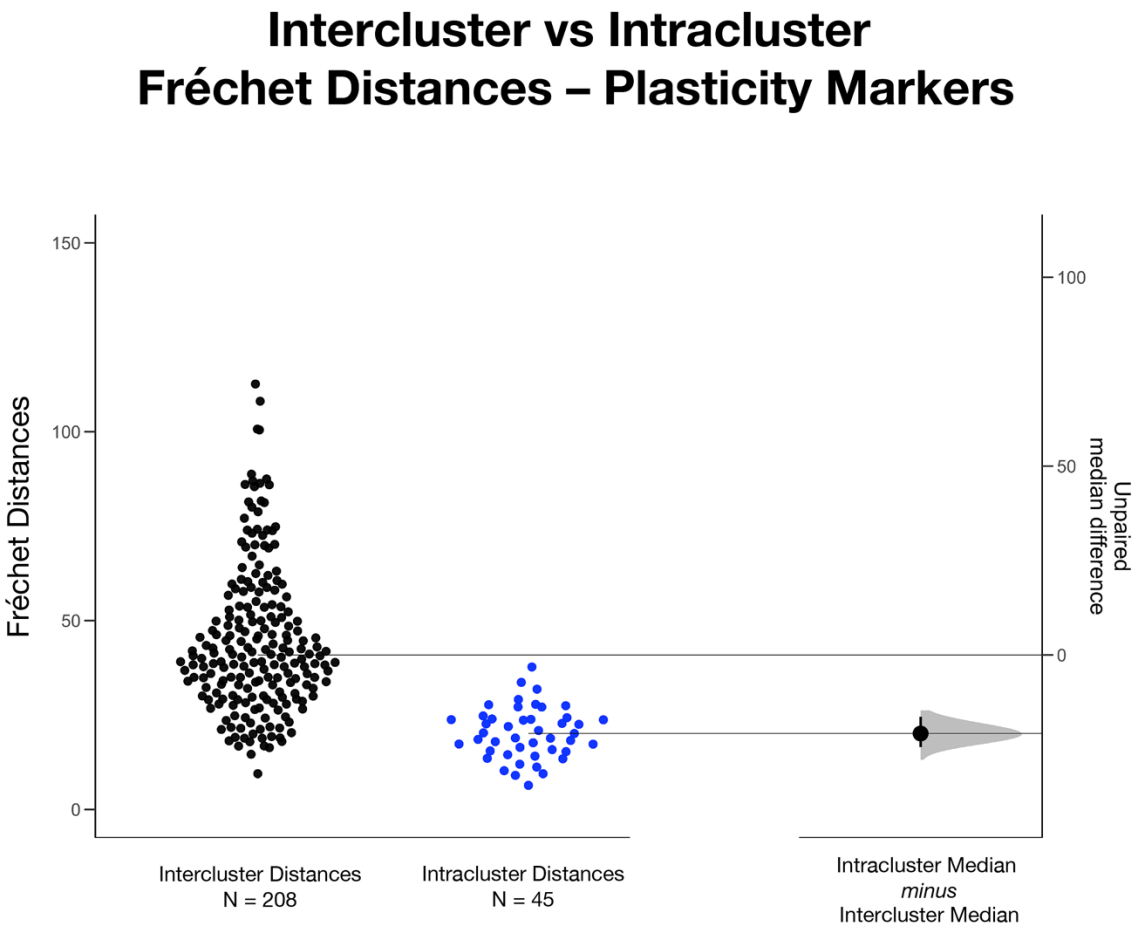
Intercluster vs Intracluster
Fréchet Distances – Plasticity Markers
Fréchet Distances
150
100
50
0
100
50
0
Unpaired
median difference
Intercluster Distances
N = 208
Intracluster Distances
N = 45
Intracluster Median
minus
Intercluster Median

Figure 17. Median difference between intercluster and intracluster Fréchet distances – plasticity marker data. The black dots in the swarm plot indicate the Fréchet distances between the 23 plasticity markers in varying clusters (i.e. intercluster distances). The Fréchet distances between proteins in the same cluster, with the exception of protein self-comparisons, are indicated by the collection of blue dots. The Fréchet distances themselves can be seen on the y-axis on the left. The median intercluster Fréchet distance is 40.9, while the median intercluster distance is 20.1. The difference between the median value of these two sets of Fréchet distances is plotted on the second y-axis on the right. Estimation statistics was used to compute a bootstrap interval for the difference (-20.8, [95CI -24.4, -16.3]).

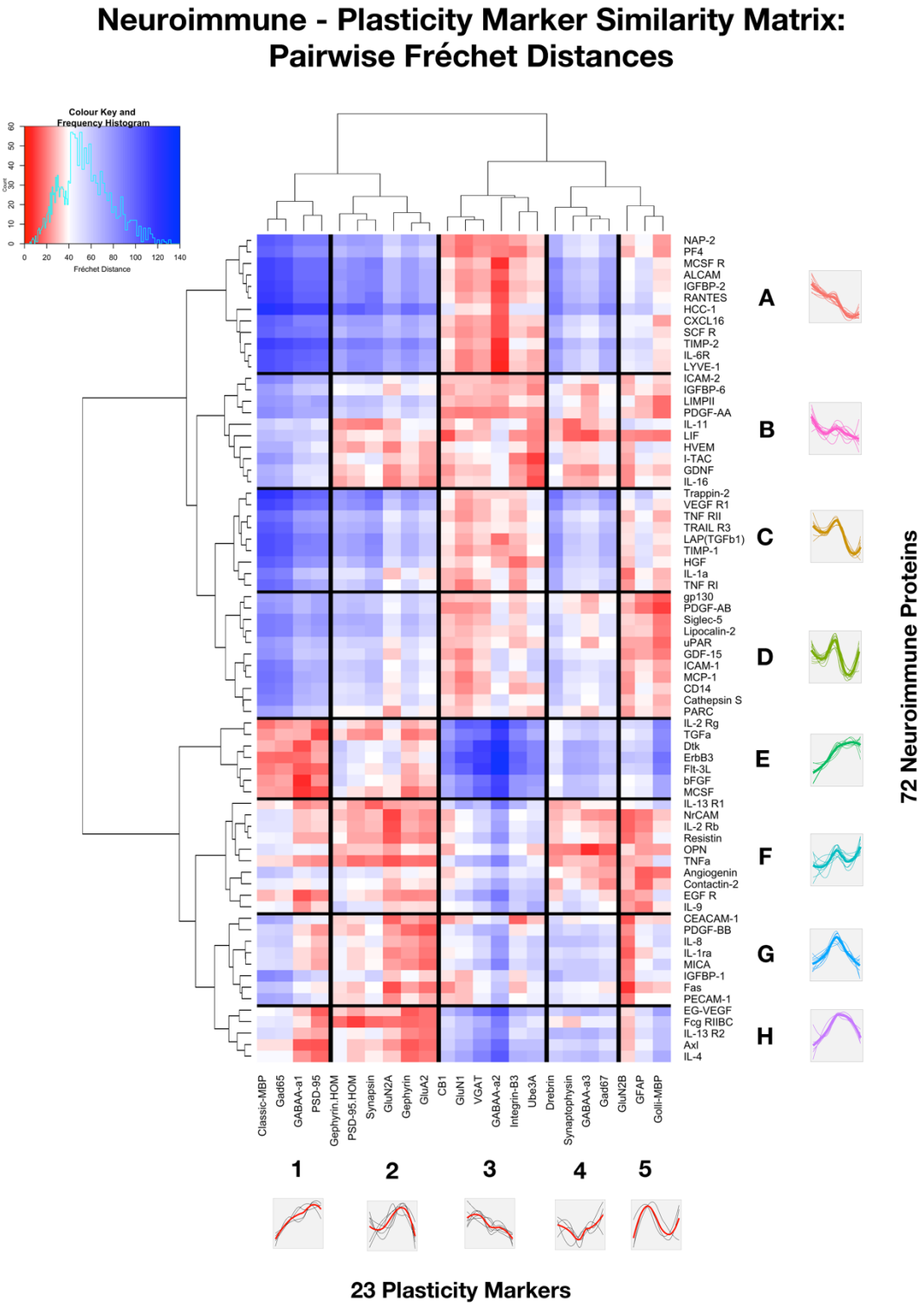
Neuroimmune - Plasticity Marker Similarity Matrix:
Pairwise Fréchet Distances
Colour Key and
Frequency Histogram
Count
Fréchet Distance
NAP-2
PF4
MCSF R
ALCAM
IGFBP-2
RANTES
HCC-1
CXCL16
SCF R
TIMP-2
IL-6R
LYVE-1
ICAM-2
IGFBP-6
LIMPII
PDGF-AA
IL-11
LIF
HVEM
I-TAC
GDNF
IL-16
Trappin-2
VEGF R1
TNF RII
TRAIL R3
LAP(TGFb1)
TIMP-1
HGF
IL-1a
TNF RI
gp130
PDGF-AB
Siglec-5
Lipocalin-2
uPAR
GDF-15
ICAM-1
MCP-1
CD14
Cathepsin S
PARC
IL-2 Rg
TGFa
Dtk
ErbB3
Flt-3L
bFGF
MCSF
IL-13 R1
NrCAM
IL-2 Rb
Resistin
OPN
TNFa
Angiogenin
Contactin-2
EGF R
IL-9
CEACAM-1
PDGF-BB
IL-8
IL-1ra
MICA
IGFBP-1
Fas
PECAM-1
EG-VEGF
Fcg RIIBC
IL-13 R2
Axl
IL-4
A
B
C
D
E
F
G
H
72 Neuroimmune Proteins
Classic-MBP
Gad65
GABAA-a1
PSD-95
Gephyrin.HOM
PSD-95.HOM
Synapsin
GluN2A
Gephyrin
GluA2
CB1
GluN1
VGAT
GABAA-a2
Integrin-B3
Ube3A
Drebrin
Synaptophysin
GABAA-a3
Gad67
GluN2B
GFAP
Golli-MBP
1
2
3
4
5
23 Plasticity Markers

Figure 18. Fréchet distance matrix for measuring similarity between neuroimmune and plasticity marker clusters. Pairwise Fréchet distances between 72 neuroimmune trajectories and 23 plasticity marker trajectories. A total of 1656 distances were calculated and each of the proteins are organized according to their ward.D2 cluster designation. The clusters and their average curves are displayed on the plot. The values range from ~4.7 to ~126.3, and the median Fréchet distance is ~ 42.8. Red cells correspond to smaller Fréchet distances and indicate a greater degree of similarity, while larger Fréchet distances are coloured blue and indicate lower levels of similarity. The same colour scale as Figure 9 has been used to facilitate the comparison of results. The wide range of Fréchet distances indicates that neuroimmune and classic neural plasticity marker trajectories share some common trajectories but also contain trajectories unique to each set of proteins.

Estimation statistics were applied to produce a bootstrap CI for the median difference scores between the two protein sets (**Figure 19**). The analysis revealed that certain trajectories patterns are common between the plasticity and neuroimmune proteins, while other trajectories are unique. Plasticity Cluster 1 generally increases across the lifespan, until ~ 25 years when expression levels begin to decrease. Unsurprisingly, estimation statistics reveal that the proteins in this cluster have trajectories very similar to the neuroimmune Cluster E: +0.6 [95CI -5.3, +7.3] which also increases across the lifespan until ~ 20 years, followed by a slight decrease into aging. Plasticity Cluster 2 shows a slow increase in protein levels in infancy and peaks in expression during adolescence, with decreasing protein levels into aging. Based on the Fréchet distances, proteins in this cluster follow similar patterns to neuroimmune Cluster H: +5.1, [95CI -1.8, +13.0]. Plasticity Cluster 3 decreases across the lifespan, this pattern is also seen in neuroimmune Clusters A: +1.2, [95CI [-3.0, +5.7] and to a lesser extent Cluster B: +2.8, 95CI [-0.8, +6.4], which shows a transient increase in expression during infancy and early childhood. Plasticity Cluster 4 is a unique trajectory, where there are higher expression levels in early development and in older adults with very low levels of expression in young children at ~ 1-2 years of age. This expression pattern is not seen in the neuroimmune proteins. Finally, plasticity Cluster 5 shows an undulating pattern, with high levels of protein in infancy and in older adults, while there are low levels of protein expression in neonates and during adolescence. Neuroimmune Cluster D: +2.9 [95CI -1.0, +11.3], Cluster F: +3.8, [95CI -1.9, +12.2] and Cluster G: +9.3, [95CI -2.5, +20.0] show overlapping median distances with Plasticity Cluster 5.

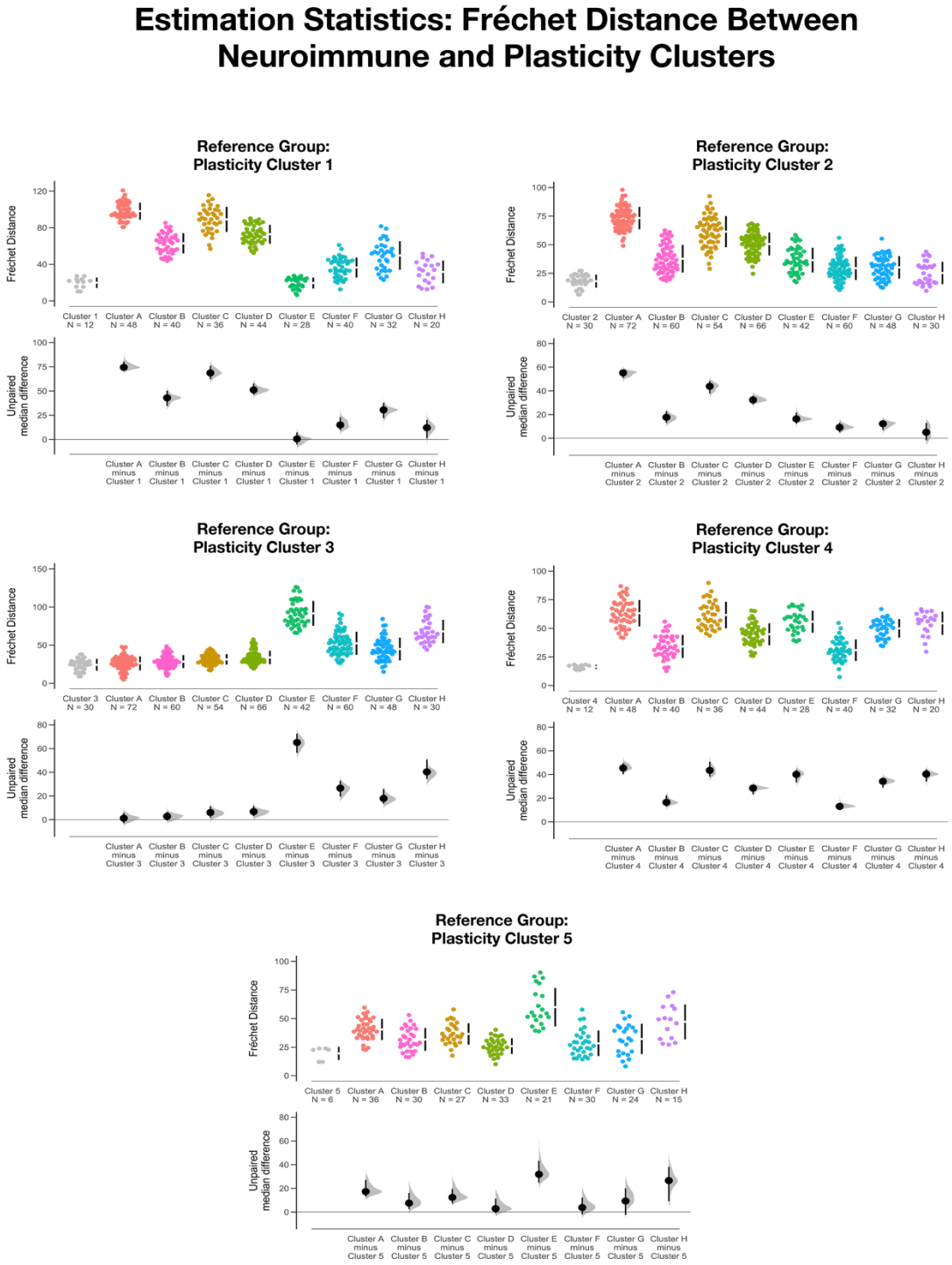
Estimation Statistics: Fréchet Distance Between Neuroimmune and Plasticity Clusters
Reference Group: Plasticity Cluster 1
Reference Group: Plasticity Cluster 2
Reference Group: Plasticity Cluster 3
Reference Group: Plasticity Cluster 4
Reference Group: Plasticity Cluster 5
Fréchet Distance
Unpaired median difference

Figure 19. Estimation statistics for measuring the similarity between neuroimmune and plasticity marker cluster trajectories. Swarm plots of intracluster Fréchet distances and pairwise Fréchet distances between proteins of varying clusters. This stamp collection of estimation plots includes five graphs, corresponding to the five plasticity marker clusters. In an individual plot the first category corresponds to the reference group: Fréchet distances between proteins in the same plasticity cluster. Subsequent categories indicate the Fréchet distances between proteins in the reference cluster and each of the eight neuroimmune clusters (i.e. the test clusters). An unpaired median difference score (test cluster median *minus* reference cluster median) is indicated along with bootstrapped CIs for each median difference score. CIs that overlap with a median difference of zero indicate clusters with similar patterns.

However, there are only three proteins in Plasticity Cluster 5; this small number of proteins results in larger confidence intervals when performing the estimation statistics.

Grouping the individual protein distances together to calculate median Fréchet distances between neuroimmune and plasticity clusters reveals that these two protein collections do not share extremely similar trajectories (**Figure 20**). Recall that the median intracluster Fréchet distance for neuroimmune proteins was ~ 17.3. This value indicates the strength of the relationship between neuroimmune proteins in the same cluster. Comparatively, the median Fréchet distance between neuroimmune and plasticity marker trajectories is ~ 42.8, which is more than double the neuroimmune intracluster median distance. Of these clusters, the highest degree of similarity occurs between plasticity Cluster 1 and neuroimmune Cluster E. The median Fréchet distance between the proteins in these two clusters is ~ 22.0. Plasticity Cluster 1 is composed of proteins with known functions in the regulation of the critical period for experience-dependent plasticity in the visual cortex. Consequently, the proteins in neuroimmune Cluster E are candidates for plasticity and neurodevelopment processes. There are a total of six proteins in Cluster E: macrophage colony stimulating factor 1 (MCSF), ErbB3, basic fibroblast growth factor (bFGF), fms-related tyrosine kinase 3 ligand (Flt-3L), cytokine receptor common subunit gamma (IL2RG), protransforming growth factor alpha (TGFα), and tyrosine-protein kinase receptor TYRO3 (Dtk/Tyro3).

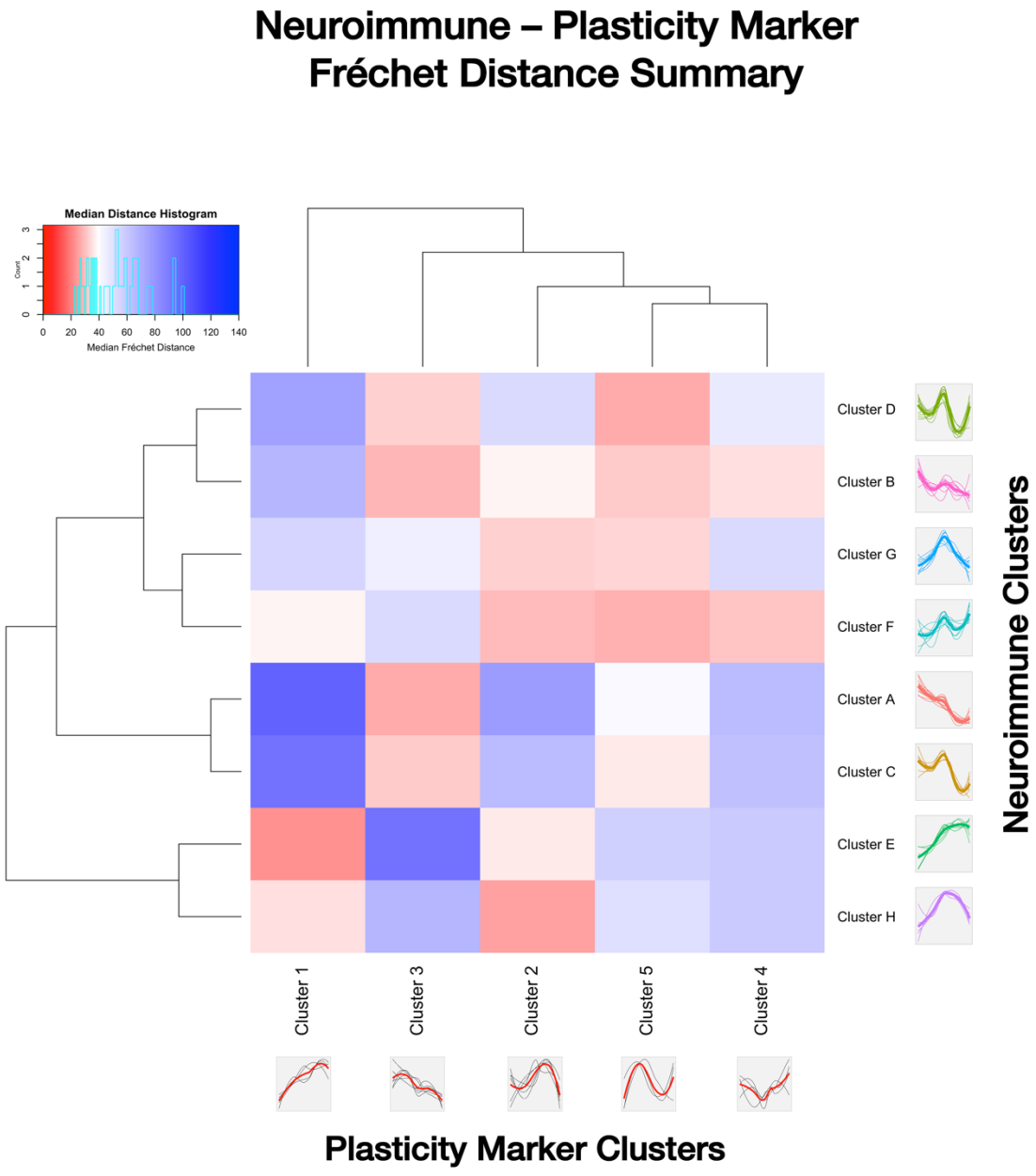
Neuroimmune – Plasticity Marker
Fréchet Distance Summary
Median Distance Histogram
Count
0
1
2
3
0
20
40
60
80
100
120
140
Median Fréchet Distance
Cluster D
Cluster B
Cluster G
Cluster F
Cluster A
Cluster C
Cluster E
Cluster H
Neuroimmune Clusters
Cluster 1
Cluster 3
Cluster 2
Cluster 5
Cluster 4
Plasticity Marker Clusters

Figure 20. Neuroimmune-plasticity marker cluster Fréchet distance summary. Median Fréchet distances between the two sets of protein clusters. Plasticity clusters are visualized as the columns, neuroimmune clusters are visualized as the rows. Dendrograms organize the order of the clusters according to the similarities in median Fréchet distances. Red cells correspond to smaller Fréchet distances and indicate a greater degree of similarity, while larger Fréchet distances are coloured blue and indicate lower levels of similarity. The same colour scale as Figure 9 has been used to facilitate the comparison of neuroimmune Fréchet distances with the plasticity marker distances.

Several of these proteins and their genes have important roles in the development of the visual cortex. For example, ErbB3 (Makinodan et al., 2012) and Tyro3 (Akkermann et al., 2017) are required for normal developmental myelination. MCSF on the other hand, mediates GABAergic circuitry in the mouse visual cortex (Michaelson et al., 1996). Furthermore, TGFα is implicated in regulating the survival of glial cells in the Drosophila visual system (Hidalgo et al., 2006), while bFGF prevents neuronal apoptosis and promotes plasticity after injury in the rat visual system (Chadi & Fuxe, 1998; Hendrickson et al., 2012).

Overall, the average Cluster E trajectory increases across the lifespan into adulthood, with decreasing levels into aging. As many of the aforementioned functions associated with proteins in neuroimmune Cluster E are neuroprotective, a loss or decline in the expression of these proteins may contribute to the detrimental effects associated with the aging process. Furthermore, the dysregulation of these proteins is implicated in neurological disorders such as MS (Katiyar et al., 2018; Shafit-Zagardo et al., 2018; Woodbury & Ikezu, 2013), mood disorders (Kéri et al., 2014; Tang et al. 2017), and psychiatric disorders like schizophrenia (Janova et al., 2017; Roy et al., 2007).

Approach Two: Comparison of neuroimmune and plasticity marker trajectories

To approach the question of plasticity and neuroimmune trajectory similarities through an alternate lens, we performed unsupervised hierarchical clustering on the combined set of all 95 protein trajectories. The WSS method (**Figure 21**) and the ward.D2 method together revealed eight clusters ranging in size from seven proteins to 18 proteins (**Figure 22**).

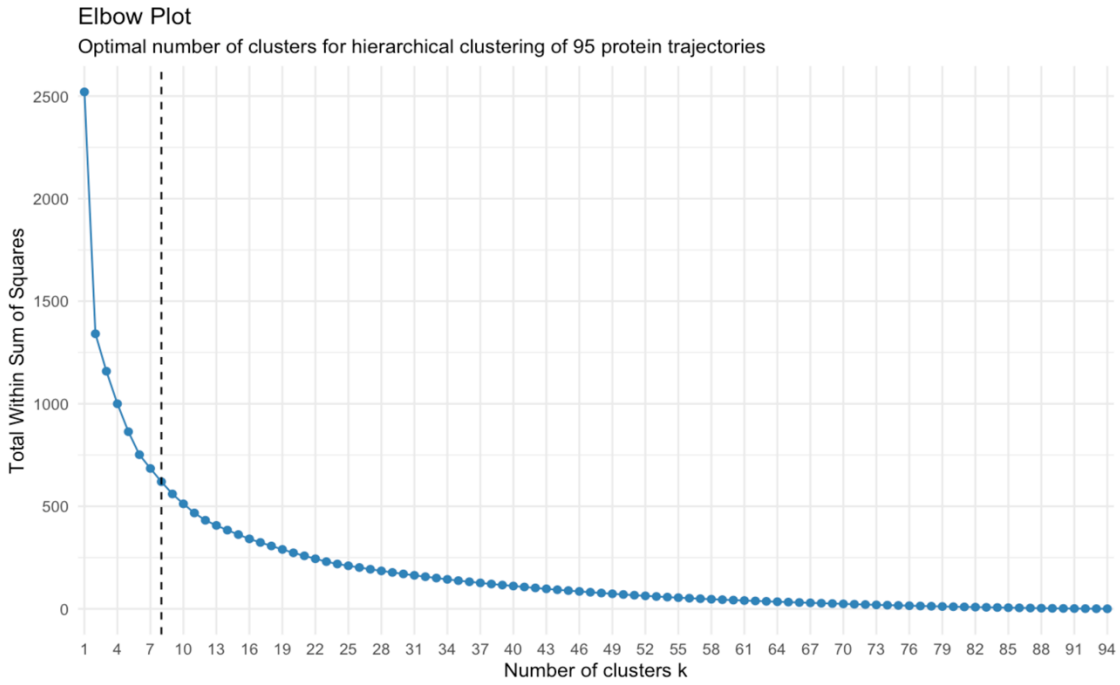
Elbow Plot
Optimal number of clusters for hierarchical clustering of 95 protein trajectories
Total Within Sum of Squares
2500
2000
1500
1000
500
0
1 4 7 10 13 16 19 22 25 28 31 34 37 40 43 46 49 52 55 58 61 64 67 70 73 76 79 82 85 88 91 94
Number of clusters k

Figure 21. Total Within Sum of Square calculations for determining the optimal number of clusters. WSS values (a measure of the compactness of clusters) corresponding to the hierarchical clustering of all 95 lifespan trajectories. A range of cluster numbers were assessed from one to 94. The x-axis indicates the number of clusters and the y-axis indicates the total WSS for that cluster number. The WSS values decrease as the number of clusters increases. The bend in the curve indicates the point at which a balance is reached between minimizing the WSS and creating too many clusters. Here, the "elbow method" for determining the optimal number of clusters reveals a bend at 8 ± 2 clusters.

A Ward.D2 Hierarchical Clustering Dendrogram: 95 Protein Trajectories

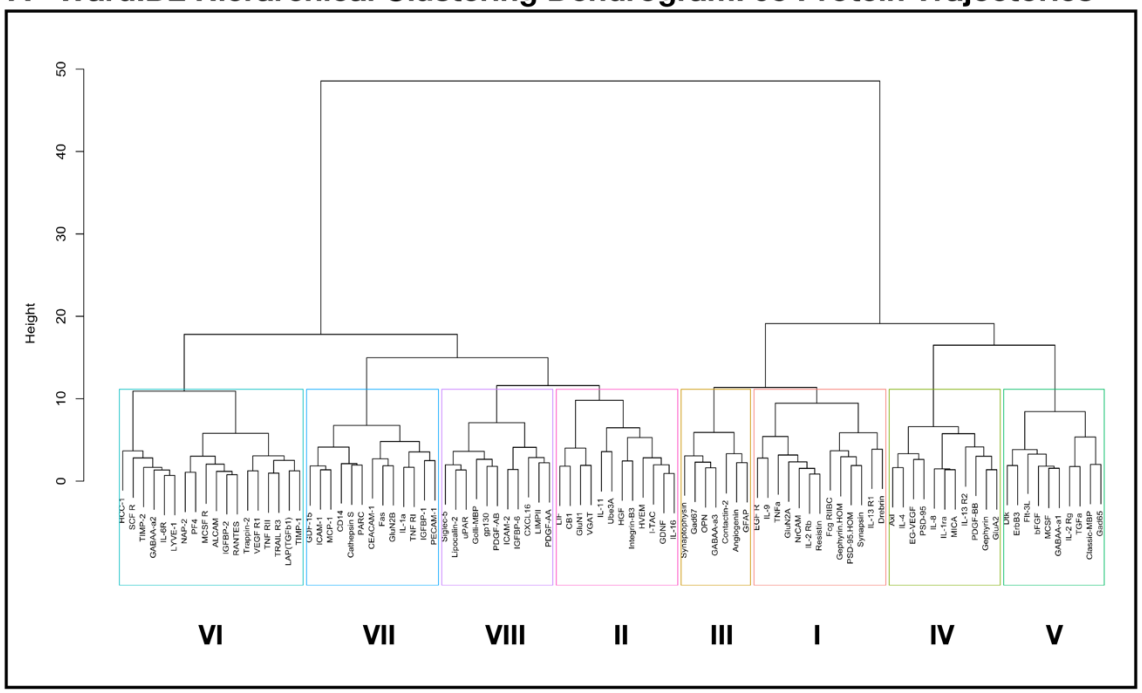

B Average LOESS Curves ordered by number of SynGO terms

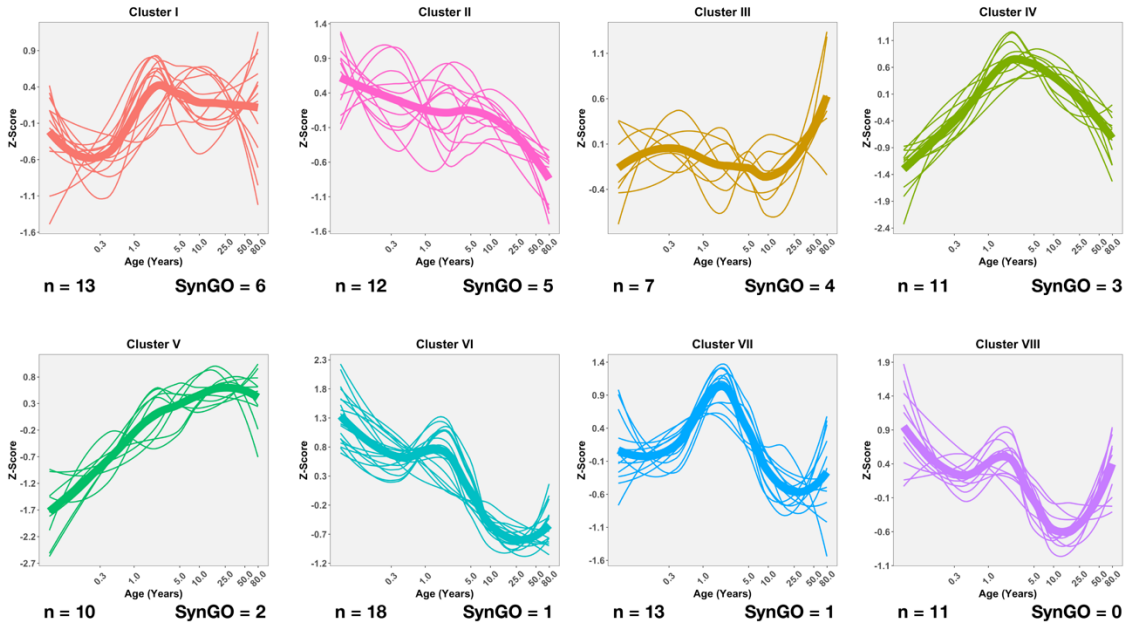

Figure 22. Ward. D2 hierarchical clustering of neuroplasticity marker trajectories. Hierarchical relationships and cluster designations for 95 neuroimmune and classic neural plasticity markers. **(A)** Hierarchical clustering dendrogram, in which the height is a reflection of the proximity between the trajectories, with smaller values indicating a closer relationship. Here, the eight clusters are identified by coloured boxes. The dendrogram is cut at a height of ~ 12 and the clusters are labelled "I" through "VIII" in order of the number of SynGO proteins (i.e. with recognized synapse-related functions) in each cluster. **(B)** Average curves for the eight identified clusters. Age is plotted on a logarithmic scale, and protein levels (z-score) are shown. Thick lines represent the average curves, while the thin lines indicate individual protein trajectories. The number of proteins (n) in each cluster are indicated, this number ranges from seven to 18. The total number of SynGO proteins in a cluster range from zero to six.

Clusters were organized by the number of synapse-related proteins. As proteins in the neuroimmune collection also have synapse-related functions, the SynGO database was used to annotate the 95 proteins with their known synaptic functions. Clusters were labelled "I" to "VIII" in order of decreasing number of SynGO annotated proteins (Cluster I: n = 13, AU = 0.80, SynGO = 6; Cluster II: n = 12, AU = 0.73, SynGO = 5; Cluster III: n = 7, AU = 0.70, SynGO = 4; Cluster IV: n = 11, AU = 0.81, SynGO = 3; Cluster V: n = 10, AU = 0.93, SynGO = 2; Cluster VI: n= 18, AU = 0.73, SynGO = 1; Cluster VII: n = 13, AU = 0.77, SynGO = 1; Cluster VIII: n = 11, AU = 0.88, SynGO = 0). Importantly, clustering did not reveal strictly linear patterns, rather these molecular marker clusters all show non-linear lifespan trajectories.

Similar to the neuroimmune Fréchet analysis, intracluster distances (Mdn = 19.5) were compared to intercluster distances (Mdn = 44.0). The median difference: -24.5, [95CI -25.7, -23.2] indicates once again, that the intracluster median is much smaller than the intercluster median (**Figure 23**).

Cluster I: Regulating ODP, E: I balance, and efficacy of synaptic transmission

Cluster I contains six proteins annotated by SynGO (**Figure 24**), the largest number of all eight clusters. These include the excitatory scaffolding protein PSD-95 and the inhibitory scaffolding protein gephyrin (measured in homogenate samples). The relative levels of these two proteins are used as a proxy for the postsynaptic E: I balance (Yan et al., 2017). Thus, neuroimmune proteins in Cluster I may also play roles in maintaining the E: I balance in human V1C. Accordingly, TNFα, a quintessential proinflammatory cytokine, is also part of Cluster I. This molecule is widely implicated in

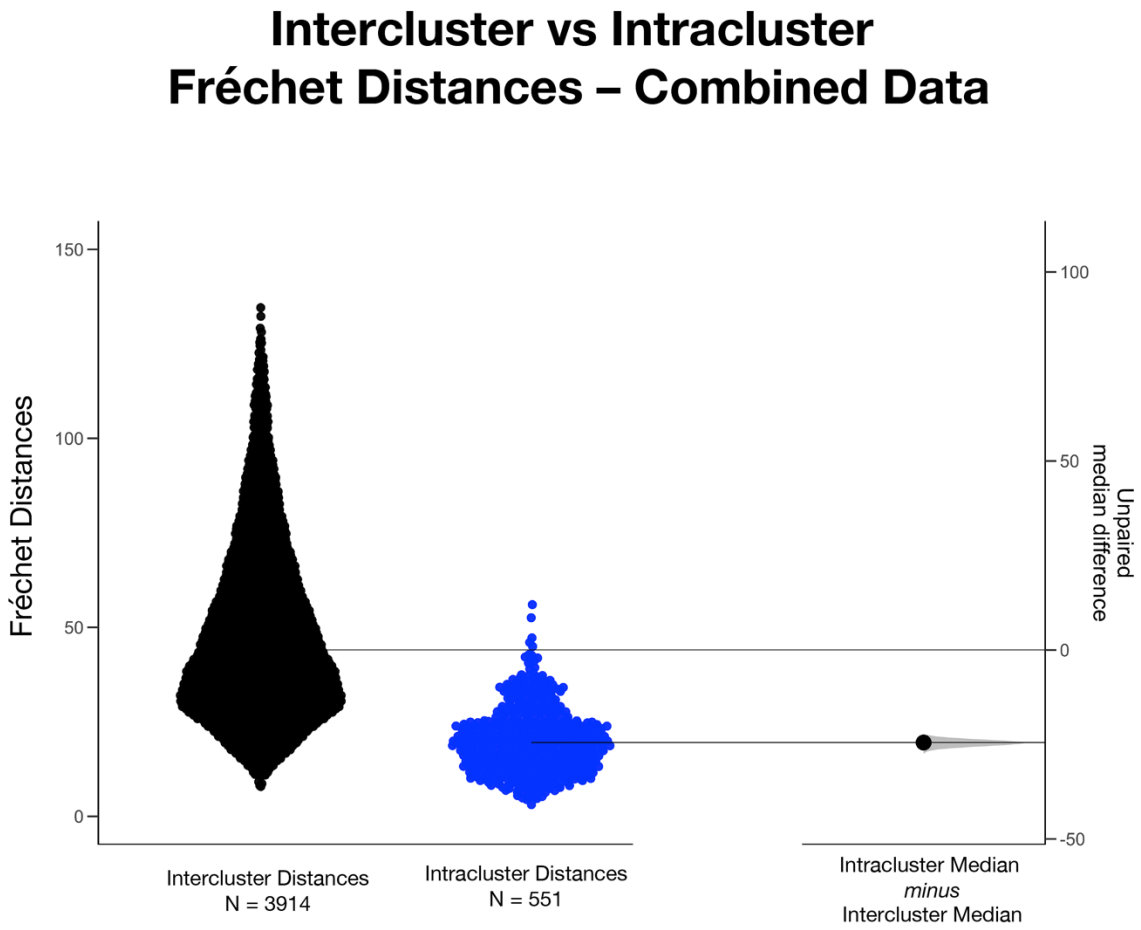
Intercluster vs Intracluster
Fréchet Distances – Combined Data
Fréchet Distances
150
100
50
0
100
50
0
-50
Unpaired
median difference
Intercluster Distances
N = 3914
Intracluster Distances
N = 551
Intracluster Median
minus
Intercluster Median

Figure 23. Median difference between intercluster and intracluster Fréchet distances – combined data. This figure corresponds to the data set produced by combining all 72 neuroimmune proteins with the 23 plasticity markers. The black dots in the swarm plot indicate the Fréchet distances between the proteins assigned to varying clusters. (i.e. intercluster distances). The Fréchet distances between proteins in the same cluster, with the exception of protein self-comparisons, are indicated by the collection of blue dots. The Fréchet distances themselves can be seen on the y-axis on the left. The median intercluster Fréchet distance is 44.0, while the median intercluster distance is 19.5. The difference between the median value of these two sets of Fréchet distances is plotted on the second y-axis on the right. Estimation statistics was used to compute a bootstrap interval for the difference (-24.5, [95CI -25.7, -23.2]).


Ward.D2 Hierarchical Clusters:
Individual Protein LOESS Curves
Cluster I
Drebrin
EGF R
Fcg RIIBC
Gephyrin.HOM
GluN2A
IL-13 R1
IL-2 Rb
IL-9
NrCAM
PSD-95.HOM
Resistin
Synapsin
TNFa
Cluster II
CB1
GDNF
GluN1
HGF
HVEM
I-TAC
IL-11
IL-16
Integrin-B3
LIF
Ube3A
VGAT
Cluster III
Angiogenin
Contactin-2
GABAA-a3
Gad67
GFAP
OPN
Synaptophysin
Cluster IV
Axl
EG-VEGF
Gephyrin
GluA2
IL-13 R2
IL-1ra
IL-4
IL-8
MICA
PDGF-BB
PSD-95
Cluster V
bFGF
Classic-MBP
Dtk
ErbB3
Flt-3L
GABAA-a1
Gad65
IL-2 Rg
MCSF
TGFa
Cluster VI
ALCAM
GABAA-a2
HCC-1
IGFBP-2
IL-6R
LAP(TGFb1)
LYVE-1
MCSF R
NAP-2
PF4
RANTES
SCF R
TIMP-1
TIMP-2
TNF RII
TRAIL R3
Trappin-2
VEGF R1
Cluster VII
Cathepsin S
CD14
CEACAM-1
Fas
GDF-15
GluN2B
ICAM-1
IGFBP-1
IL-1a
MCP-1
PARC
PECAM-1
TNF RI
Cluster VIII
CXCL16
Golli-MBP
gp130
ICAM-2
IGFBP-6
LIMPII
Lipocalin-2
PDGF-AA
PDGF-AB
Siglec-5
uPAR
Protein
Z-Score
Age (Years)
0.3
1.0
5.0
10.0
25.0
50.0
80.0

Figure 24. LOESS regression curves and SynGO classification for a set of 95 neuroimmune and classic neural plasticity proteins. Individual protein trajectories (as revealed by LOESS regression). Proteins have been grouped according to ward.D2 cluster designation. Age is plotted on a logarithmic scale on the x-axis, while protein levels (z-score) are plotted on the y-axis. Legends that specify the proteins in each cluster are found to the right of the plot with arrows indicating proteins that have known synapse-related functions according to the SynGO database. Clusters have been organized from most to least amount of SynGO annotated terms.

activity-dependent synaptic scaling (Stellwagen & Malenka, 2006) and in regulating the inhibitory synaptic strength in the mouse (Stellwagen et al., 2005).

Another candidate synaptic process for immune proteins in Cluster I is regulating synaptic efficacy. The protein drebrin has roles in structural plasticity where it regulates the morphology of dendritic spines for efficient synaptic transmission (Takahashi & Naito, 2017). This functional role is shared with the NrCAM, which plays roles in dendritic spine remodelling (Mohan et al., 2018). Synapsin too, is involved in regulating presynaptic transmission efficiency, by modulating the number of vesicles available to fuse with the synaptic membrane (Hilfiker et al., 1999).

Finally, Cluster I contains proteins known to regulate the opening and closing of the critical period for ODP. Increases in PSD-95 are associated with closing the critical period (Huang et al., 2015). Furthermore, a developmental shift to more GluN2A and less GluN2B also reduces ODP (Philpot et al., 2003; Philpot et al., 2007; Quinlan et al., 1999). Overall, Cluster I seems to represent proteins that regulate the critical period for ODP, the E: I balance, and the efficacy of synaptic transmission.

Cluster II: Modulating GABA release and synapse formation

On the other hand, Cluster II contains proteins that are associated with modulating the release of GABA. Two members of this cluster are the cannabinoid receptor 1 (CB1) and the vesicular inhibitory amino acid transporter (VGAT). While CB1 acts as a retrograde control of neurotransmitter release from the presynaptic terminal (Castillo et al., 2012; Kano et al., 2009), VGAT is responsible for the uptake of glycine or GABA into vesicles (McIntire et al., 1997; Sagné et al., 1997). Here, we find that GDNF also

clusters with CB1 and VGAT in our analysis. GDNF has been found in the developing brain to promote the differentiation and migration of cortical GABAergic neurons (Pozas & Ibáñez, 2005). Additionally, GDNF is localized at both the pre-synapse and the post-synapse suggesting that it plays a role in the formation of synapses (Ledda et al., 2007). This is important, as Cluster II also contains classic plasticity protein Integrin-β3 that orchestrates pre- and postsynaptic events (Chavis & Westbrook, 2001). Similarly, hepatocyte growth factor (HGF), another neuroimmune protein, enhances the formation of excitatory synapses (Xie et al., 2016). This suggests that another candidate plasticity process for neuroimmune proteins in Cluster II is synapse formation.

Cluster III: Temporal and spatial regulation and synaptic transmission kinetics

Cluster III contains four synapse-related proteins including gamma-aminobutyric acid receptor subunit alpha-3 ($GABA_A\alpha3$), glutamate decarboxylase 67 (GAD67), synaptophysin and contactin-2. Of particular interest are synaptophysin and contactin-2, which have been implicated in spatial and temporal regulation of development in mice hippocampal neurons (Stottmann & Rivas, 1998). Notably, these two proteins are not colocalized, in terms of time and cortical layer (Stottmann & Rivas, 1998). In our data, these proteins show fluctuating patterns across the lifespan, however, their peaks in expression are completely out of phase. This suggests that the proteins in Cluster III may be involved in spatial and temporal regulation of visual cortical development. Furthermore, synaptophysin has also been implicated in mediating the kinetics of endocytosis at synapses (Kwon & Chapman, 2011). Thus, another candidate function for proteins in Cluster III is the regulation of synaptic transmission kinetics. For example,

$GABA_A\alpha3$ is an immature subunit and has slower kinetics than the mature $GABA_A\alpha1$ (Gingrich et al., 1995). There are also variances in the kinetics of glutamate decarboxylase enzymes. GAD67 is the slower variant (compared to GAD65) of proteins that catalyze the formation of GABA (Battaglioli et al., 2003). Therefore, changes in Cluster III protein levels, and the developmental period during which these shifts occur, may indicate changing synaptic transmission kinetics.

Cluster IV and V: Maturation of synapses and regulating CNS myelination

A candidate process for proteins in Cluster IV is the maturation of glutamatergic synapses. Both the synaptoneurosome measurement of PSD-95 and GluA2 are part of this cluster. Increases in the expression of PSD-95 stabilizes activity-dependent synapses leading to the maturation of silent excitatory synapses and ending the critical period for ODP (Huang et al., 2015). Cluster V, on the other hand, is associated with myelination during the critical period, which has been traditionally considered a break in plasticity (Bavelier et al., 2010; Lyckman et al., 2008; McGee et al., 2005; Siu et al., 2015). In addition to the classic-myelin basic protein (MBP) which is responsible for the contraction of the myelin sheath around axons in response to activity (Wake et al., 2011), numerous immune markers of the tyrosine kinase family are also part of this cluster including Tyro3 and ErbB3. Tyro3 directly regulates myelination in the central nervous system (Attermann et al., 2017), while ERBB3 deletions in mice lead to developmental alterations in myelin and are associated with behavioural changes due to abnormal experience dependent plasticity (Makinodan et al., 2012). Many of the proteins in neuroimmune Cluster E, are part of the combined Cluster V, this includes bFGF which

also is implicated in oligodendrocyte myelin production (Woodbury & Ikezu, 2013). In addition, different members of the FGF protein family have been linked to the differentiation of excitatory and inhibitory synapses and regulating the E:I tone (Dabrowski & Umemori, 2016; Terauchi et al., 2010). GAD65, the protein responsible for the synthesis of the on-demand pool of GABA (Feldblum et al., 1993), is also part of this cluster. Therefore, in addition to myelination and plasticity, proteins in this cluster may participate in homeostatic plasticity to maintain appropriate levels of excitation and inhibition.

Neuroimmune only cluster: Links to IL-6 function

The final three clusters are composed of less than three proteins with known synaptic function, as annotated by SynGO. Of particular interest is the cluster with no synaptic proteins, as it contains the Golli-MBP, a molecular link between the nervous and immune systems (Pribyl et al., 1993). This cluster shows a unique pattern not observed in our plasticity marker proteins. These proteins have peaks in expression during early childhood, only to decrease rapidly to very low levels of expression in adolescence, followed by a sharp increase into aging. Specifically, the levels of expression seen in older adults ~ 79 years old (i.e. in aging), are roughly equal to the expression levels in young children ~2 years of age. In order to determine other proteins that these molecular mechanisms interact with, we used the STRINGdb to generate an integrated network using a list of predicted functional partners (**Figure 25**).

A. STRINGdb Functional Network

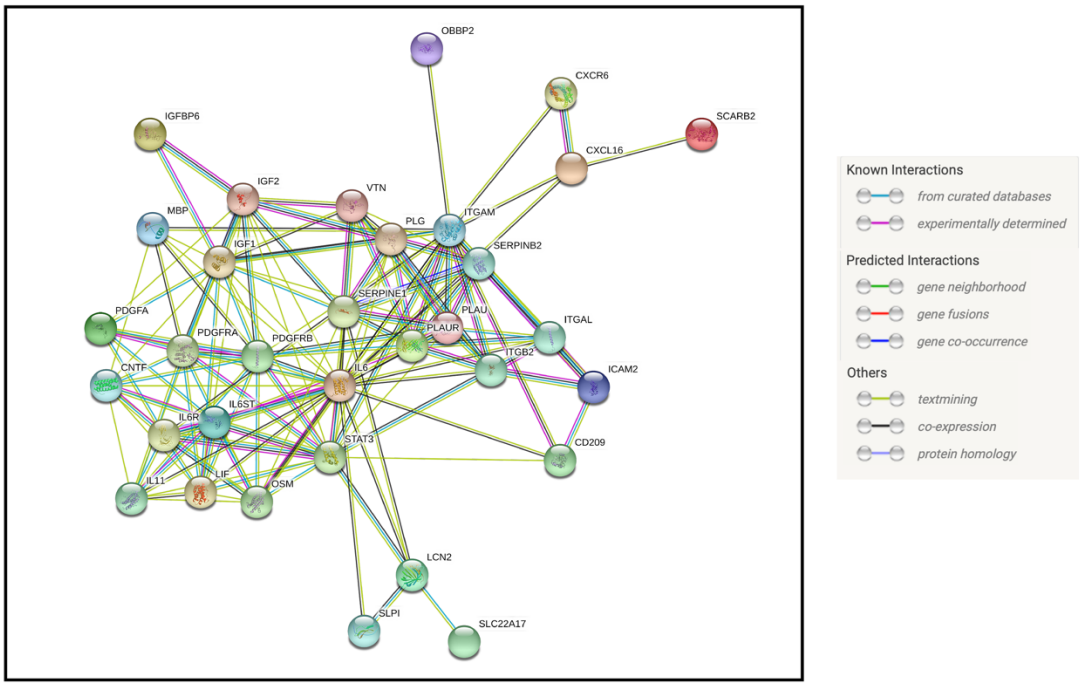

B. Functional Network GO Analysis

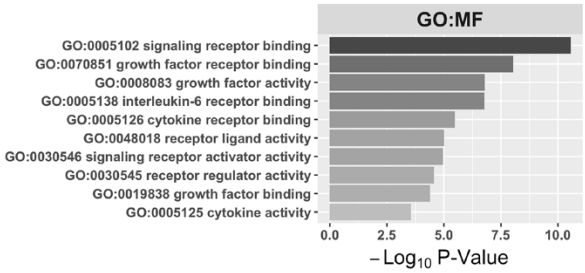

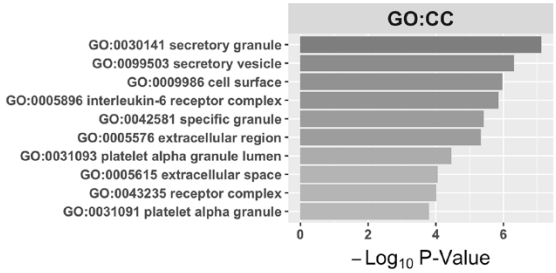

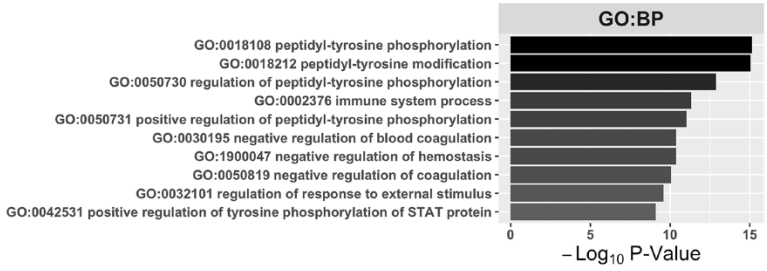

Figure 25. Functional network analysis and GO enrichment analysis of the neuroimmune cluster. When clustering all 95 neuroimmune and plasticity marker trajectories together one cluster was composed of proteins with neuroimmune functions alone, none of the proteins in this cluster were recognized by SynGO. **(A)** STRINGdb was used to determine functional partners that interact with the proteins in the neuroimmune cluster. Each node (i.e. sphere) represents a gene that encodes for the proteins in the cluster or one of the predicted functional partners. Lines between these nodes indicate a functional relationship based on: experimental evidence, documented relationships in other databases, gene neighbourhoods, knowledge of gene fusion, or gene co-occurrence. Finally, partners are also predicted by text mining, co-expression, and protein homology. Each one of these lines of evidence are colour coded. In the case that multiple forms of evidence support the functional connectedness of two proteins, multiple lines will connect the corresponding nodes. **(B)** GO enrichment analysis of the enriched molecular functions, cellular components and biological processes of the neuroimmune-only cluster members and their predicted functional partners. P-values were -log transformed and are indicated on the x-axis. GO term names, including the GO term ID, are indicated on the y-axis. Terms have been sorted from top to bottom in order of increasing p-value. Smaller p-values (i.e. larger -log(p-values)) are coloured black, while larger p-values are filled with a translucent grey shade. Note that all terms listed meet the threshold for statistical significance ($p < 0.05$).

Completing a GO analysis on the network of proteins reveals that they are enriched for molecular functions including signalling receptor binding ($p < 0.001$), growth factor activity ($p < 0.001$) and IL-6 receptor binding ($p < 0.001$). In terms of cellular components these proteins are found in secretory granules ($p < 0.001$), the cell surface ($p < 0.001$) and are part of the IL-6 receptor complex ($p < 0.001$). Finally, these molecules are part of biological processes associated with peptidyl-tyrosine phosphorylation ($p < 0.001$), peptidyl-tyrosine modification ($p < 0.001$) and immune system processes ($p < 0.001$) in general. While many of these terms overlap the enrichment results for the entire collection of 72 neuroimmune proteins, the STRINGdb analysis places IL-6 at the center of the functional network. Moreover, the enrichment analysis reveals IL-6 related functions. IL-6 is a pleiotropic cytokine that has been analyzed extensively in the context of neuropsychiatric disease and is often used as an indicator of inflammatory state (Borovcanin et al., 2017; Erta et al., 2012; Ng et al., 2018). The association of IL-6 with this cluster raises the question of whether these diseases are truly a case of neuroprogression, or whether they could also be interpreted as neuroregression, as protein levels for these proteins are as high in young children as they are in older adults.

Overall, both approaches to understanding the relationship between neuroimmune and classic plasticity marker trajectories reveal that shared developmental patterns are indicative of shared plasticity and development related functions.

Profiling development of human V1C

Lifespan trajectories reveal that protein levels are similar at extremely different periods of the lifespan. In order to determine whether protein expression alone is able to

identify sample age, we performed RSKC on the neuroimmune expression and the plasticity marker expression. This unsupervised clustering algorithm received only protein expression values, with no information about the age of the cases. A prediction-based resampling method revealed that the optimal number of clusters for the plasticity marker data set was six. In order to use the plasticity markers as a guide to unpack neuroimmune human development profiles, six was used as the optimal number of clusters for both collections of proteins.

First, we clustered the cases using solely the neuroimmune protein expression values and calculated the median age and interquartile range (IQR) for each cluster. We obtained clusters with progressing median age (Cluster A: Mdn = 0.26 years, IQR [0.16, 0.30]; Cluster B: 0.35 years, IQR [0.29, 0.37]; Cluster C: 2.21 years, IQR[1.78, 2.78]; Cluster D: 5.39 years, IQR[4.56, 8.14]; Cluster E: 15.22 years, IQR[12.45, 22.98]; Cluster F: 70.61 years, IQR[65.45, 73.81]) (**Figure 26**). The youngest two clusters consist of cases of similar age as the difference between the median ages is only 0.09 years. As the case clusters are formed based on protein expression vectors, this may indicate separate biological states that occur during the same period of the lifespan. The rest of the clusters are relatively discrete, where the IQR of cluster ages do not overlap.

The RSKC algorithm weights proteins based on their importance to creating the case clusters. Here, the proteins with the greatest weights are tissue inhibitors of metalloproteinases 2 (TIMP-2), Flt-3L, vascular endothelial growth factor receptor 1 (VEGF R1). These proteins show great changes in their protein expression levels across the lifespan.

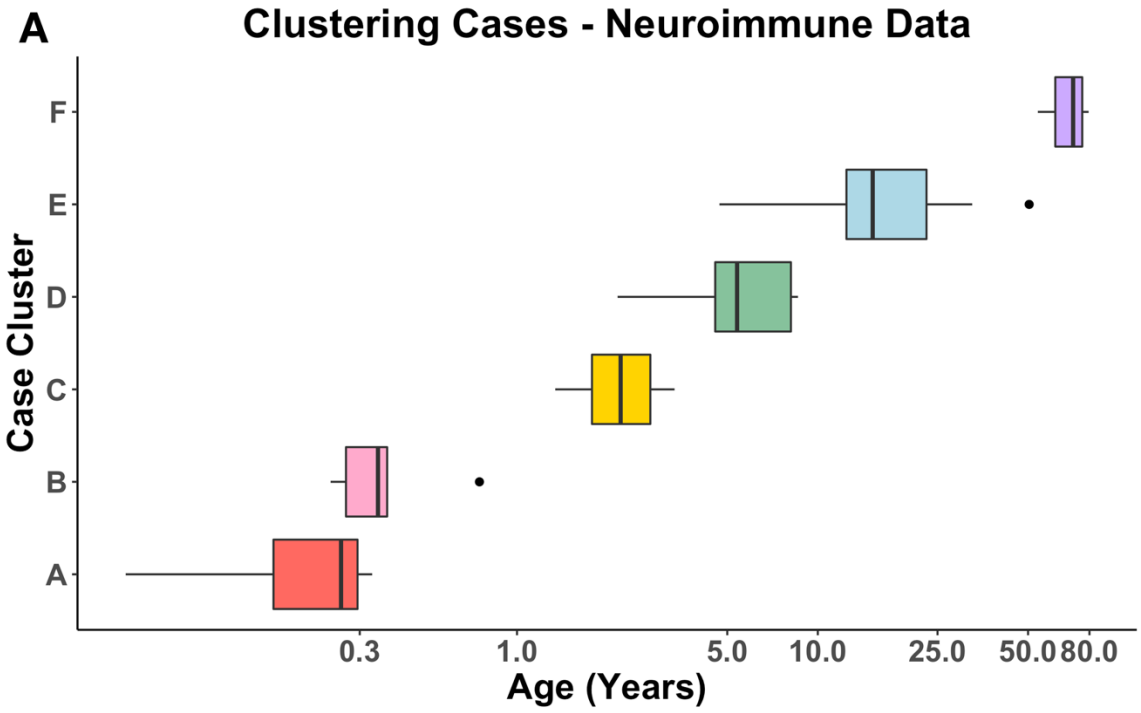
A
Clustering Cases - Neuroimmune Data
Case Cluster
F
E
D
C
B
A
0.3
1.0
5.0
10.0
25.0
50.0
80.0
Age (Years)

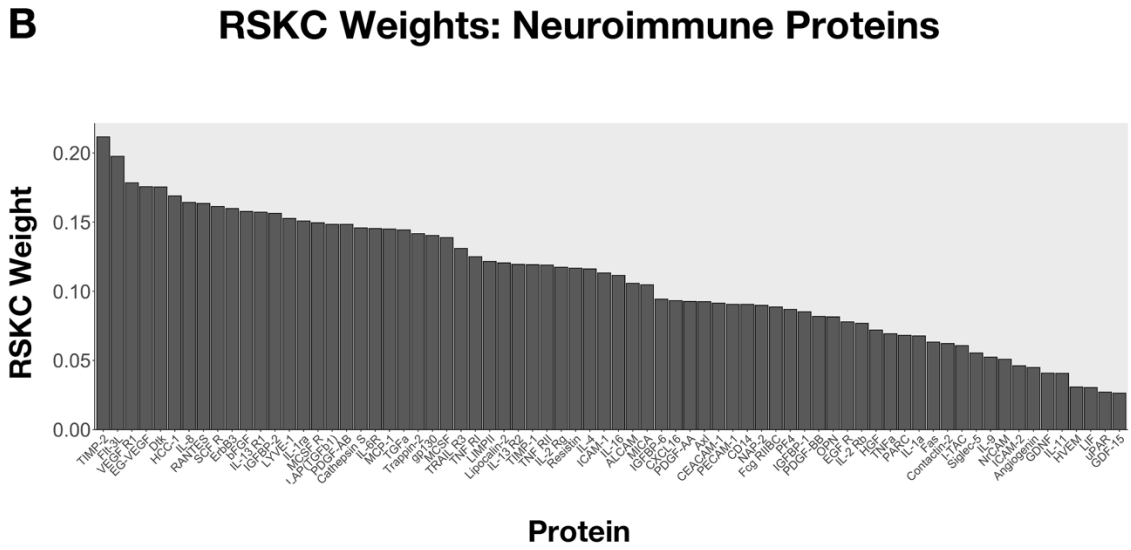
B
RSKC Weights: Neuroimmune Proteins
RSKC Weight
0.20
0.15
0.10
0.05
0.00
Protein

Figure 26. Box plots of the RSKC case clusters derived from neuroimmune expression vectors. Cases were clustered together based on the log2 expression values of 72 neuroimmune proteins. **(A)** High-dimensional clustering using the RSKC algorithm reveals 6 clusters. Cluster IQRs were calculated and plotted to reveal progressing median age. Age is plotted on a logarithmic scale on the x-axis, and the clusters themselves are plotted on the y-axis from youngest to oldest median age. Box plot whiskers indicate the minimum and maximum values that fall within 1.5* IQR. Values outside this range are considered outliers and are indicated as black dots. If none of the values in a cluster are larger than the 75th percentile and within 1.5*IQR, then an upper whisker is not depicted. If none of the values are smaller than the 25th percentile and within 1.5*IQR, then a lower whisker is not depicted. **(B)** RSKC weights assigned to the 72 proteins reflect their importance in forming the case clusters. Proteins are organized from largest to smallest weight.

In comparison, the proteins that are weighed the least are leukemia inhibitory factor (LIF) and urokinase receptor (uPAR). These have relatively less fluctuation in protein levels across the lifespan. The outlier here is growth differentiation factor (GDF-15), which shows an undulating pattern and yet is the lowest weighted protein. This suggests that fluctuation and high magnitude of change across the lifespan is not sufficient to weight a protein highly. Thus, it seem that more subtle patterns are emphasized in the weighting of proteins during RSKC.

To create a profile of human development, we took the protein expression values, multiplied them by their RSKC weights and calculated a sum of these weighted expression values for each case. The summed values were z-scored to scale the values and obtain total protein levels across the lifespan (**Figure 27**). This analysis revealed increasing neuroimmune protein levels during early development with a peak in expression in young children. These expression levels then decrease.

Clustering the same cases using the plasticity marker data (**Figure 28**), we find once again that the clusters show progressing median age (Cluster A: Mdn = 0.33 years, IQR[0.27, 0.35]; Cluster B: 0.75 years, IQR[0.56, 2.66]; Cluster C: 4.71 years, IQR[1.34, 9.13]; Cluster D: 8.14 years, IQR[5.39, 15.22]; Cluster E: 12.86 years, IQR[9.89, 18.11]; Cluster F: 61.60 years, IQR[51.30, 71.26]). In contrast to the neuroimmune data however, the youngest two cases do not have overlapping age IQRs. Here, the intermediate clusters (i.e. Cluster B to Cluster E) all have overlapping IQRs, while the youngest and oldest clusters stand apart.

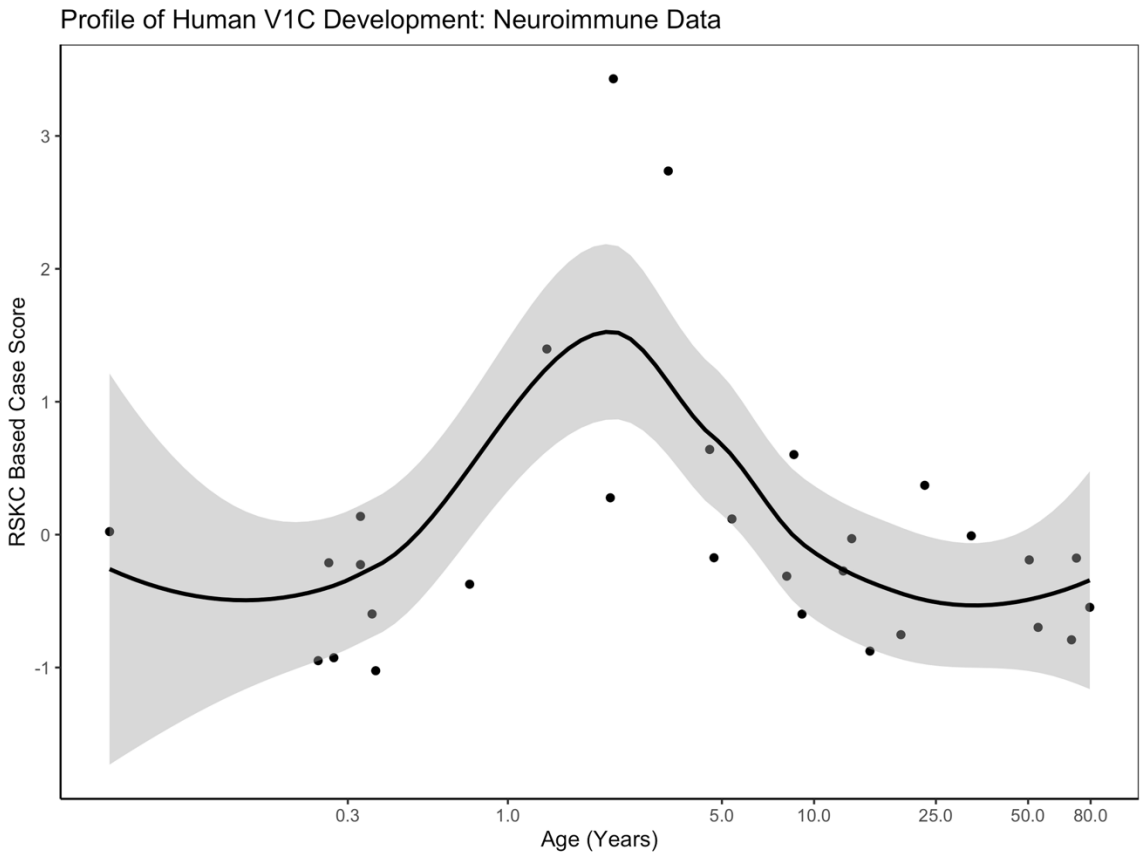
Profile of Human V1C Development: Neuroimmune Data
RSKC Based Case Score
3
2
1
0
-1
0.3
1.0
5.0
10.0
25.0
50.0
80.0
Age (Years)

Figure 27. Profile of human V1 development using neuroimmune weighted expression. Cases were given a score based on the total weighted expression across all 72 neuroimmune proteins. Weighted expression was obtained by multiplying each protein's expression values by its RSKC weight. The sum of these weighted expression values was calculated for each case. Values were scaled by calculating a z-score. Age is plotted on a logarithmic scale on the x-axis. Weighted expression levels are plotted on the y-axis. A LOESS curve was fit to these values. There is a wave of increased neuroimmune expression in early childhood between 2-3 years of age, expression levels are similar during the neonatal period and in aging.

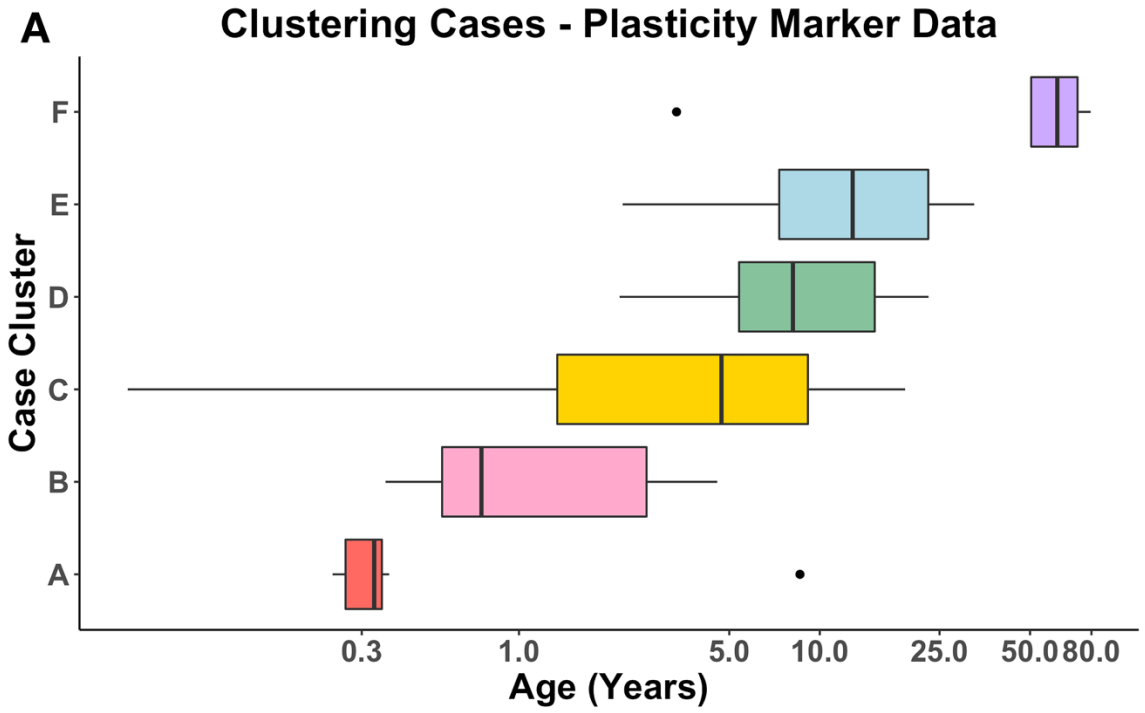
A
Clustering Cases - Plasticity Marker Data
Case Cluster
F
E
D
C
B
A
0.3
1.0
5.0
10.0
25.0
50.0
80.0
Age (Years)

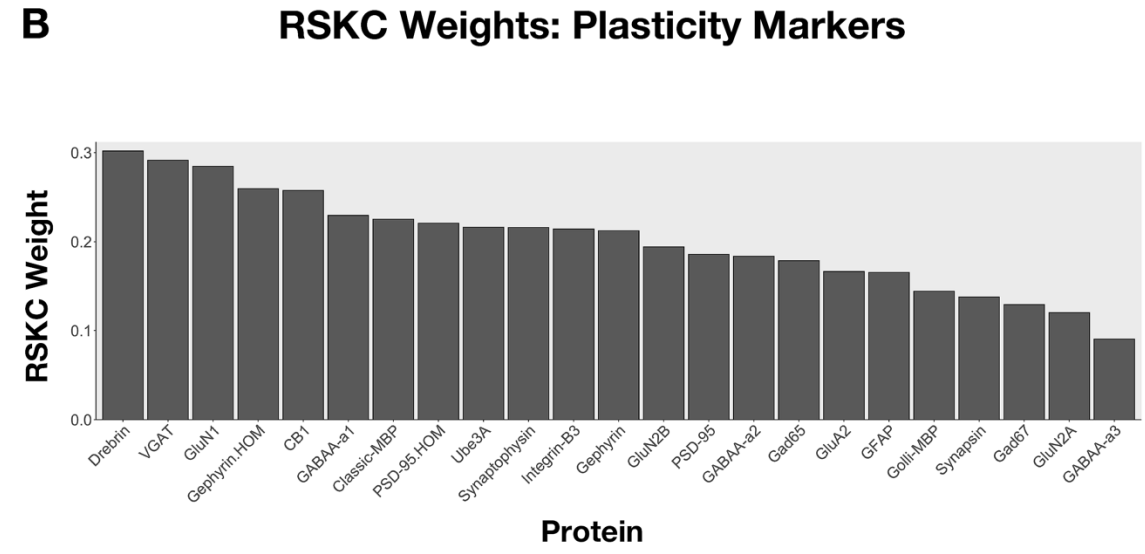
B
RSKC Weights: Plasticity Markers
RSKC Weight
0.3
0.2
0.1
0.0
Drebrin
VGAT
GluN1
Gephyrin.HOM
CB1
GABAA-a1
Classic-MBP
PSD-95.HOM
Ube3A
Synaptophysin
Integrin-B3
Gephyrin
GluN2B
PSD-95
GABAA-a2
Gad65
GluA2
GFAP
Golli-MBP
Synapsin
Gad67
GluN2A
GABAA-a3
Protein

Figure 28. Box plots of the RSKC case clusters derived from classic neural plasticity marker expression vectors. Cases were clustered together based on the relative expression values of 23 plasticity trajectories. **(A)** High-dimensional clustering using the RSKC algorithm reveals 6 clusters. Cluster IQR were calculated and plotted to reveal progressing median age. Age is plotted on a logarithmic scale on the x-axis, and the clusters themselves are plotted on the y-axis from youngest to oldest median age. Box plot whiskers indicate the minimum and maximum values that fall within 1.5* IQR. Values outside this range and considered outliers and are indicated as black dots. If none of the values in a cluster are larger than the 75th percentile and within 1.5*IQR, then an upper whisker is not depicted. If none of the values are smaller than the 25th percentile and within 1.5*IQR, then a lower whisker is not depicted. **(B)** RSKC weights assigned to the 23 trajectories reflecting their importance in forming the case clusters. Proteins are organized from largest to smallest weight.

This reveals greater interindividual variability during early childhood and adolescence in the profile of classic plasticity markers as compared to neuroimmune profiles. In weighting the proteins, there are no apparent trends in the synaptic data set. Proteins from the same cluster, with similar patterns are weighted differently. In the neuroimmune data set 33 proteins were assigned low weights, with magnitudes below 0.1. Comparatively, only $GABA_A\alpha3$ in the plasticity marker data set was assigned a weight less than 0.1. This indicates that almost all synaptic proteins were important in forming case clusters that show age progression.

To compare the cluster designations, we calculated a Jaccard similarity coefficient (J) and found only a 21% similarity between the clustering results (**Figure 29**). While both collection of proteins show progressing median age, the similarity measure further confirms that the nuances of their development in the human V1C are varied. When comparing clustering results between individual clusters we found that the greatest level of similarity occurs between Cluster F (J = 0.667) which has a median age corresponding to late adulthood (55+ years old). Here, 100% of the cases placed in the oldest cluster (Cluster F) when clustering with neuroimmune data, are placed in the oldest cluster when clustering with the plasticity marker data. Cluster D, which has a median age corresponding to late childhood (5-11 years old), also shows a moderate degree of similarity between the two data sets. 60% of the cases which fall into neuroimmune Cluster D data also fall into plasticity marker Cluster D. The resulting Jaccard similarity coefficient for the two Cluster Ds is J = 0.429.

Case Cluster Comparison: Neuroimmune vs Plasticity Markers Data

A

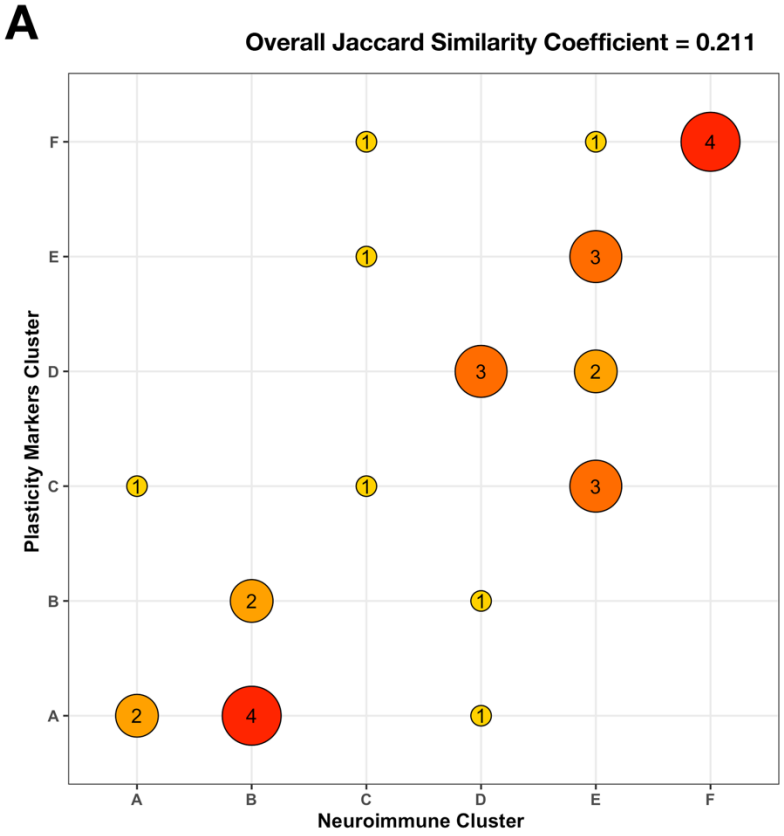

B

Age (Years)	Neuroimmune Proteins	Plasticity Markers
0.05	A	C
0.24	B	A
0.26	A	A
0.27	B	A
0.33	B	A
0.33	A	A
0.36	B	B
0.37	B	A
0.75	B	B
1.34	C	C
2.16	D	D
2.21	C	E
3.34	C	F
4.56	D	B
4.71	E	C
5.39	D	D
8.14	D	D
8.59	D	A
9.13	E	C
12.45	E	E
13.27	E	E
15.22	E	D
19.21	E	C
22.98	E	D
32.61	E	E
50.43	E	F
53.90	F	F
69.30	F	F
71.91	F	F
79.50	F	F

C

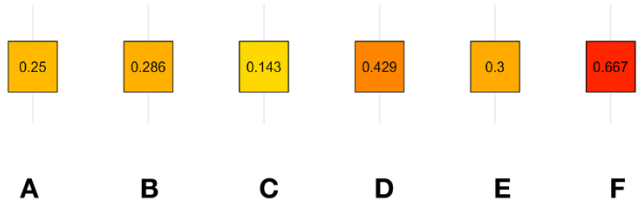

Jaccard Similarity Coefficient per Cluster

Figure 29. Jaccard similarity coefficient between neuroimmune and plasticity expression-based case-cluster designations. Clustering the 30 cases using the neuroimmune expression, or the plasticity marker expression, both reveal clusters with progressing median age. Nonetheless, the composition of the clusters is not the same. **(A)** Bubble plot indicating the neuroimmune cluster designation on the x-axis and the plasticity marker designation on the y-axis. Each bubble indicates the number of cases that were classified at the intersection on point. For example, two cases were assigned to the youngest cluster "A" when clustering with the neuroimmune data and the classic plasticity marker data. Bubbles are coloured from yellow to red, with yellow representing a smaller number and red representing larger numbers. The size of bubbles also increases as the number increases. At the top right corner of the plot, the Jaccard similarity coefficient between the overall clustering results is indicated (i.e. ~0.211) **(B)** Table indicating the age of the cases and their cluster designation when using with either the neuroimmune expression or classic plasticity marker expression as the RSKC input. **(C)** Jaccard similarity coefficient indicating the similarity of individual clusters between the neuroimmune and classic plasticity marker RSKC results.

On the other hand, during the early postnatal periods as well as infancy, early childhood and adolescence, neuroimmune and classic neural developmental patterns do not coincide. Accordingly, the Jaccard similarity coefficients of the remaining clusters drops to 0.300 or lower. This illustrates that the developmental profile of neuroimmune and classic neural plasticity markers are not the same in the human V1C.

Overall, protein expression alone is sufficient to form age-based clusters, as both data sets reveal clusters with progressing median age, albeit with different median ages. This is important as protein expression levels are similar at drastically different stages of the lifespan. Nonetheless, the relative levels of protein expression provide enough information to group cases of similar age together using their protein expression vectors.

Heightened expression of viral receptors during childhood in the human V1C

The visual cortex has dense microvasculature (Schmid et al., 2019) and is therefore vulnerable to viral infections that compromise the integrity of the BBB (Spindler & Hsu, 2012). As evidenced by the results of our GO cellular component analysis, many of the proteins explored in this study are cell surface receptors that may be hijacked by viruses to infect host cells. We used the UniProt database to determine a list of viral receptors using the keyword “Host cell receptor for virus entry (KW-1183)” and matched the results to our list of proteins. We found that seven of the proteins explored in this study are receptors that facilitate entry for human viruses. To explore whether there are any relationships between their trajectories and their viral functions, we plotted all seven trajectories and found a wave of heightened viral receptor expression in early childhood, before 5 years of age (**Figure 30**).

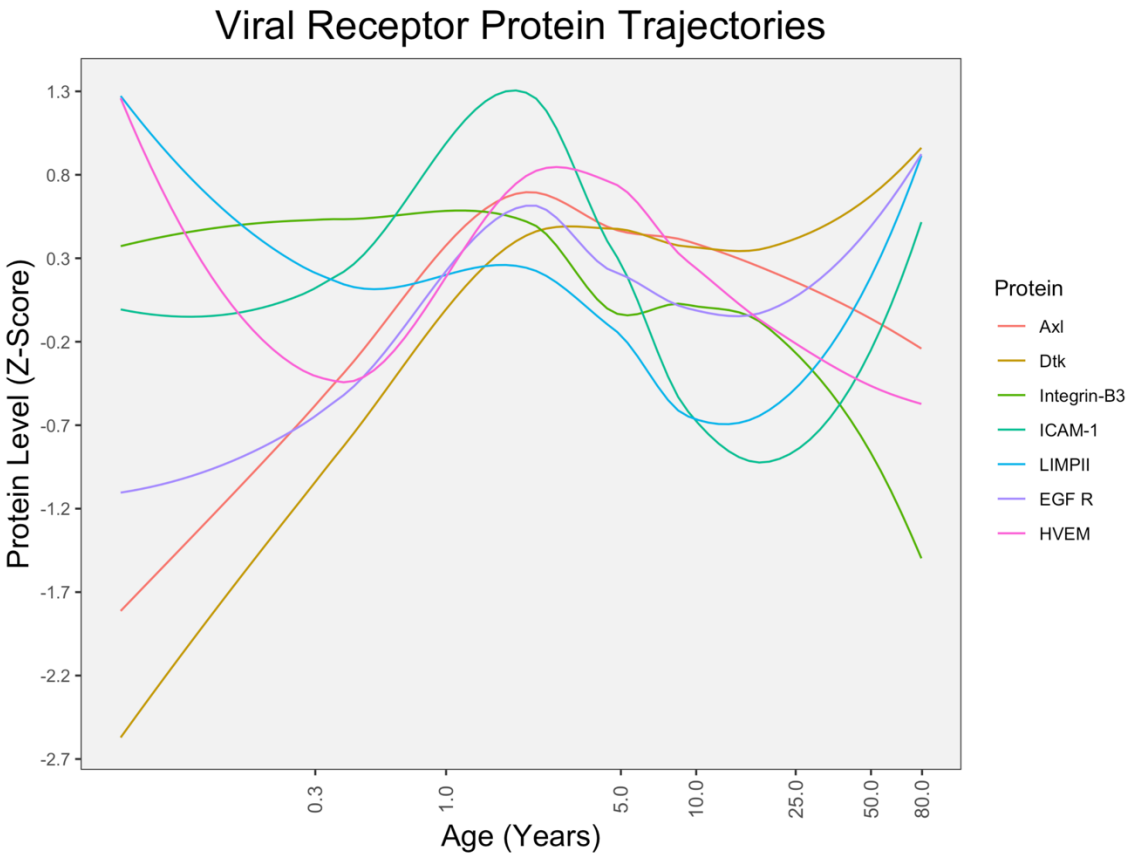
Viral Receptor Protein Trajectories
Protein Level (Z-Score)
1.3
0.8
0.3
-0.2
-0.7
-1.2
-1.7
-2.2
-2.7
0.3
1.0
5.0
10.0
25.0
50.0
80.0
Age (Years)
Protein
Axl
Dtk
Integrin-B3
ICAM-1
LIMPII
EGF R
HVEM

Figure 30. Viral receptor protein trajectories across the lifespan. UniProt search reveals that seven proteins in our collection of molecular markers are receptors for viruses that infect humans. The lifespan trajectory of all seven proteins has been plotted on the same graph for comparison of their developmental profiles. Age is plotted on a logarithmic scale on the x-axis and the protein levels (z-score) are indicated on the y-axis. A legend can be found indicating the color that has been assigned to each protein.

Next, we mapped the receptors to specific viruses and viral families (Qi et al., 2020). We found that the seven receptors are associated with 7 different viral families including Arenaviridae, Filoviridae, Flaviviridae, Hantaviridae, Orthomyxoviridae, Picornaviridae and Herpesviridae (**Figure 31**). These viral receptors were associated with 14 different viruses. Tyro3 and tyrosine-protein kinase receptor UFO (Axl) act as receptors for the same set of viruses including lymphocytic chroiomeningitis mammarenavirus, lassa mammarenavirus, margurgvirus and ebola virus. Interestingly, these two proteins show very similar trajectories until ~5 years of age at which point the trajectories veer off into opposite directions. More specifically, Tyro3 increases into aging while Axl decreases into aging. Furthermore, many of these proteins including intercellular adhesion molecule 1 (ICAM-1), Integrin-β3, lysosome membrane protein 2 (LIMPII) are receptors for various strains of Coxsackievirus, which causes hand foot and mouth disease (HFMD) and occurs most commonly in young children less than 5 years old (Liu et al., 2019). Note that these proteins also show peaks in expression during early childhood (absolute max for ICAM-1, Integrin-β3; local max for LIMPII). Of the remaining proteins epidermal growth factor receptor (EGF R) is a viral receptor for the influenza A virus, herpes virus entry mediator A (HVEM) is a receptor for herpes. Additionally, Integrin-β3 is also a receptor for West Nile Virus. As most of the viral receptors show peaks in expression during early childhood, there is reason to believe that this period of development presents increased risk of viral insult in the brain, which not only disrupts the functioning of neural circuits but can predispose individuals to psychiatric disorders in later development (Atluri et al., 2015; Hornig & Lipkin, 2001).

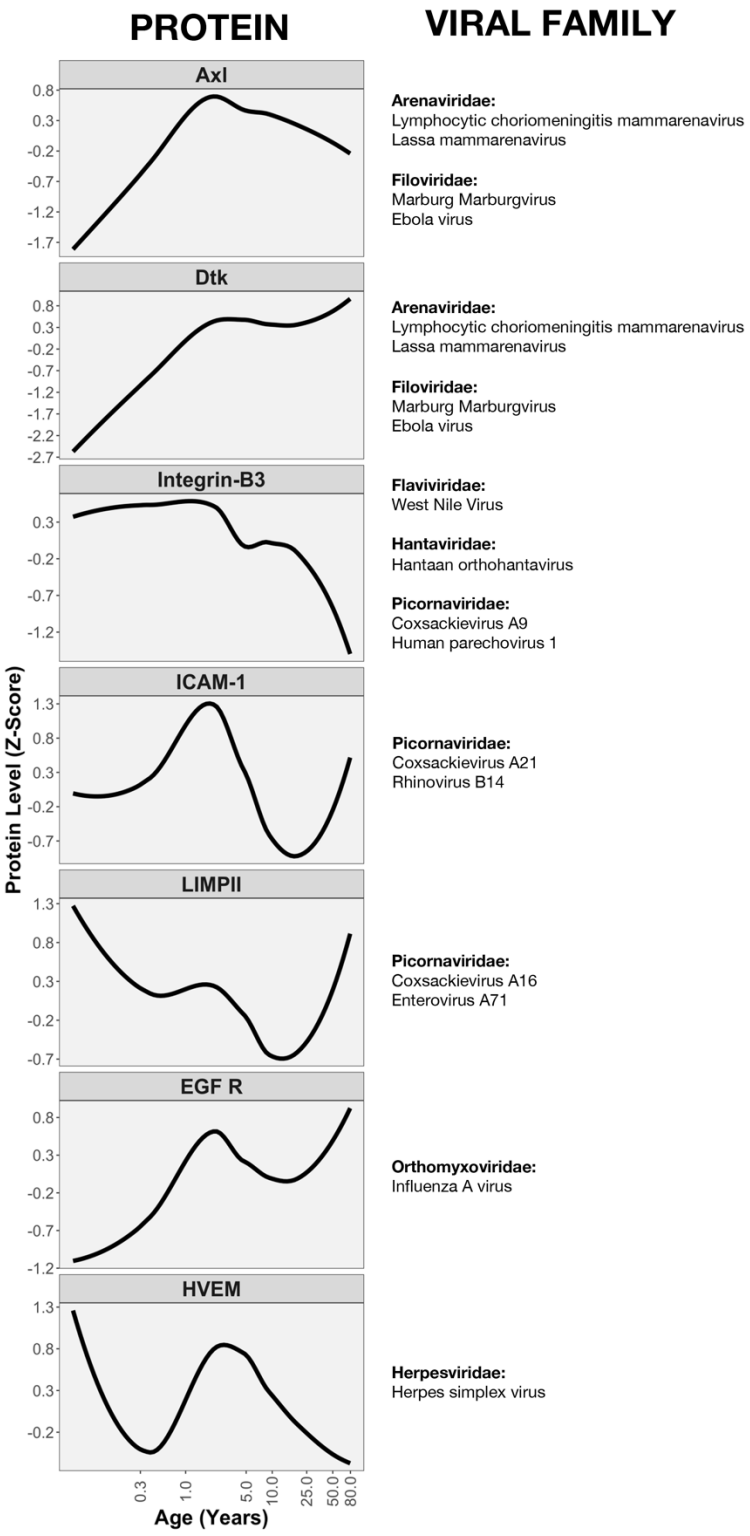
PROTEIN
VIRAL FAMILY
Axl
Arenaviridae:
Lymphocytic choriomeningitis mammarenavirus
Lassa mammarenavirus
Filoviridae:
Marburg Marburgvirus
Ebola virus
Dtk
Arenaviridae:
Lymphocytic choriomeningitis mammarenavirus
Lassa mammarenavirus
Filoviridae:
Marburg Marburgvirus
Ebola virus
Integrin-B3
Flaviviridae:
West Nile Virus
Hantaviridae:
Hantaan orthohantavirus
Picornaviridae:
Coxsackievirus A9
Human parechovirus 1
ICAM-1
Picornaviridae:
Coxsackievirus A21
Rhinovirus B14
LIMPII
Picornaviridae:
Coxsackievirus A16
Enterovirus A71
EGF R
Orthomyxoviridae:
Influenza A virus
HVEM
Herpesviridae:
Herpes simplex virus
Protein Level (Z-Score)
Age (Years)
0.3
1.0
5.0
10.0
25.0
50.0
80.0

Figure 31. Viral families, strains and associated receptors. Of the 93 unique proteins in our combined data set, 7 proteins are receptors for viruses that infect humans. The lifespan trajectory of all seven proteins has been plotted with age on a logarithmic scale on the x-axis and the protein levels (z-score) on the y-axis. The name of the viral family that the receptor is associated with is indicated in bold letters, with specific viruses indicated underneath. Note that some proteins are associated with one viral family and one specific viral strain, while other proteins are receptors for multiple viral families and numerous viral strains.

2.4 Discussion

The aim of this study was to characterize the lifespan trajectories of 72 neuroimmune proteins in the human VIC. We found that these molecular mechanisms show a range of undulating patterns across the lifespan. Importantly, immune markers do not globally increase into aging. The "inflammaging" model suggests that aging is a progressive increase in proinflammatory state, resulting in a reduced ability to deal with stressors (Franceschi et al., 2000). This model has been used to describe neurodegenerative disorders such as AD (Giunta et al., 2008) as well as neuropsychiatric disorders such as schizophrenia (Nguyen et al., 2017). Diseases are therefore described as brain states with high levels of inflammation characteristic of later stages of life (Franceschi et al., 2018). In our data set however, proteins that are traditionally considered to be proinflammatory like interleukin-8 (IL-8) show lower levels of expression in aging when compared to early postnatal development.

While the protein trajectories reveal complex and dynamic lifespan trajectories, we recognized that some expression patterns were shared amongst proteins. Ward.D2 hierarchical clustering identified eight trajectory clusters for our neuroimmune markers. Fréchet distances along with estimation statistics revealed that none of the clusters had overlapping median Fréchet scores, allowing us to be confident that the eight clusters are truly different. Lehallier et al. (2019) examined the lifespan profiles of almost 3,000 plasma proteins and found that these also grouped into eight clusters. Similar to our study, they found that the developmental profile of these plasma proteins is not strictly linear, but rather undulating across the lifespan (Lehallier et al., 2019). While the number

of proteins assessed in that paper is much higher than that of our study, a similar number of unique trajectories was found. As a result, it seems that human brain development, at the level of protein expression, follows a limited number of undulating trajectories.

A GO enrichment analysis was used to pick out the top 25 molecular functions, cellular components and biological processes that are enriched in our collection of neuroimmune proteins. We found that these terms had to do with signalling, cytokine activity, receptor activity, the cell surface, extracellular regions and phosphorylation. As our protein collection is composed of immune markers measured in a membrane sample preparation, these findings are not new or unexpected. We found no clear relationship between the lifespan trajectories and their functions when we examined the clusters individually. This revealed that protein clusters are composed of proteins with a range of biological functions.

Nonetheless, we did find functional relationships when evaluating the similarity between neuroimmune and classic plasticity marker development. Two parallel approaches were taken to assess this similarity. In the first approach, cluster designations were maintained and eight neuroimmune clusters were compared to five classic plasticity clusters. The similarity between these groups of proteins was assessed using the Fréchet distance metric. This analysis revealed that select proteins in both data sets show increasing expression across the lifespan, with a small decrease into aging. Included in this list of proteins are classic MBP and neuroimmune markers that regulate myelination in the CNS; such as Tyro3 (Attermann et al., 2017), ErbB3 (Makinodan et al., 2012) and bFGF (Woodbury & Ikezu, 2013). These results indicate that proteins regulating CNS

myelination increase in expression for most of the lifespan, especially in early development when the brain is highly plastic.

The second approach to comparing these two collections of proteins involved clustering all 95 protein trajectories together. Using the classic neural proteins as a guide, we revealed that immune proteins with roles in synaptic scaling and synaptic transmission like TNFα (Stellwagen et al., 2005; Stellwagen & Malenka, 2006) are clustered with classic neural proteins like PSD-95, synapsin and drebrin, which are also associated with the synaptic plasticity and transmission (Hilfiker et al., 1999; Huang et al., 2015; Takahashi & Naito, 2017). Other clusters revealed that proteins involved in GABAergic signalling cluster together and that proteins regulating the critical period for ODP cluster together. This suggests that regulators of synaptic plasticity follow similar expression patterns in the human V1C, whether they be classically neural or classically immune.

Notably, one of the clusters obtained from partitioning the combined data set was composed only of proteins with immune functions. This cluster demonstrated increasing expression levels from adolescence (at ~13 years) to late stages of the lifespan (~79 years). While this pattern supports the popular view that there is an increase in inflammation in aging, and that these increases are exacerbated in disease, the proteins in the "immune-only" cluster have equally high levels of expression during early childhood. Studies looking at inflammation, disease and aging in general tend to compare inflammatory expression levels between young adults and older adults. They are also likely to compare expressions between adults with neurological disorders to age-matched

controls. Very little work, however, has compared the inflammatory levels of older adults, or those affected by disease, to neonates, infants and young children. Our data suggests that we may find that older adults, and those suffering from neuropsychiatric disease, have comparable inflammatory expression levels to unaffected young children. This may indicate differing roles for neuroimmune proteins at different points in the lifespan.

Overall, taking a set of plasticity markers that regulate experience-dependent plasticity in the human V1C, we show that certain lifespan expression patterns are shared by the two classes of proteins. Specifically, both collections contain markers with increasing, and undulating patterns of expression. Analyzing these shared developmental patterns revealed shared functions. Additionally, we found that while some classic plasticity markers have reduced expression in early childhood, this pattern was not observed in any neuroimmune clusters.

Next, to characterize the human V1C development we clustered the cases in our study based on protein expression. We observed that protein expression is sufficient to group cases together by their age. These clusters show progressing median age. This is unexpected as many proteins have similar expression levels during drastically different points in the lifespan, such as during early childhood and in aging. Our findings suggest that the relative levels of proteins are varied in individuals of drastically different ages. Furthermore, when clustering using the neuroimmune proteins we find that there *are* overlapping clusters composed of neonates and infants. We interpret these overlapping clusters as different biological states that exist during the similar stages of the lifespan.

Comparatively, the case clusters mostly overlap when partitioning them using classic neural protein expression. The only cluster that stands on its own, regardless of clustering with neuroimmune or classic plasticity data is that composed of older adults (55+ years). As the cluster corresponding to older adults is discrete from all others, the profile of older adults seems the most robust. Finally, we compared the case cluster designations obtained from neuroimmune and classic plasticity marker data. We found that the cases designated to the oldest cluster overlap the most between these two data sets. Nonetheless, developmental profiles are quite varied in the intervening years.

In light of the novel coronavirus outbreak, the interactions between viral antigens and the human immune system have been the topic of immense investigation. Many of the proteins in this study are located on the cell surface and are candidates for viral interaction. Therefore, we investigated whether our collection of proteins are receptors for any human viruses. We found that seven of our proteins act as viral entry receptors for seven different families of viruses and 14 different viral strains. Interestingly, all of these viruses are known to attack the CNS (Anastasina et al., 2017; Conrady et al., 2010; Huang & Shih 2015; Kakooza-Mwesige et al., 2019; Kang & McGavern, 2008; Studahl, 2003). The majority of these viruses show increased levels of expression before five years of age in our data set. Particularly, three of the seven proteins are receptors for varying strains of HFMD. Notably, this disease most commonly affects children less than five years old (Liu et al., 2019), which overlaps with the developmental period where there is high expression for these immune markers. These results show that early childhood represents a period of heightened vulnerability to viral infection in the brain.

Nevertheless, the relationship between neuroimmune proteins and viral infection is not solely negative. Counterintuitively, some of the proteins that mediate viral entry also promote the integrity of the BBB. Axl and Tyro3 are part of the TAM family of proteins that maintain the integrity of the BBB in the event of viral infection (Shafit-Zagardo et al., 2018; Wang et al., 2020). Moreover, these proteins are thought to have protective roles in the CNS through suppressing the levels of proinflammatory cytokines and promoting stem cell survival (Ji et al., 2013).

In conclusion, unpacking the lifespan trajectories of neuroimmune markers has significant implications for translational research and the development of therapeutics for psychiatric and neurodevelopmental disorders. As neuroimmune markers are considered to be central to the pathological conditions, understanding which immune proteins have elevated levels, and most importantly *when* these elevations occur, will be instrumental in developing treatments that are timely and effective. Similarly, charting the patterns of neuroimmune development is essential in verifying whether patterns observed in mice models of psychiatric and neurodevelopmental disorders actually translate to humans.

Chapter 3. General Discussion

3.1 Summary of Main Findings

My thesis contributes to the understanding of how neuroimmune proteins change across the lifespan. As most studies focus on animal models and measure gene expression, my thesis fills the knowledge gap about how protein levels of cytokines, chemokines, growth factors and other inflammatory factors change across the lifespan in the human cortex. Furthermore, my thesis compares these neuroimmune markers to classic neural proteins, to determine whether they show similar patterns. Finally, I explore different functions for these neuroimmune proteins and connect these functions to the lifespan trajectories.

Neuroimmune proteins expressed in the human V1C show a wide range of developmental profiles. Some proteins increase across the lifespan, while others decrease. We also observed that the majority of proteins had undulating trajectories, following a series of increases and decreases in protein levels across the lifespan. While the development of neuroimmune proteins in the human cortex could not be explained by a common trajectory, we also did not observe 72 unique trajectories. Rather eight common trajectory patterns were determined using hierarchical clustering.

Through the GO analysis we determined that trajectories and function in the human V1C do not map onto one another in a one-to-one relationship. In other words, proteins with similar trajectories were not associated with the same set of functions. Nonetheless, by calculating the Fréchet distance between classic neural proteins and neuroimmune markers we found that proteins (in both data sets) involved in myelination show increasing patterns into adulthood with slight decreases in protein levels into aging.

A parallel approach to comparing the neuroimmune and plasticity clusters, involved clustering all 95 trajectories together. This analysis revealed that certain lifespan expression patterns are common to both neuroimmune and classic neural proteins, while other patterns are unique. In particular, while some proteins in the plasticity marker collection show the lowest level of protein expression in early childhood (ex. drebrin, synaptophysin, $GABA_A\alpha3$, and GAD67) this expression pattern is not seen in the neuroimmune data. On the other hand, a collection of neuroimmune proteins show an undulating pattern not seen in the plasticity marker data. These proteins increase from almost no expression in adolescence to high expression levels in late adulthood. Nonetheless, this is only part of the picture, as these proteins have similarly high levels of expression in early childhood. Using online databases to determine functional partners for these proteins reveals that they are connected to IL-6 function, which is a commonly studied cytokine used to measure proinflammatory states in a range of neurological disorders (Erta et al., 2012). As childhood is a period of great brain plasticity, these results suggest that proteins with high expression levels in early childhood and in late adulthood may have differing functions across the lifespan.

Finally, clustering the cases together using protein expression revealed that protein levels are sufficient to identify cases of similar age. Nonetheless, the developmental profile revealed by the two collections of proteins was not the same. While neuroimmune data showed heterogeneous biological states during the neonatal-infancy period, plasticity markers show greater heterogeneity from infancy to early adulthood. Using the RSKC protein weightings we found that there is a period of

heightened immune expression in early childhood. Interestingly, the viral receptors present in our data all show peaks in expression during this time. As viral infections can cross the BBB and infect the CNS (Spindler & Hsu, 2012), this heightened expression represents a wave of increased susceptibility to CNS viral infection.

3.2 Significance

Immune proteins are implicated in a host of neurodevelopmental processes. They are involved in all stages of the lifespan and in all brain regions, from embryonic development to the early postnatal sculpting of circuits in the visual cortex, they are even involved in neurogenesis and plasticity in the adult hippocampus (Boulanger, 2009). Due to their extensive involvement in mediating brain development, immune proteins have also been implicated in many neurodevelopmental, neuropsychiatric and neurodegenerative disorders (Garay & McAllister, 2010). Despite the fact that elevation in inflammatory levels are associated with normal and pathological conditions, very little is actually known about the lifespan expression of immune proteins in the human cortex. Many studies exploring these molecular markers and their typical and atypical development use animal models and are not reflective of human expression levels. Moreover, levels of mRNA expression - not protein expression - are usually measured. As proteins carry out biological functions in our cells and form the cellular components, it is important to understand how they change across the lifespan (Carlyle et al., 2017). Consequently, this study aims to address the gap in our knowledge about how immune proteins develop across the lifespan in the human cortex and whether their development varies from that of classic neural proteins. As these markers play important roles in development, we charted their expression in the visual cortex, which is an exemplary model for studying neurodevelopment and plasticity.

Undulating trajectories explain neuroimmune development in human V1C

The traditional view of visual cortical development is hierarchical. The findings from perceptual (Aslin & Smith, 1988) and anatomical data (Huttenlocher & Dabholkar, 1997) suggest that the V1C matures first and that the maturation of association cortices follows subsequently. Studies in our lab, however, have found that classic neural proteins including glutamatergic receptor proteins, GABAergic receptor proteins and myelin-related proteins show protracted development well into adulthood (Pinto et al., 2010; Siu et al., 2015, Siu et al., 2017). Despite the fact that neuroimmune proteins regulate the development of these proteins, very little was known about how neuroimmune protein expression compares. Our findings show that immune proteins are not monotonic, rather they show lifelong, changing patterns of expression. As the levels of neuroimmune proteins are dynamic across the lifespan, this further supports the idea that the visual cortex is constantly changing and that contrary to the hierarchical view, V1C maturation is not achieved in the first few years of life.

While the expression profiles of neuroimmune proteins is complex, we do not observe a unique trajectory for each protein. Rather there are a number of limited, undulating expression patterns that are shared by the set of neuroimmune proteins assessed in this paper. As measurements for nearly 3,000 human plasma proteins also reveal a small number of clusters with undulating expression (Lehallier et al., 2019), this suggests that higher order molecular mechanisms orchestrate protein development in a limited, specific number of non-linear patterns.

Immune markers in the human V1C have pleiotropic, even opposing functions

Neuroimmune proteins are considered pleiotropic as they have both immunological roles and development roles in the CNS (Boulanger, 2009; Stolp, 2013). Our findings support this understanding of immune proteins in the brain. While we were not able to find a one-to-one relationship between neural function and immune protein trajectories, this is probably due to the fact that a single protein is involved with a range of neural processes. Furthermore, a single protein can also have opposing functions. For example, through our study of viral receptors in the brain we find that immune proteins can act as viral receptors that mediate entry into host cells (Qi et al., 2020). It is interesting that these molecular mechanisms also have protective effects that maintain the integrity of the BBB and supposed to prevent viral entry into the CNS (Shafit-Zagardo et al., 2018; Wang et al., 2020). In addition, it has been shown that the type of cell releasing a cytokine, the target cell and the amount of the cytokine released, are a few of the factors that determine the function of a neuroimmune molecule (Cavaillon, 2001). For instance, whether or not a cytokine will have pro- or anti-inflammatory effects (Cavaillon, 2001). As a result, to simply measure the levels of cytokines in plasma is not sufficient to indicate a proinflammatory state.

Elevated immune expression levels in young children and in older adults

In this study we found that a group of neuroimmune proteins show a unique developmental pattern not observed in the classic plasticity marker collection of proteins. Here, the protein expression levels increase from very low levels in adolescence to high protein expression in older adults. This pattern has been used as evidence for the

inflammaging model that describes aging as an increase in proinflammatory state (Franceschi et al., 2000). Additionally, neurological disorders have been described (in part) as accelerated aging due to the findings that immune protein expression levels are high in these individuals. To provide a few examples, a study looing looking at depression and suicide measured elevated TNFα, IL1-B and IL-6 mRNA levels in the post-mortem brain tissue of affected individuals (Pandey, 2017). These results were taken as evidence that depression is a case of neuroprogression (Pandey, 2017). Another study looked at the levels of proteins in the TNF pathway and also found increased levels in teens with schizophrenia and bipolar disorder (Hoseth et al., 2017). Interestingly, these studies use age-matched controls or adult controls as their reference group. In contrast, it is uncommon to see studies compare affected individuals with unaffected young children. Our results suggest that the picture is incomplete when considering inflammation in just adults. We find that many of these proteins with high levels of expression in older adults also have high levels of expression in neonates and early childhood. Thus, presenting the possibility that proteins have varying roles throughout development.

Brain development profile varies between immune and classic neural markers

We used protein expression to profile human V1 development. We found that protein expression was sufficient to identify and group proteins together by similar age. This is especially interesting, as individual proteins in both data sets show almost-equal levels of expression at varying developmental stages (ex. young children and older adults have similar levels of TRAIL R3). The formation of clusters with progressing median age using just protein expression suggests that it is not the magnitude of expression, but

rather the complex relationship between protein levels allows the identification of sample ages. This being said, the profiles produced by neuroimmune and classic neural proteins is highly different. Neuroimmune proteins show heterogeneity in the neonatal-infancy periods, where two overlapping clusters are produced. Contrastingly, overlapping clusters are not observed in the neonatal period when clustering classic plasticity markers. Rather, we find that the clusters overlap in IQR for the rest of the lifespan, with the exception of older adults. This suggests that developmental programmes for different classes of proteins are distinct in the human V1C. Finally using the RSKC weighted expression we found that there is a wave of increased immune expression around 2 years of age. Of the seven proteins that act as mediates of viral entry, three of them are receptors for HFMD which peaks in children less than 5 years old. Our findings suggest that the increased expression of viral receptors in the child CNS heightens vulnerability to viral infection and may contribute to repeated childhood infections (AlKhater, 2009)

3.3 Methodological Considerations

Strengths: Approach to data collection

Neuroimmune protein expression was measured using a multiplex ELISA. A major strength of this approach is that it enables the simultaneous detection of hundreds of proteins. Using this method, I was able to create a lifespan expression database for many neuroimmune proteins that have not been studied in the human visual cortex. Another strength of this approach is its high specificity and sensitivity to protein targets (Sakamoto et al., 2018). Additionally, an ELISA enables the measurement of absolute concentration values as opposed to relative expression.

On the other hand, western blots were used to detect the expression of classic plasticity markers. This tool also has high sensitivity and specificity to the protein target (Ghosh et al., 2014). Moreover, the synaptoneurosome preparation used in the study facilitates the enrichment of low abundance synaptic proteins for detection by western blot (Murphy et al., 2014). Both the multiplex ELISA and the western blot techniques result in the reliable detection of protein targets.

Limitations: Approach to data collection

Western blots and multiplex ELISAs do not convey cell-type related information. Moreover, they do not provide specify protein localization in terms of cortical layer, and with respect to cell components. Neuroanatomical studies and immunohistochemistry techniques will be required to identify which cortical layers and neuronal (or glial) components these proteins are preferentially expressed in. Another limitation of this study is that the western blot technique is semi-quantitative. Consequently, relative

expression is reported not protein concentration (Mahmood & Yang, 2012). Furthermore, in the multiplex ELISA, each protein antibody was arrayed in quadruplicate in the *same* sample. In contrast, multiple runs of the western blot enabled the measurement of a single protein in different samples from the same tissue donor. Finally, the small sample size (n = 30) results in a lower level of statistical power for the study.

Data analysis considerations

Modern high-dimensional data analysis tools were used to evaluate the resulting data. My study falls under the category of discovery research, where a data-driven approach is used to unpack novel protein interactions. I begin to create a pipeline for analyzing numerous proteins simultaneously and using their developmental patterns to identify biological significance.

Clustering is highly effective in revealing subtle patterns in protein expression. When visually comparing two trajectories it may seem that they are similar. Nonetheless, this may not truly be the case. Features of the curve - such as when fluctuations in expression occur - are important factors in interpreting time-series data, and they are not easily quantifiable by eye. In this study we reveal eight different clusters using the ward.D2 hierarchical clustering method. Ward.D2 is well suited for answering our research question as it is an agglomerative method, this means that a bottom-up approach is used in grouping protein trajectories together (Murtagh & Legendre, 2014). The algorithm functions by grouping together proteins that are similar to each other. The strength of this approach is that previous knowledge about the proteins does not bias the

formation of these clusters. Rather the protein-protein relationships are based in their lifespan expression.

A separate metric called the Fréchet distance was used to measure the similarity of trajectories within and between clusters identified by the ward.D2 method. Fréchet distances are better suited to our data than a standard Pearson correlation, as the Fréchet similarity measure was designed for times series data. Specifically, in computing Fréchet distances the order of points, and their positions are taken into account (Eiter & Mannila, 1994). Additionally, I used the "sum" algorithm for calculating the Fréchet distance in this study. This method has the added benefit of representing the degree of variation between curves at multiple points across the entire trajectory, as opposed to indicating only the largest distance between the curves (Genolini & Guichard, 2016).

One limitation to consider is the small cluster sizes in this study. Clustering was completed on the neuroimmune data set, the plasticity marker data set and a combined data set. Dividing these collections of proteins into five or eight groups results in small clusters; some containing only three to six members. As a result, these smaller clusters are not suitable for significance testing when performing GO enrichment on a cluster-by-cluster basis, nor are they well-suited for estimation statistics analyses on intracluster Fréchet distances.

On the other hand, RSKC was used for clustering cases together as it is designed for situations in which the number of objects to be clustered is roughly equal to, or less than the dimensions used for clustering those objects. In this study, neuroimmune data resulted in more compact case clusters than plasticity markers, this may in part be due to

the smaller number of proteins in the classic neural protein data set. There are two advantages to using RSKC for the formation of case clusters. First, RSKC is good at dealing with outliers (Kondo et al., 2016). The algorithm will identify outliers while clustering and remove them from the process initially (Kondo et al., 2016). These outliers are incorporated at the end, when all other objects have been clustered, by determining which of the clusters the outliers most closely resemble (Kondo et al., 2016). Secondly, RSKC provides weights for the clustering dimensions. One of the challenges with clustering high-dimensional data is that dimensions are not equally important; some proteins may be noise variables. RSKC is capable of determining noise variables and will assign low weights to these variables (Kondo et al., 2016). In this study, RSKC weightings reveal which proteins facilitate the formation of clusters with progressing median age and it also identifies proteins that did not contribute to this process.

3.4 Future Directions

The present study begins to unpack how neuroimmune proteins change across the lifespan and whether their expression patterns are comparable to classic neural proteins. The next step will be to explore whether a similar number of unique trajectories are detected in the human V1C on a larger number of proteins. Furthermore, as there is only a 40% correlation between protein and gene expression levels (Vogel & Marcotte, 2012), the question of how immune genes develop across the lifespan is of particular interest. In addition, future studies may address questions about whether neuroimmune proteins preferentially expressed in certain brain cell types are differentially expressed across the lifespan. Finally, regional comparisons can be carried out to determine whether visual association areas show the same or different protein trajectories. These will help further our understanding of the robustness of protein developmental trajectories and may uncover varying functions for these proteins in different regions of the brain.

Chapter 4. References

Airaksinen, M. S., & Saarma, M. (2002). The GDNF family: Signalling, biological functions and therapeutic value. *Nature Reviews Neuroscience*, *3*(5), 383–394. https://doi.org/10.1038/nrn812

Akkermann, R., Aprico, A., Perera, A. A., Bujalka, H., Cole, A. E., Xiao, J., Field, J., Kilpatrick, T. J., & Binder, M. D. (2017). The TAM receptor Tyro3 regulates myelination in the central nervous system. *Glia*, *65*(4), 581–591. https://doi.org/10.1002/glia.23113

AlKhater, S. A. (2009). Approach to the child with recurrent infections. *Journal of Family & Community Medicine*, *16*(3), 77–82. Retrieved from https://www.ncbi.nlm.nih.gov/pmc/articles/PMC3377046/

Anastasina, M., Domanska, A., Palm, K., & Butcher, S. (2017). Human picornaviruses associated with neurological diseases and their neutralization by antibodies. *Journal of General Virology*, *98*(6), 1145–1158. https://doi.org/10.1099/jgv.0.000780

Ashburner, M., Ball, C. A., Blake, J. A., Botstein, D., Butler, H., Cherry, J. M., Davis, A. P., Dolinski, K., Dwight, S. S., Eppig, J. T., Harris, M. A., Hill, D. P., Issel-Tarver, L., Kasarskis, A., Lewis, S., Matese, J. C., Richardson, J. E., Ringwald, M., Rubin, G. M., & Sherlock, G. (2000). Gene Ontology: tool for the unification of biology. *Nature Genetics*, *25*(1), 25–29. https://doi.org/10.1038/75556

Ashwood, P., Krakowiak, P., Hertz-Picciotto, I., Hansen, R., Pessah, I., & Water, J. V. D. (2011). Elevated plasma cytokines in autism spectrum disorders provide evidence of immune dysfunction and are associated with impaired behavioral outcome. *Brain, Behavior, and Immunity*, *25*(1), 40–45. https://doi.org/10.1016/j.bbi.2010.08.003

Aslin, R. N., & Smith, L. B. (1988). Perceptual Development. *Annual Review of Psychology*, *39*(1), 435–473. https://doi.org/10.1146/annurev.ps.39.020188.002251

Atluri, V. S. R., Hidalgo, M., Samikkannu, T., Kurapati, K. R. V., & Nair, M. (2015). Synaptic Plasticity and Neurological Disorders in Neurotropic Viral Infections. *Neural Plasticity*, *2015*, 1–14. https://doi.org/10.1155/2015/138979

Battaglioli, G., Liu, H., & Martin, D. L. (2003). Kinetic differences between the isoforms of glutamate decarboxylase: implications for the regulation of GABA synthesis. *Journal of Neurochemistry*, *86*(4), 879–887. https://doi.org/10.1046/j.1471-4159.2003.01910.x

Bavelier, D., Levi, D. M., Li, R. W., Dan, Y., & Hensch, T. K. (2010). Removing Brakes on Adult Brain Plasticity: From Molecular to Behavioral Interventions. *Journal of Neuroscience*, *30*(45), 14964–14971. https://doi.org/10.1523/jneurosci.4812-10.2010

Beattie, E. C., Stellwagen, D., Morishita, W., Bresnahan, J. C., Ha, B. K., Zastrow, M. V., Beattie, M. S., & Malenka, R. C. (2002). Control of Synaptic Strength by Glial TNFalpha. *Science*, *295*(5563), 2282–2285. https://doi.org/10.1126/science.1067859

Bilbo, S. D., & Schwarz, J. M. (2009). Early-life programming of later-life brain and behavior: a critical role for the immune system. *Frontiers in Behavioral Neuroscience*, *3*. https://doi.org/10.3389/neuro.08.014.2009

Bilbo, S. D., & Schwarz, J. M. (2012). The immune system and developmental programming of brain and behavior. *Frontiers in Neuroendocrinology*, *33*(3), 267–286. https://doi.org/10.1016/j.yfrne.2012.08.006

Bjartmar, L., Huberman, A. D., Ullian, E. M., Rentería, R. C., Liu, X., Xu, W., Prezioso, J., Susman, M. W., Stellwagen, D., Stokes, C. C., Cho, R., Worley, P., Malenka, R. C., Ball, S., Peachey, N. S., Copenhagen, D., Chapman, B., Nakamoto, M., Barres, B. A., & Perin, M. S. (2006). Neuronal Pentraxins Mediate Synaptic Refinement in the Developing Visual System. *Journal of Neuroscience*, *26*(23), 6269–6281. https://doi.org/10.1523/jneurosci.4212-05.2006

Bohlson, S. S., O'Conner, S. D., Hulsebus, H. J., Ho, M.-M., & Fraser, D. A. (2014). Complement, C1q, and C1q-Related Molecules Regulate Macrophage Polarization. *Frontiers in Immunology*, *5*. https://doi.org/10.3389/fimmu.2014.00402

Borovcanin, M. M., Jovanovic, I., Radosavljevic, G., Pantic, J., Janicijevic, S. M., Arsenijevic, N., & Lukic, M. L. (2017). Interleukin-6 in Schizophrenia—Is There a Therapeutic Relevance? *Frontiers in Psychiatry*, *8*(221). https://doi.org/10.3389/fpsyt.2017.00221

Boulanger, L. M. (2009). Immune Proteins in Brain Development and Synaptic Plasticity. *Neuron*, *64*(1), 93–109. https://doi.org/10.1016/j.neuron.2009.09.001

Buka, S. L., Tsuang, M. T., Torrey, E. F., Klebanoff, M. A., Bernstein, D., & Yolken, R. H. (2001). Maternal Infections and Subsequent Psychosis Among Offspring. *Archives of General Psychiatry*, *58*(11), 1032–1037. https://doi.org/10.1001/archpsyc.58.11.1032

Carlyle, B. C., Kitchen, R. R., Kanyo, J. E., Voss, E. Z., Pletikos, M., Sousa, A. M. M., Lam, T. T., Gerstein, M. B., Sestan, N., & Nairn, A. C. (2017). A multiregional proteomic survey of the postnatal human brain. *Nature Neuroscience*, *20*(12), 1787–1795. https://doi.org/10.1038/s41593-017-0011-2

Castillo, P. E., Younts, T. J., Chávez, A. E., & Hashimotodani, Y. (2012). Endocannabinoid Signaling and Synaptic Function. *Neuron*, *76*(1), 70–81. https://doi.org/10.1016/j.neuron.2012.09.020

Cavaillon, J. M. (2001). Pro- versus anti-inflammatory cytokines: myth or reality. *Cellular and Molecular Biology (Noisy-Le-Grand, France)*, *47*(4), 695–702. Retrieved from https://www.researchgate.net/publication/11843030_Pro-_versus_anti-inflammatory_cytokines_Myth_or_reality

Çavuş, I., Reinhart, R. M. G., Roach, B. J., Gueorguieva, R., Teyler, T. J., Clapp, W. C., Ford, J. M., Krystal, J. H., & Mathalon, D. H. (2012). Impaired Visual Cortical Plasticity in Schizophrenia. *Biological Psychiatry*, *71*(6), 512–520. https://doi.org/10.1016/j.biopsych.2012.01.013

Chadi, G., & Fuxe, K. (1998). Analysis of trophic responses in lesioned brain: focus on basic fibroblast growth factor mechanisms. *Brazilian Journal of Medical and Biological Research*, *31*(2), 231–241. https://doi.org/10.1590/s0100-879x1998000200007

Chaitanya, G. V., Omura, S., Sato, F., Martinez, N. E., Minagar, A., Ramanathan, M., Guttman, B. W., Zivadinov, R., Tsunoda, I., & Alexander, J. S. (2013). Inflammation induces neuro-lymphatic protein expression in multiple sclerosis brain neurovasculature. *Journal of Neuroinflammation*, *10*(1), 1–14. https://doi.org/10.1186/1742-2094-10-125

Chavis, P., & Westbrook, G. (2001). Integrins mediate functional pre- and postsynaptic maturation at a hippocampal synapse. *Nature*, *411*(6835), 317–321. https://doi.org/10.1038/35077101

Chen, W. S., & Bear, M. F. (2007). Activity-dependent regulation of NR2B translation contributes to metaplasticity in mouse visual cortex. *Neuropharmacology*, *52*(1), 200–214. https://doi.org/10.1016/j.neuropharm.2006.07.003

Chu, W.-M. (2013). Tumor necrosis factor. *Cancer Letters*, *328*(2), 222–225. https://doi.org/10.1016/j.canlet.2012.10.014

Coiro, P., Padmashri, R., Suresh, A., Spartz, E., Pendyala, G., Chou, S., Jung, Y., Meays, B., Roy, S., Gautam, N., Alnouti, Y., Li, M., & Dunaevsky, A. (2015). Impaired synaptic development in a maternal immune activation mouse model of neurodevelopmental disorders. *Brain, Behavior, and Immunity*, *50*, 249–258. https://doi.org/10.1016/j.bbi.2015.07.022

Conrady, C. D., Drevets, D. A., & Carr, D. J. (2010). Herpes simplex type I (HSV-1) infection of the nervous system: Is an immune response a good thing? *Journal of Neuroimmunology*, *220*(1-2), 1–9. https://doi.org/10.1016/j.jneuroim.2009.09.013

Corriveau, R. A., Huh, G. S., & Shatz, C. J. (1998). Regulation of Class I MHC Gene Expression in the Developing and Mature CNS by Neural Activity. *Neuron*, *21*(3), 505–520. https://doi.org/10.1016/s0896-6273(00)80562-0

Crair, M. C., Gillespie, D. C., & Stryker, M. P. (1998). The Role of Visual Experience in the Development of Columns in Cat Visual Cortex. *Science*, *279*(5350), 566–570. https://doi.org/10.1126/science.279.5350.566

D-Krab. Abstract technology and science of intelligence connectivity network in Human brain, vector illustration [digital image]. Stock vector ID: 457211164. Retrieved from https://www.shutterstock.com/image-vector/abstract-technology-science-intelligence-connectivity-network-457211164

Dabrowski, A., & Umemori, H. (2016). Buttressing a balanced brain: Target-derived FGF signaling regulates excitatory/inhibitory tone and adult neurogenesis within the maturating hippocampal network. *Neurogenesis*, *3*(1). https://doi.org/10.1080/23262133.2016.1168504

Datwani, A., McConnell, M. J., Kanold, P. O., Micheva, K. D., Busse, B., Shamloo, M., Smith, S. J., & Shatz, C. J. (2009). Classical MHCI Molecules Regulate Retinogeniculate Refinement and Limit Ocular Dominance Plasticity. *Neuron*, *64*(4), 463–470. https://doi.org/10.1016/j.neuron.2009.10.015

Derecki, N. C., Cronk, J. C., Lu, Z., Xu, E., Abbott, S. B. G., Guyenet, P. G., & Kipnis, J. (2012). Wild-type microglia arrest pathology in a mouse model of Rett syndrome. *Nature*, *484*(7392), 105–109. https://doi.org/10.1038/nature10907

Draftsboy. Eppendorf tube vector. Biology lab equipment icon [digital image]. Stock vector ID: 1769474504. Retrieved from https://www.shutterstock.com/image-vector/eppendorf-tube-vector-biology-lab-equipment-1769474504

Eiter, T., & Mannila, H. (1994). *Computing discrete Fréchet distance*. Technical Report CD-TR 94/64, Christian Doppler Laboratory for Expert Systems, TU Vienna, Austria. Retrieved from http://www.kr.tuwien.ac.at/staff/eiter/et-archive/cdtr9464.pdf

Elmer, B. M., & Mcallister, A. K. (2012). Major histocompatibility complex class I proteins in brain development and plasticity. *Trends in Neurosciences*, *35*(11), 660–670. https://doi.org/10.1016/j.tins.2012.08.001

Erta, M., Quintana, A., & Hidalgo, J. (2012). Interleukin-6, a Major Cytokine in the Central Nervous System. *International Journal of Biological Sciences*, *8*(9), 1254–1266. https://doi.org/10.7150/ijbs.4679

Espinosa, J. S., & Stryker, M. P. (2012). Development and Plasticity of the Primary Visual Cortex. *Neuron*, *75*(2), 230–249. https://doi.org/10.1016/j.neuron.2012.06.009

Extender_01. Gel electrophoresis device with loaded sample vector illustration [digital image]. Stock vector ID: 190696757. Retrieved from https://www.shutterstock.com/image-vector/gel-electrophoresis-device-loaded-sample-vector-190696757

Fagiolini, M., Fritschy, J. M., Löw, K., Möhler, H., Rudolph, U., & Hensch, T. K. (2004). Specific GABAA Circuits for Visual Cortical Plasticity. *Science*, *303*(5664), 1681–1683. https://doi.org/10.1126/science.1091032

Fatemi, S. H., & Folsom, T. D. (2009). The Neurodevelopmental Hypothesis of Schizophrenia, Revisited. *Schizophrenia Bulletin*, *35*(3), 528–548. https://doi.org/10.1093/schbul/sbn187

Feldblum, S., Erlander, M. G., & Tobin, A. J. (1993). Different distributions of GAD65 and GAD67 mRNAS suggest that the two glutamate decarboxylases play distinctive functional roles. *Journal of Neuroscience Research*, *34*(6), 689–706. https://doi.org/10.1002/jnr.490340612

Forrester, J. V., Mcmenamin, P. G., & Dando, S. J. (2018). CNS infection and immune privilege. *Nature Reviews Neuroscience*, *19*(11), 655–671. https://doi.org/10.1038/s41583-018-0070-8

Franceschi, C., Bonafè, M., Valensin, S., Olivieri, F., Luca, M. D., Ottaviani, E., & Benedictis, G. D. (2000). Inflamm-aging: An Evolutionary Perspective on Immunosenescence. *Annals of the New York Academy of Sciences*, *908*(1), 244–254. https://doi.org/10.1111/j.1749-6632.2000.tb06651.x

Franceschi, C., Garagnani, P., Parini, P., Giuliani, C., & Santoro, A. (2018). Inflammaging: a new immune–metabolic viewpoint for age-related diseases. *Nature Reviews Endocrinology*, *14*(10), 576–590. https://doi.org/10.1038/s41574-018-0059-4

Frankle, W., Lerma, J., & Laruelle, M. (2003). The Synaptic Hypothesis of Schizophrenia. *Neuron*, *39*(2), 205–216. https://doi.org/10.1016/s0896-6273(03)00423-9

Galea, I., Bechmann, I., & Perry, V. H. (2007). What is immune privilege (not)? *Trends in Immunology*, *28*(1), 12–18. https://doi.org/10.1016/j.it.2006.11.004

Ganguli, R., Yang, Z., Shurin, G., Chengappa, K., Brar, J. S., Gubbi, A. V., & Rabin, B. S. (1994). Serum interleukin-6 concentration in schizophrenia: Elevation associated with duration of illness. *Psychiatry Research*, *51*(1), 1–10. https://doi.org/10.1016/0165-1781(94)90042-6

Garay, P. A., Hsiao, E. Y., Patterson, P. H., & Mcallister, A. (2013). Maternal immune activation causes age- and region-specific changes in brain cytokines in offspring throughout development. *Brain, Behavior, and Immunity*, *31*, 54–68. https://doi.org/10.1016/j.bbi.2012.07.008

Garay, P., & McAllister, K. (2010). Novel roles for immune molecules in neural development: implications for neurodevelopmental disorders. *Frontiers in Synaptic Neuroscience*, *2*(136), 1–16. https://doi.org/10.3389/fnsyn.2010.00136

Garcia-Martin, E., Gavin, A., Garcia-Campayo, J., Vilades, E., Orduna, E., Polo, V., Larrosa, J. M., Pablo, L. E., & Satue, M. (2019). Visual Function and Retinal Changes in Patients with Bipolar Disorder. *Retina*, *39*(10), 2012–2021. https://doi.org/10.1097/iae.0000000000002252

The Gene Ontology Consortium. (2019). The Gene Ontology Resource: 20 years and still GOing strong. *Nucleic Acids Research*, *47*(D1), D330–D338. https://doi.org/10.1093/nar/gky1055

Genolini, C., & Guichard, E. (2016). *K-Means for Longitudinal Data using Shape-Respecting Distance*. cran.r-project.org. Retrieved from https://cran.r-project.org/web/packages/kmlShape/kmlShape.pdf.

Ghosh, R., Gilda, J. E., & Gomes, A. V. (2014). The necessity of and strategies for improving confidence in the accuracy of western blots. *Expert Review of Proteomics*, *11*(5), 549–560. https://doi.org/10.1586/14789450.2014.939635

Gingrich, K. J., Roberts, W. A., & Kass, R. S. (1995). Dependence of the GABAA receptor gating kinetics on the alpha-subunit isoform: implications for structure-function relations and synaptic transmission. The Journal of Physiology, 489(2), 529–543. https://doi.org/10.1113/jphysiol.1995.sp021070

Giunta, B., Fernandez, F., Nikolic, W. V., Obregon, D., Rrapo, E., Town, T., & Tan, J. (2008). Inflammaging as a prodrome to Alzheimer's disease. *Journal of Neuroinflammation*, *5*(1), 51. https://doi.org/10.1186/1742-2094-5-51

Glen, S. (2016, December 2). *Jaccard Index / Similarity Coefficient*. Statistics How To: Jaccard Index / Similarity Coefficient. Retrieved from https://www.statisticshowto.com/jaccard-index/.

Glynn, M. W., Elmer, B. M., Garay, P. A., Liu, X.-B., Needleman, L. A., El-Sabeawy, F., & Mcallister, A. K. (2011). MHCI negatively regulates synapse density during the establishment of cortical connections. *Nature Neuroscience*, *14*(4), 442–451. https://doi.org/10.1038/nn.2764

Goines, P., & Water, J. V. D. (2010). The immune system's role in the biology of autism. *Current Opinion in Neurology*, *23*(2), 111–117. https://doi.org/10.1097/wco.0b013e3283373514

Goswami, R., & Kaplan, M. H. (2011). A Brief History of IL-9. *The Journal of Immunology*, *186*(6), 3283–3288. https://doi.org/10.4049/jimmunol.1003049

Hendrickson, M. L., Ling, C., & Kalil, R. E. (2012). Degeneration of Axotomized Projection Neurons in the Rat dLGN: Temporal Progression of Events and Their Mitigation by a Single Administration of FGF2. *PLoS ONE*, *7*(11). https://doi.org/10.1371/journal.pone.0046918

Hensch, T. K. (2004). Critical Period Regulation. *Annu. Rev. Neurosci.*, *27*, 549–579. https://doi.org/10.1002/chin.200446297

Hensch, T. K., & Quinlan, E. M. (2018). Critical periods in amblyopia. *Visual Neuroscience*, *35*. https://doi.org/10.1017/s0952523817000219

Hensch, T. K., Fagiolini, M., Mataga, N., Stryker, M. P., Baekkeskov, S., & Kash, S. F. (1998). Local GABA Circuit Control of Experience-Dependent Plasticity in Developing Visual Cortex. *Science*, *282*(5393), 1504–1508. https://doi.org/10.1126/science.282.5393.1504

Heynen, A. J., Yoon, B.-J., Liu, C.-H., Chung, H. J., Huganir, R. L., & Bear, M. F. (2003). Molecular mechanism for loss of visual cortical responsiveness following brief monocular deprivation. *Nature Neuroscience*, *6*(8), 854–862. https://doi.org/10.1038/nn1100

Hidalgo, A., Learte, A. R., Mcquilton, P., Pennack, J., & Zhu, B. (2006). Neurotrophic and Gliatrophic Contexts in Drosophila. *Brain, Behavior and Evolution*, *68*(3), 173–180. https://doi.org/10.1159/000094086

Hilfiker, S., Pieribone, V. A., Czernik, A. J., Kao, H.-T., Augustine, G. J., & Greengard, P. (1999). Synapsins as regulators of neurotransmitter release. *Philosophical Transactions of the Royal Society of London. Series B: Biological Sciences*, *354*(1381), 269–279. https://doi.org/10.1098/rstb.1999.0378

Hornig, M., & Lipkin, W. I. (2001). Infectious and immune factors in the pathogenesis of neurodevelopmental disorders: Epidemiology, hypotheses, and animal models. *Mental Retardation and Developmental Disabilities Research Reviews*, *7*(3), 200–210. https://doi.org/10.1002/mrdd.1028

Hoseth, E. Z., Ueland, T., Dieset, I., Birnbaum, R., Shin, J. H., Kleinman, J. E., Hyde, T. M., Mørch, R. H., Hope, S., Lekva, T., Abraityte, A. J., Michelsen, A. E., Melle, I., Westlye, L. T., Ueland, T., Djurovic, S., Aukrust, P., Weinberger, D. R., & Andreassen, O. A. (2017). A Study of TNF Pathway Activation in Schizophrenia and Bipolar Disorder in Plasma and Brain Tissue. *Schizophrenia Bulletin*, *43*(4), 881–890. https://doi.org/10.1093/schbul/sbw183

Hou, Y., Dan, X., Babbar, M., Wei, Y., Hasselbalch, S. G., Croteau, D. L., & Bohr, V. A. (2019). Ageing as a risk factor for neurodegenerative disease. *Nature Reviews Neurology*, *15*(10), 565–581. https://doi.org/10.1038/s41582-019-0244-7

Huang, H.-I., & Shih, S.-R. (2015). Neurotropic Enterovirus Infections in the Central Nervous System. *Viruses*, *7*(11), 6051–6066. https://doi.org/10.3390/v7112920

Huang, X., Stodieck, S. K., Goetze, B., Cui, L., Wong, M. H., Wenzel, C., Hosang, L., Dong, Y., Löwel, S., & Schlüter, O. M. (2015). Progressive maturation of silent synapses governs the duration of a critical period. *Proceedings of the National Academy of Sciences*, *112*(24), E3131–E3140. https://doi.org/10.1073/pnas.1506488112

Hubel, D. H., & Wiesel, T. N. (1963). Receptive Fields Of Cells In Striate Cortex Of Very Young, Visually Inexperienced Kittens. *Journal of Neurophysiology*, *26*(6), 994–1002. https://doi.org/10.1152/jn.1963.26.6.994

Hubel, D. H., Wiesel, T. N., & LeVay, S. (1977). Plasticity of ocular dominance columns in monkey striate cortex. *Philosophical Transactions of the Royal Society of London. B, Biological Sciences*, *278*(961), 377–409. https://doi.org/10.1098/rstb.1977.0050

Huh, G. S., Boulanger, L. M., Du, H., Riquelme, P. A., Brotz, T. M., & Shatz, C. J. (2000). Functional Requirement for Class I MHC in CNS Development and Plasticity. *Science*, *290*(5499), 2155–2159. https://doi.org/10.1126/science.290.5499.2155

Huttenlocher, P. R., & Dabholkar, A. S. (1997). Regional differences in synaptogenesis in human cerebral cortex. *The Journal of Comparative Neurology*, *387*(2), 167–178. https://doi.org/10.1002/(sici)1096-9861(19971020)387:23.0.co;2-z

Ip, J. P. K., Mellios, N., & Sur, M. (2018). Rett syndrome: insights into genetic, molecular and circuit mechanisms. *Nature Reviews Neuroscience*, *19*(6), 368–382. https://doi.org/10.1038/s41583-018-0006-3

Iwai, Y., Fagiolini, M., Obata, K., & Hensch, T. K. (2003). Rapid Critical Period Induction by Tonic Inhibition in Visual Cortex. *The Journal of Neuroscience*, *23*(17), 6695–6702. https://doi.org/10.1523/jneurosci.23-17-06695.2003

Janova, H., Arinrad, S., Balmuth, E., Mitjans, M., Hertel, J., Habes, M., Bittner, R. A., Pan, H., Goebbels, S., Begemann, M., Gerwig, U. C., Langner, S., Werner, H. B., Kittel-Schneider, S., Homuth, G., Davatzikos, C., Völzke, H., West, B. L., Reif, A., … Nave, K.-A. (2017). Microglia ablation alleviates myelin-associated catatonic signs in mice. *Journal of Clinical Investigation*, *128*(2), 734–745. https://doi.org/10.1172/jci97032

Ji, R., Tian, S., Lu, H. J., Lu, Q., Zheng, Y., Wang, X., Ding, J., Li, Q., & Lu, Q. (2013). TAM Receptors Affect Adult Brain Neurogenesis by Negative Regulation of Microglial Cell Activation. *The Journal of Immunology*, *191*(12), 6165–6177. https://doi.org/10.4049/jimmunol.1302229

Johnson, R. A., & Wichern, D. W. (2007). *Applied multivariate statistical analysis*. Upper Saddle River, NJ: Prentice hall. Retrieved from https://www.webpages.uidaho.edu/~stevel/519/Applied%20Multivariate%20Statistical%20Analysis%20by%20Johnson%20and%20Wichern.pdf

Kakooza-Mwesige, A., Tshala-Katumbay, D., & Juliano, S. L. (2019). Viral infections of the central nervous system in Africa. *Brain Research Bulletin*, *145*, 2–17. https://doi.org/10.1016/j.brainresbull.2018.12.019

Kaneko, M., Hanover, J. L., England, P. M., & Stryker, M. P. (2008). TrkB kinase is required for recovery, but not loss, of cortical responses following monocular deprivation. *Nature Neuroscience*, *11*(4), 497–504. https://doi.org/10.1038/nn2068

Kaneko, M., Stellwagen, D., Malenka, R. C., & Stryker, M. P. (2008). Tumor Necrosis Factor-α Mediates One Component of Competitive, Experience-Dependent Plasticity in Developing Visual Cortex. *Neuron*, *58*(5), 673–680. https://doi.org/10.1016/j.neuron.2008.04.023

Kang, S. S., & McGavern, D. B. (2008). Lymphocytic choriomeningitis infection of the central nervous system. *Frontiers in Bioscience*, *Volume*(13), 4529–4543. https://doi.org/10.2741/3021

Kano, M., Ohno-Shosaku, T., Hashimotodani, Y., Uchigashima, M., & Watanabe, M. (2009). Endocannabinoid-Mediated Control of Synaptic Transmission. *Physiological Reviews*, *89*(1), 309–380. https://doi.org/10.1152/physrev.00019.2008

Karlsson, H., Bachmann, S., Schroder, J., Mcarthur, J., Torrey, E. F., & Yolken, R. H. (2001). Retroviral RNA identified in the cerebrospinal fluids and brains of individuals with schizophrenia. *Proceedings of the National Academy of Sciences*, *98*(8), 4634–4639. https://doi.org/10.1073/pnas.061021998

Kassambara, A. (2017). *Practical guide to cluster analysis in R: unsupervised machine learning* (1st ed.). CreateSpace Independent Publishing Platform. Retrieved from https://www.datanovia.com/en/wp-content/uploads/dn-tutorials/book-preview/clustering_en_preview.pdf

Katiyar, A., Sharma, S., Singh, T. P., & Kaur, P. (2018). Identification of Shared Molecular Signatures Indicate the Susceptibility of Endometriosis to Multiple Sclerosis. *Frontiers in Genetics*, *9*. https://doi.org/10.3389/fgene.2018.00042

Katz, L. C., & Crowley, J. C. (2002). Development of cortical circuits: Lessons from ocular dominance columns. *Nature Reviews Neuroscience*, *3*(1), 34–42. https://doi.org/10.1038/nrn703

Kéri, S., Szabó, C., & Kelemen, O. (2014). Blood biomarkers of depression track clinical changes during cognitive-behavioral therapy. *Journal of Affective Disorders*, *164*, 118–122. https://doi.org/10.1016/j.jad.2014.04.030

Kerschensteiner, D., & Guido, W. (2017). Organization of the dorsal lateral geniculate nucleus in the mouse. *Visual Neuroscience*, *34*. https://doi.org/10.1017/s0952523817000062

Kiavue, N., Cabel, L., Melaabi, S., Bataillon, G., Callens, C., Lerebours, F., Pierga, J.-Y., & Bidard, F.-C. (2019). ERBB3 mutations in cancer: biological aspects, prevalence and therapeutics. *Oncogene*, *39*(3), 487–502. https://doi.org/10.1038/s41388-019-1001-5

Kioussis, D., & Pachnis, V. (2009). Immune and Nervous Systems: More Than Just a Superficial Similarity? *Immunity*, *31*(5), 705–710. https://doi.org/10.1016/j.immuni.2009.09.009

Kondo, Y., Salibian-Barrera, M., & Zamar, R. (2016). RSKC: AnRPackage for a Robust and Sparse K-Means Clustering Algorithm. *Journal of Statistical Software*, *72*(5). https://doi.org/10.18637/jss.v072.i05

Koopmans, F., van Nierop, P., Andres-Alonso, M., Byrnes, A., Cijsouw, T., Coba, M. P., Cornelisse, L. N., Farrell, R. J., Goldschmidt, H. L., Howrigan, D. P., Hussain, N. K., Imig, C., de Jong, A. P. H., Jung, H., Kohansalnodehi, M., Kramarz, B., Lipstein, N., Lovering, R. C., MacGillavry, H., … Verhage, M. (2019). SynGO: An Evidence-Based, Expert-Curated Knowledge Base for the Synapse. *Neuron*, *103*(2), 217–234. https://doi.org/10.1016/j.neuron.2019.05.002

Kraus, W. L. (2015). Editorial: Would You Like A Hypothesis With Those Data? Omics and the Age of Discovery Science. *Molecular Endocrinology*, *29*(11), 1531–1534. https://doi.org/10.1210/me.2015-1253

Kwon, S. E., & Chapman, E. R. (2011). Synaptophysin Regulates the Kinetics of Synaptic Vesicle Endocytosis in Central Neurons. *Neuron*, *70*(5), 847–854. https://doi.org/10.1016/j.neuron.2011.04.001

Lambo, M. E., & Turrigiano, G. G. (2013). Synaptic and Intrinsic Homeostatic Mechanisms Cooperate to Increase L2/3 Pyramidal Neuron Excitability during a Late Phase of Critical Period Plasticity. *Journal of Neuroscience*, *33*(20), 8810–8819. https://doi.org/10.1523/jneurosci.4502-12.2013

Law, P. C., Gurvich, C. T., Ngo, T. T., & Miller, S. M. (2017). Evidence that eye-movement profiles do not explain slow binocular rivalry rate in bipolar disorder: support for a perceptual endophenotype. *Bipolar Disorders*, *19*(6), 465–476. https://doi.org/10.1111/bdi.12515

LeBlanc, J. J., DeGregorio, G., Centofante, E., Vogel-Farley, V. K., Barnes, K., Kaufmann, W. E., Fagiolini, M., & Nelson, C. A. (2015). Visual evoked potentials detect cortical processing deficits in Rett syndrome. *Annals of Neurology*, *78*(5), 775–786. https://doi.org/10.1002/ana.24513

Ledda, F., Paratcha, G., Sandoval-Guzmán, T., & Ibáñez, C. F. (2007). GDNF and GFRα1 promote formation of neuronal synapses by ligand-induced cell adhesion. *Nature Neuroscience*, *10*(3), 293–300. https://doi.org/10.1038/nn1855

Lehallier, B., Gate, D., Schaum, N., Nanasi, T., Lee, S. E., Yousef, H., Moran Losada, P., Berdnik, D., Keller, A., Verghese, J., Sathyan, S., Franceschi, C., Milman, S., Barzilai, N., & Wyss-Coray, T. (2019). Undulating changes in human plasma proteome profiles across the lifespan. *Nature Medicine*, *25*(12), 1843–1850. https://doi.org/10.1038/s41591-019-0673-2

Leonard, H., Cobb, S., & Downs, J. (2016). Clinical and biological progress over 50 years in Rett syndrome. *Nature Reviews Neurology*, *13*(1), 37–51. https://doi.org/10.1038/nrneurol.2016.186

Leoncini, S., De Felice, C., Signorini, C., Zollo, G., Cortelazzo, A., Durand, T., Galano, J.-M., Guerranti, R., Rossi, M., Ciccoli, L., & Hayek, J. (2015). Cytokine Dysregulation inMECP2- andCDKL5-Related Rett Syndrome: Relationships with Aberrant Redox Homeostasis, Inflammation, andω-3 PUFAs. *Oxidative Medicine and Cellular Longevity*, *2015*, 1–18. https://doi.org/10.1155/2015/421624

Levay, S., Stryker, M. P., & Shatz, C. J. (1978). Ocular dominance columns and their development in layer IV of the cat's visual cortex: A quantitative study. *The Journal of Comparative Neurology*, *179*(1), 223–244. https://doi.org/10.1002/cne.901790113

LeVay, S., Wiesel, T. N., & Hubel, D. H. (1980). The development of ocular dominance columns in normal and visually deprived monkeys. *The Journal of Comparative Neurology*, *191*(1), 1–51. https://doi.org/10.1002/cne.901910102

LI-COR Inc. *Multiplexing*. LI-COR - Compare Proteins Accurately. LI-COR, Inc. Retrieved from https://www.licor.com/bio/guide/westerns/compare_proteins.

LI-COR, Inc. (2013). *Odyssey Classic Imaging System Tutorial Guide*. Lincoln, NE; LI-COR, Inc. Retrieved from https://www.licor.com/documents/hy54sfzujqjj8xolcth5.

Lin, Y., Bloodgood, B. L., Hauser, J. L., Lapan, A. D., Koon, A. C., Kim, T.-K., Hu, L. S., Malik, A. N., & Greenberg, M. E. (2008). Activity-dependent regulation of inhibitory synapse development by Npas4. *Nature*, *455*(7217), 1198–1204. https://doi.org/10.1038/nature07319

Little, R. J. A. (1988). Missing-Data Adjustments in Large Surveys. *Journal of Business & Economic Statistics*, *6*(3), 287. https://doi.org/10.2307/1391878

Liu, X.-F., Sun, X.-M., Sun, X.-W., Yang, Y.-Q., Huang, C.-H., & Wen, H. (2019). Epidemiological study on hand, foot and mouth disease in Tongzhou District, Beijing, 2013–2017. *Journal of International Medical Research*, *47*(6), 2615–2625. https://doi.org/10.1177/0300060519841974

Lord, C., Brugha, T. S., Charman, T., Cusack, J., Dumas, G., Frazier, T., Jones, E. J. H., Jones, R. M., Pickles, A., State, M. W., Taylor, J. L., & Veenstra-VanderWeele, J. (2020). Autism spectrum disorder. *Nature Reviews Disease Primers*, *6*(1), 5. https://doi.org/10.1038/s41572-019-0138-4

Luchtefeld, M., Schunkert, H., Stoll, M., Selle, T., Lorier, R., Grote, K., Sagebiel, C., Jagavelu, K., Tietge, U. J. F., Assmus, U., Streetz, K., Hengstenberg, C., Fischer, M., Mayer, B., Maresso, K., El Mokhtari, N. E., Schreiber, S., Müller, W., Bavendiek, U., … Schieffer, B. (2007). Signal transducer of inflammation gp130 modulates atherosclerosis in mice and man. *Journal of Experimental Medicine*, *204*(8), 1935–1944. https://doi.org/10.1084/jem.20070120

Lunghi, C., Sframeli, A. T., Lepri, A., Lepri, M., Lisi, D., Sale, A., & Morrone, M. C. (2018). A new counterintuitive training for adult amblyopia. *Annals of Clinical and Translational Neurology*, *6*(2), 274–284. https://doi.org/10.1002/acn3.698

Lyckman, A. W., Horng, S., Leamey, C. A., Tropea, D., Watakabe, A., Van Wart, A., McCurry, C., Yamamori, T., & Sur, M. (2008). Gene expression patterns in visual cortex during the critical period: Synaptic stabilization and reversal by visual deprivation. *Proceedings of the National Academy of Sciences*, *105*(27), 9409–9414. https://doi.org/10.1073/pnas.0710172105

Mahar, I., Labonte, B., Yogendran, S., Isingrini, E., Perret, L., Davoli, M. A., Rachalski, A., Giros, B., Turecki, G., & Mechawar, N. (2017). Erratum: Disrupted hippocampal neuregulin-1/ErbB3 signaling and dentate gyrus granule cell alterations in suicide. *Translational Psychiatry*, *7*(9), e1243. https://doi.org/10.1038/tp.2017.214

Mahmood, T., & Yang, P. -C. (2012). Western blot: technique, theory, and trouble shooting. *North American journal of medical sciences*, *4*(9), 429–434. https://doi.org/10.4103/1947-2714.100998

Makinodan, M., Rosen, K. M., Ito, S., & Corfas, G. (2012). A Critical Period for Social Experience-Dependent Oligodendrocyte Maturation and Myelination. *Science*, *337*(6100), 1357–1360. https://doi.org/10.1126/science.1220845

Man, H.-Y. (2011). GluA2-lacking, calcium-permeable AMPA receptors — inducers of plasticity? *Current Opinion in Neurobiology*, *21*(2), 291–298. https://doi.org/10.1016/j.conb.2011.01.001

Mao, Y. Q. (2014, May 1). *Advertorial: High-Throughput Cytokine Quantification Using Quantibody® Arrays*. GEN - Genetic Engineering and Biotechnology News. Retrieved from https://www.genengnews.com/magazine/223/advertorial-high-throughput-cytokine-quantification-using-quantibody-arrays/.

Maynard, T. M., Sikich, L., Lieberman, J. A., & Lamantia, A.-S. (2001). Neural Development, Cell-Cell Signaling, and the "Two-Hit" Hypothesis of Schizophrenia. *Schizophrenia Bulletin*, *27*(3), 457–476. https://doi.org/10.1093/oxfordjournals.schbul.a006887

McAllister, A. K., & Water, J. V. D. (2009). Breaking Boundaries in Neural-Immune Interactions. *Neuron*, *64*(1), 9–12. https://doi.org/10.1016/j.neuron.2009.09.038

McGee, A. W., Yang, Y., Fischer, Q. S., Daw, N. W., & Strittmatter, S. N. (2005). Experience-Driven Plasticity of Visual Cortex Limited by Myelin and Nogo Receptor. *Science*, *309*(5744), 2222–2226. https://doi.org/10.1126/science.1114362

McIntire, S. L., Reimer, R. J., Schuske, K., Edwards, R. H., & Jorgensen, E. M. (1997). Identification and characterization of the vesicular GABA transporter. *Nature*, *389*(6653), 870–876. https://doi.org/10.1038/39908

Mednick, S. A., Machon, R. A., Huttunen, M. O., & Bonett, D. (1988). Adult Schizophrenia Following Prenatal Exposure to an Influenza Epidemic. *Archives of General Psychiatry*, *45*(2), 189. https://doi.org/10.1001/archpsyc.1988.01800260109013

Mi, H., Muruganujan, A., Tang, H., Huang, X., Thomas, P. D., Mills, C., & Kang, D. (2019). PANTHER version 14: more genomes, a new PANTHER GO-slim and improvements in enrichment analysis tools. *Nucleic Acids Research*, *47*(D1), D419–D426. https://doi.org/10.1093/nar/gky1038

Michaelson, M. D., Bieri, P. L., Mehler, M. F., Xu, H., Arezzo, J. C., Pollard, J. W., & Kessler, J. A. (1996). CSF-1 deficiency in mice results in abnormal brain development. *Development*, *122*(9), 2661–2672. Retrieved from https://dev.biologists.org/content/122/9/2661.long

Minakova, E., & Warner, B. B. (2018). Maternal immune activation, central nervous system development and behavioral phenotypes. *Birth Defects Research*, *110*(20), 1539–1550. https://doi.org/10.1002/bdr2.1416

Mohan, V., Wyatt, E. V., Gotthard, I., Phend, K. D., Diestel, S., Duncan, B. W., Wienburg, R. J., Tripathy, A., & Maness, P. F. (2018). Neurocan Inhibits Semaphorin 3F Induced Dendritic Spine Remodeling Through NrCAM in Cortical Neurons. *Frontiers in Cellular Neuroscience*, *12*. https://doi.org/10.3389/fncel.2018.00346

MP Biomedicals. *Fastprep24-classic-bead-beater*. Retrieved from https://www.mpbio.com/us/fastprep-24-classic-instrument-1-each.

Murphy, K. M., Balsor, J., Beshara, S., Siu, C., & Pinto, J. G. (2014). A high-throughput semi-automated preparation for filtered synaptoneurosomes. *Journal of Neuroscience Methods*, *235*, 35–40. https://doi.org/10.1016/j.jneumeth.2014.05.036

Murtagh, F., & Legendre, P. (2014). Ward's Hierarchical Agglomerative Clustering Method: Which Algorithms Implement Ward's Criterion? *Journal of Classification*, *31*(3), 274–295. https://doi.org/10.1007/s00357-014-9161-z

Ng, A., Tam, W. W., Zhang, M. W., Ho, C. S., Husain, S. F., Mcintyre, R. S., & Ho, R. C. (2018). IL-1β, IL-6, TNF- α and CRP in Elderly Patients with Depression or Alzheimer's disease: Systematic Review and Meta-Analysis. *Scientific Reports*, *8*(1). https://doi.org/10.1038/s41598-018-30487-6

Nguyen, T. T., Eyler, L. T., & Jeste, D. V. (2017). Systemic Biomarkers of Accelerated Aging in Schizophrenia: A Critical Review and Future Directions. *Schizophrenia Bulletin*, *44*(2), 398–408. https://doi.org/10.1093/schbul/sbx069

Nicholson, L. B. (2016). The immune system. *Essays in Biochemistry*, *60*(3), 275–301. https://doi.org/10.1042/ebc20160017

Nutma, E., Willison, H., Martino, G., & Amor, S. (2019). Neuroimmunology - the past, present and future. *Clinical & Experimental Immunology*, *197*(3), 278–293. https://doi.org/10.1111/cei.13279

O'Brien, R. J., Xu, D., Petralia, R. S., Steward, O., Huganir, R. L., & Worley, P. (1999). Synaptic Clustering of AMPA Receptors by the Extracellular Immediate-Early Gene Product Narp. *Neuron*, *23*(2), 309–323. https://doi.org/10.1016/s0896-6273(00)80782-5

Pandey, G. N. (2017). Inflammatory and Innate Immune Markers of Neuroprogression in Depressed and Teenage Suicide Brain. *Modern Trends in Pharmacopsychiatry Neuroprogression in Psychiatric Disorders*, 79–95. https://doi.org/10.1159/000470809

Patel, K. R., Cherian, J., Gohil, K., & Atkinson, D. (2014). Schizophrenia: Overview and Treatment Options. *Pharmacy and Therapeutics*, *39*(9), 638–645. Retrieved from https://www.ncbi.nlm.nih.gov/pmc/articles/PMC4159061/

Perna, G., Iannone, G., Alciati, A., & Caldirola, D. (2016). Are Anxiety Disorders Associated with Accelerated Aging? A Focus on Neuroprogression. *Neural Plasticity*, *2016*, 1–19. https://doi.org/10.1155/2016/8457612

Philpot, B. D., Cho, K. K., & Bear, M. F. (2007). Obligatory Role of NR2A for Metaplasticity in Visual Cortex. *Neuron*, *53*(4), 495–502. https://doi.org/10.1016/j.neuron.2007.01.027

Philpot, B. D., Espinosa, J. S., & Bear, M. F. (2003). Evidence for Altered NMDA Receptor Function as a Basis for Metaplasticity in Visual Cortex. *The Journal of Neuroscience*, *23*(13), 5583–5588. https://doi.org/10.1523/jneurosci.23-13-05583.2003

Philpot, B. D., Sekhar, A. K., Shouval, H. Z., & Bear, M. F. (2001). Visual Experience and Deprivation Bidirectionally Modify the Composition and Function of NMDA Receptors in Visual Cortex. *Neuron*, *29*(1), 157–169. https://doi.org/10.1016/s0896-6273(01)00187-8

Pinto, J. G. A., Hornby, K. R., Jones, D. G., & Murphy, K. M. (2010). Developmental changes in GABAergic mechanisms in human visual cortex across the lifespan. *Frontiers in Cellular Neuroscience*, *4*, 16. https://doi.org/10.3389/fncel.2010.00016

Pozas, E., & Ibáñez, C. F. (2005). GDNF and GFRα1 Promote Differentiation and Tangential Migration of Cortical GABAergic Neurons. *Neuron*, *45*(5), 701–713. https://doi.org/10.1016/j.neuron.2005.01.043

Pribyl, T. M., Campagnoni, C. W., Kampf, K., Kashima, T., Handley, V. W., Mcmahon, J., & Campagnoni, A. T. (1993). The human myelin basic protein gene is included within a 179-kilobase transcription unit: expression in the immune and central nervous systems. *Proceedings of the National Academy of Sciences*, *90*(22), 10695–10699. https://doi.org/10.1073/pnas.90.22.10695

Qi, F., Qian, S., Zhang, S., & Zhang, Z. (2020). Single cell RNA sequencing of 13 human tissues identify cell types and receptors of human coronaviruses. https://doi.org/10.1101/2020.02.16.951913

Quinlan, E. M., Philpot, B. D., Huganir, R. L., & Bear, M. F. (1999). Rapid, experience-dependent expression of synaptic NMDA receptors in visual cortex in vivo. *Nature Neuroscience*, *2*(4), 352–357. https://doi.org/10.1038/7263

R Core Team (2020). R: A language and environment for statistical computing. R Foundation for Statistical Computing, Vienna, Austria. URL https://www.R-project.org/.

Rajendran, L., & Paolicelli, R. C. (2018). Microglia-Mediated Synapse Loss in Alzheimer's Disease. *The Journal of Neuroscience*, *38*(12), 2911–2919. https://doi.org/10.1523/jneurosci.1136-17.2017

Ramey, J. A. (2012, August 31). *Package 'clusterval'*. clusteval: Evaluation of Clustering Algorithms. Retrieved from https://cran.r-project.org/web/packages/clusteval/clusteval.pdf.

Raudvere, U., Kolberg, L., Kuzmin, I., Arak, T., Adler, P., Peterson, H., & Vilo, J. (2019). g:Profiler: a web server for functional enrichment analysis and conversions of gene lists (2019 update). *Nucleic Acids Research*, *47*(W1), W191–W198. https://doi.org/10.1093/nar/gkz369

RayBiotech, Inc. (2019). *Quantibody® Human Cytokine Antibody Array 4000*. Norcross, GA; RayBiotech, Inc. Retrieved from https://doc.raybiotech.com/pdf/Manual/QAH-CAA-4000.pdf.

Reardon, C., Murray, K., & Lomax, A. E. (2018). Neuroimmune Communication in Health and Disease. *Physiological Reviews*, *98*(4), 2287–2316. https://doi.org/10.1152/physrev.00035.2017

Reimer, R. J., Schuske, K., Edwards, R. H., Jorgensen, E. M., & McIntire, S. L. (1997). Identification and characterization of the vesicular GABA transporter. *Nature*, *389*(6653), 870–876. https://doi.org/10.1038/39908

Roy, K., Murtie, J. C., El-Khodor, B. F., Edgar, N., Sardi, S. P., Hooks, B. M., Benoit-Marand, M., Chen, C., Moore, H., O'Donnell, P., Brunner, D., & Corfas, G. (2007). Loss of erbB signaling in oligodendrocytes alters myelin and dopaminergic function, a potential mechanism for neuropsychiatric disorders. *Proceedings of the National Academy of Sciences*, *104*(19), 8131–8136. https://doi.org/10.1073/pnas.0702157104

RStudio Team (2020). RStudio: Integrated Development for R. RStudio, PBC, Boston, MA URL http://www.rstudio.com/.

Rubin, D. B. (1986). Statistical Matching Using File Concatenation with Adjusted Weights and Multiple Imputations. *Journal of Business & Economic Statistics*, *4*(1), 87. https://doi.org/10.2307/1391390

Rumpel, S., Hatt, H., & Gottmann, K. (1998). Silent Synapses in the Developing Rat Visual Cortex: Evidence for Postsynaptic Expression of Synaptic Plasticity. *The Journal of Neuroscience*, *18*(21), 8863–8874. https://doi.org/10.1523/jneurosci.18-21-08863.1998

Sadreev, I. I., Chen, M. Z. Q., Welsh, G. I., Umezawa, Y., Kotov, N. V., & Valeyev, N. V. (2014). A Systems Model of Phosphorylation for Inflammatory Signaling Events. *PLoS ONE*, *9*(10). https://doi.org/10.1371/journal.pone.0110913

Sagné, C., Mestikawy, S. E., Isambert, M.-F., Hamon, M., Henry, J.-P., Giros, B., & Gasnier, B. (1997). Cloning of a functional vesicular GABA and glycine transporter by screening of genome databases. *FEBS Letters*, *417*(2), 177–183. https://doi.org/10.1016/s0014-5793(97)01279-9

Saiz, J. (2016, October 10). *Jaccard Index Calculation In R*. Jose's blog. Retrieved from https://jootse84.github.io/notes/jaccard-index-calculation-in-R.

Sakamoto, S., Putalun, W., Vimolmangkang, S., Phoolcharoen, W., Shoyama, Y., Tanaka, H., & Morimoto, S. (2018). Correction to: Enzyme-linked immunosorbent assay for the quantitative/qualitative analysis of plant secondary metabolites. *Journal of Natural Medicines*, *72*(1), 43–43. https://doi.org/10.1007/s11418-017-1163-9

Saunders, K. J., Mcculloch, D. L., & Kerr, A. M. (1995). Visual Function In Rett Syndrome. *Developmental Medicine & Child Neurology*, *37*(6), 496–504. https://doi.org/10.1111/j.1469-8749.1995.tb12037.x

Sawalha, A., Webb, R., Han, S., Kelly, J., Kaufman, K., Kimberly, R., Alarcón-Riquelme, M., James, J., Vyse, T., Gilkeson, G., Choi, C.-B., Scofield, H., Bae, S.-C., Nath, S., & Harley, J. (2008). Sa.9. Common Variants within MECP2 Confer Risk of Systemic Lupus Erythematosus. *Clinical Immunology*, *127*, S83. https://doi.org/10.1016/j.clim.2008.03.230

Schafer, D. P., & Stevens, B. (2010). Synapse elimination during development and disease: immune molecules take centre stage. *Biochemical Society Transactions*, *38*(2), 476–481. https://doi.org/10.1042/bst0380476

Schmid, F., Barrett, M. J., Jenny, P., & Weber, B. (2019). Vascular density and distribution in neocortex. *NeuroImage*, *197*, 792–805. https://doi.org/10.1016/j.neuroimage.2017.06.046

Shafit-Zagardo, B., Gruber, R. C., & Dubois, J. C. (2018). The role of TAM family receptors and ligands in the nervous system: From development to pathobiology. *Pharmacology & Therapeutics*, *188*, 97–117. https://doi.org/10.1016/j.pharmthera.2018.03.002

Shatz, C. J. (2009). MHC Class I: An Unexpected Role in Neuronal Plasticity. *Neuron*, *64*(1), 40–45. https://doi.org/10.1016/j.neuron.2009.09.044

Silverstein, S., Keane, B. P., Blake, R., Giersch, A., Green, M., & Kã©Ri, S. (2015). Vision in schizophrenia: why it matters. *Frontiers in Psychology*, *6*. https://doi.org/10.3389/fpsyg.2015.00041

Siu, C. R. (2017). *Development of human visual cortex: A neurobiological approach* (thesis). MacSphere, Hamilton. Retrieved from https://macsphere.mcmaster.ca/handle/11375/23881

Siu, C. R., Balsor, J. L., Jones, D. G., & Murphy, K. M. (2015). Classic and Golli Myelin Basic Protein have distinct developmental trajectories in human visual cortex. *Frontiers in Neuroscience*, *9*, 138. https://doi.org/10.3389/fnins.2015.00138

Siu, C. R., Beshara, S. P., Balsor, J. L., Mancini, S. J., & Murphy, K. M. (2018). Use of Synaptoneurosome Samples to Study Development and Plasticity of Human Cortex. In Synaptosomes (pp. 269-286). Humana Press, New York, NY.

Siu, C. R., Beshara, S. P., Jones, D. G., & Murphy, K. M. (2017). Development of Glutamatergic Proteins in Human Visual Cortex across the Lifespan. *The Journal of Neuroscience*, *37*(25), 6031–6042. https://doi.org/10.1523/jneurosci.2304-16.2017

Smith, G. B., & Olsen, R. W. (1995). Functional domains of GABAA receptors. *Trends in Pharmacological Sciences*, *16*(5), 162–168. https://doi.org/10.1016/s0165-6147(00)89009-4

Smith, G. B., Heynen, A. J., & Bear, M. F. (2009). Bidirectional synaptic mechanisms of ocular dominance plasticity in visual cortex. *Philosophical Transactions of the Royal Society B: Biological Sciences*, *364*(1515), 357–367. https://doi.org/10.1098/rstb.2008.0198

Smith, M. R., Readhead, B., Dudley, J. T., & Morishita, H. (2019). Critical period plasticity-related transcriptional aberrations in schizophrenia and bipolar disorder. *Schizophrenia Research*, *207*, 12–21. https://doi.org/10.1016/j.schres.2018.10.021

Smith, S. E. P., Li, J., Garbett, K., Mirnics, K., & Patterson, P. H. (2007). Maternal Immune Activation Alters Fetal Brain Development through Interleukin-6. *Journal of Neuroscience*, *27*(40), 10695–10702. https://doi.org/10.1523/jneurosci.2178-07.2007

Song, G., Xu, S., Zhang, H., Wang, Y., Xiao, C., Jiang, T., Wu, L., Zhang, T., Sun, X., Zhong, L., Zhou, C., Wang, Z., Peng, Z., Chen, J., & Wang, X. (2016). TIMP1 is a prognostic marker for the progression and metastasis of colon cancer through FAK-PI3K/AKT and MAPK pathway. *Journal of Experimental & Clinical Cancer Research*, *35*(148). https://doi.org/10.1186/s13046-016-0427-7

Spindler, K. R., & Hsu, T.-H. (2012). Viral disruption of the blood–brain barrier. *Trends in Microbiology*, *20*(6), 282–290. https://doi.org/10.1016/j.tim.2012.03.009

Stellwagen, D., & Malenka, R. C. (2006). Synaptic scaling mediated by glial TNF-α. *Nature*, *440*(7087), 1054–1059. https://doi.org/10.1038/nature04671

Stellwagen, D., Beattie, E. C., Seo, J. Y., & Malenka, R. C. (2005). Differential Regulation of AMPA Receptor and GABA Receptor Trafficking by Tumor Necrosis Factor- . *Journal of Neuroscience*, *25*(12), 3219–3228. https://doi.org/10.1523/jneurosci.4486-04.2005

Stevens, B., Allen, N. J., Vazquez, L. E., Howell, G. R., Christopherson, K. S., Nouri, N., Micheva, K. D., Mehalow, A. K., Huberman, A. D., Stafford, B., Sher, A., Litke, A. M., Lambris, J. D., Smith, S. J., John, S. W. M., & Barres, B. A. (2007). The Classical Complement Cascade Mediates CNS Synapse Elimination. *Cell*, *131*(6), 1164–1178. https://doi.org/10.1016/j.cell.2007.10.036

Stolp, H. (2013). Neuropoietic cytokines in normal brain development and neurodevelopmental disorders. *Molecular and Cellular Neuroscience*, *53*, 63–68. https://doi.org/10.1016/j.mcn.2012.08.009

Stottmann, R. W., & Rivas, R. J. (1998). Distribution of TAG-1 and synaptophysin in the developing cerebellar cortex: Relationship to Purkinje cell dendritic development. *The Journal of Comparative Neurology*, *395*(1), 121–135. https://doi.org/10.1002/(sici)1096-9861(19980525)395:13.0.co;2-2

Studahl, M. (2003). Influenza virus and CNS manifestations. *Journal of Clinical Virology*, *28*(3), 225–232. https://doi.org/10.1016/s1386-6532(03)00119-7

Syken, J., GrandPre, T., Kanold, P. O., & Shatz, C. J. (2006). PirB Restricts Ocular-Dominance Plasticity in Visual Cortex. *Science*, *313*(5794), 1795–1800. https://doi.org/10.1126/science.1128232

Szklarczyk, D., Gable, A. L., Lyon, D., Junge, A., Wyder, S., Huerta-Cepas, J., Simonovic, M., Doncheva, N. T., Morris, J. H., Bork, P., Jensen, L. J., & Mering, C. . v. o. n. (2018). STRING v11: protein–protein association networks with increased coverage, supporting functional discovery in genome-wide experimental datasets. *Nucleic Acids Research*, *47*(D1), D607–D613. https://doi.org/10.1093/nar/gky1131

Takahashi, H., & Naito, Y. (2017). Drebrin and Spine Formation. In *DREBRIN: from structure and function to physiological and pathological roles* (pp. 157–182). essay, SPRINGER Verlag, JAPAN.

Tang, M.-M., Lin, W.-J., Zhang, J.-T., Zhao, Y.-W., & Li, Y.-C. (2017). Exogenous FGF2 reverses depressive-like behaviors and restores the suppressed FGF2-ERK1/2 signaling and the impaired hippocampal neurogenesis induced by neuroinflammation. *Brain, Behavior, and Immunity*, *66*, 322–331. https://doi.org/10.1016/j.bbi.2017.05.013

Terauchi, A., Johnson-Venkatesh, E. M., Toth, A. B., Javed, D., Sutton, M. A., & Umemori, H. (2010). Distinct FGFs promote differentiation of excitatory and inhibitory synapses. *Nature*, *465*(7299), 783–787. https://doi.org/10.1038/nature09041

Tetzchner, S., Jacobsen, K. H., Smith, L., Skjeldal, O. H., Heiberg, A., & Fagan, J. F. (1996). Vision, Cognition And Developmental Characteristics Of Girls And Women With Rett Syndrome. *Developmental Medicine & Child Neurology*, *38*(3), 212–225. https://doi.org/10.1111/j.1469-8749.1996.tb15083.x

The UniProt Consortium. (2019). UniProt: a worldwide hub of protein knowledge. *Nucleic Acids Research*, *47*(D1), D506–D515. https://doi.org/10.1093/nar/gky1049

Vogel, C., & Marcotte, E. M. (2012). Insights into the regulation of protein abundance from proteomic and transcriptomic analyses. *Nature Reviews Genetics*, *13*(4), 227–232. https://doi.org/10.1038/nrg3185

Vonhoff, F., & Keshishian, H. (2017). Activity-Dependent Synaptic Refinement: New Insights from Drosophila. *Frontiers in Systems Neuroscience*, *11*. https://doi.org/10.3389/fnsys.2017.00023

Wake, H., Lee, P. R., & Fields, R. D. (2011). Control of Local Protein Synthesis and Initial Events in Myelination by Action Potentials. *Science*, *333*(6049), 1647–1651. https://doi.org/10.1126/science.1206998

Walker, J. A., & Mckenzie, A. N. J. (2017). TH2 cell development and function. *Nature Reviews Immunology*, *18*(2), 121–133. https://doi.org/10.1038/nri.2017.118,

Wang, Z.-Y., Wang, P.-G., & An, J. (2020). The Multifaceted Roles of TAM Receptors during Viral Infection. *Virologica Sinica*. https://doi.org/10.1007/s12250-020-00264-9

Webb, R., Wren, J. D., Jeffries, M., Kelly, J. A., Kaufman, K. M., Tang, Y., Frank, M. B., Merrill, J., Kimberly, R. P., Edberg, J. C., Ramsey-Goldman, R., Petri, M., Reveille, J. D., Alarcón, G. S., Vilá, L. M., Alarcón-Riquelme, M. E., James, J. A., Vyse, T. J., Moser, K. L., … Sawalha, A. H. (2009). Variants withinMECP2, a key transcription regulator, are associated with increased susceptibility to lupus and differential gene expression in patients with systemic lupus erythematosus. *Arthritis & Rheumatism*, *60*(4), 1076–1084. https://doi.org/10.1002/art.24360

White, U. A., & Stephens, J. M. (2011). The gp130 Receptor Cytokine Family: Regulators of Adipocyte Development and Function. *Current Pharmaceutical Design*, *17*(4), 340–346. https://doi.org/10.2174/138161211795164202

WhiteDragon. Plastic plate with 96 wells is widely used for molecular biology research - lab equipment [digital image]. Stock vector ID: 375965884. Retrieved from https://www.shutterstock.com/image-vector/plastic-plate-96-wells-widely-used-375965884

Wieczorek, M., Abualrous, E. T., Sticht, J., Álvaro-Benito, M., Stolzenberg, S., Noé, F., & Freund, C. (2017). Major Histocompatibility Complex (MHC) Class I and MHC Class II Proteins: Conformational Plasticity in Antigen Presentation. *Frontiers in Immunology*, *8*. https://doi.org/10.3389/fimmu.2017.00292

Wiesel, T. N., & Hubel, D. H. (1963a). Effects Of Visual Deprivation On Morphology And Physiology Of Cells In The Cat's Lateral Geniculate Body. *Journal of Neurophysiology*, *26*(6), 978–993. https://doi.org/10.1152/jn.1963.26.6.978

Wiesel, T. N., & Hubel, D. H. (1963b). Single-Cell Responses In Striate Cortex Of Kittens Deprived Of Vision In One Eye. *Journal of Neurophysiology*, *26*(6), 1003–1017. https://doi.org/10.1152/jn.1963.26.6.1003

Wiesel, T. N., Hubel, D. H., & Lam, D. M. (1974). Autoradiographic demonstration of ocular-dominance columns in the monkey striate cortex by means of transneuronal transport. *Brain Research*, *79*(2), 273–279. https://doi.org/10.1016/0006-8993(74)90416-8

Winter, C., Djodari-Irani, A., Sohr, R., Morgenstern, R., Feldon, J., Juckel, G., & Meyer, U. (2009). Prenatal immune activation leads to multiple changes in basal neurotransmitter levels in the adult brain: implications for brain disorders of neurodevelopmental origin such as schizophrenia. *The International Journal of Neuropsychopharmacology*, *12*(04), 513–524. https://doi.org/10.1017/s1461145708009206

Wiwie, C., Baumbach, J., & Röttger, R. (2015). Comparing the performance of biomedical clustering methods. *Nature Methods*, *12*(11), 1033–1038. https://doi.org/10.1038/nmeth.3583

Woodbury, M. E., & Ikezu, T. (2013). Fibroblast Growth Factor-2 Signaling in Neurogenesis and Neurodegeneration. *Journal of Neuroimmune Pharmacology*, *9*(2), 92–101. https://doi.org/10.1007/s11481-013-9501-5

Wright, A., & Vissel, B. (2012). The essential role of AMPA receptor GluR2 subunit RNA editing in the normal and diseased brain. *Frontiers in Molecular Neuroscience*, *5*(34). https://doi.org/10.3389/fnmol.2012.00034

Xie, Z., Eagleson, K. L., Wu, H.-H., & Levitt, P. (2016). Hepatocyte Growth Factor Modulates MET Receptor Tyrosine Kinase and β-Catenin Functional Interactions to Enhance Synapse Formation. *Eneuro*, *3*(4). https://doi.org/10.1523/eneuro.0074-16.2016

Yan, Q., Zhai, L., Zhang, B., & Dallman, J. E. (2017). Spatial patterning of excitatory and inhibitory neuropil territories during spinal circuit development. *Journal of Comparative Neurology*, *525*(7), 1649–1667 https://doi.org/10.1002/cne.24152

Yang, S., Wang, J., Brand, D. D., & Zheng, S. G. (2018). Role of TNF–TNF Receptor 2 Signal in Regulatory T Cells and Its Therapeutic Implications. *Frontiers in Immunology*, *9*. https://doi.org/10.3389/fimmu.2018.00784

Yarlagadda, A., Alfson, E., & Clayton, A. H. (2009). The Blood Brain Barrier and the Role of Cytokines in Neuropsychiatry. *Psychiatry (Edgmont)*, *6*(11), 18–22. Retrieved from https://www.ncbi.nlm.nih.gov/pmc/articles/PMC2801483/

Zlokovic, B. V. (2008). The Blood-Brain Barrier in Health and Chronic Neurodegenerative Disorders. *Neuron*, *57*(2), 178–201. https://doi.org/10.1016/j.neuron.2008.01.003